



NUCLEAR WASTE  
MANAGEMENT  
ORGANIZATION

SOCIÉTÉ DE GESTION  
DES DÉCHETS  
NUCLÉAIRES

Phase 2 Geoscientific Preliminary Assessment  
Acquisition, Processing and Interpretation of  
High-Resolution Airborne Geophysical Data

TOWNSHIP OF WHITE RIVER AND AREA, ONTARIO



**APM-REP-01332-0209**

**DECEMBER 2017**

*This report has been prepared under contract to the NWMO. The report has been reviewed by the NWMO, but the views and conclusions are those of the authors and do not necessarily represent those of the NWMO.*

*All copyright and intellectual property rights belong to the NWMO.*

*For more information, please contact:*

**Nuclear Waste Management Organization**

22 St. Clair Avenue East, Sixth Floor

Toronto, Ontario M4T 2S3 Canada


Tel 416.934.9814

Toll Free 1.866.249.6966

Email [contactus@nwmo.ca](mailto:contactus@nwmo.ca)

[www.nwmo.ca](http://www.nwmo.ca)



 <b>Sander Geophysics</b>	Airborne Geophysics Acquisition and Interpretation	Issue Date:	December 2017
--	--	-------------	---------------

## **PHASE 2 GEOSCIENTIFIC PRELIMINARY ASSESSMENT**

# **ACQUISITION, PROCESSING AND INTERPRETATION OF HIGH-RESOLUTION AIRBORNE GEOPHYSICAL DATA**

## **TOWNSHIP OF WHITE RIVER AND AREA, ONTARIO**

**Prepared for:**

**Nuclear Waste Management Organization (NWMO)**

**by:**

**Sander Geophysics Limited (SGL)**

**NWMO REPORT NUMBER:  
APM-REP-01332-0209**

## Signatures



Martin Bates, Ph.D.



Martin Mushayandebvu, Ph.D.

*Peter Tschirhart*  
Dec 8, 2016

Peter Tschirhart, M.Sc.

## Executive Summary

This technical report documents the results of the acquisition, processing and interpretation of high-resolution airborne geophysical data conducted as part of the Phase 2 Geoscientific Preliminary Assessment, to further assess the suitability of the White River area to safely host a deep geological repository (AMEC, 2017). This study followed the successful completion of a Phase 1 Geoscientific Desktop Preliminary Assessment (AECOM, 2014a). The desktop Phase 1 study identified four potentially suitable areas warranting further studies such as high-resolution surveys and geological mapping; two located within the Anahareo pluton, one within the Strickland pluton, and one within the Pukaskwa batholith. Of the potentially suitable areas identified during Phase 1, airborne geophysical data was only acquired for the eastern side of the Anahareo pluton and the Strickland pluton; the interpretation therefore only focuses on two of the four areas identified in Phase 1

The purpose of the Phase 2 acquisition, processing and interpretation of geophysical data was to provide an updated interpretation of the geological characteristics of the potentially suitable bedrock unit identified in Phase 1 and to provide additional information to further assess the geology of the White River area. Both magnetic and gravimetric data were acquired during the surveys in order to provide data to interpret the geometry and thickness of the potentially suitable bedrock units; the nature of geological contacts; bedrock lithologies; the degree of geological heterogeneities and the nature of intrusive phases within the plutons in the area; as well as the nature of structural features such as faults, shears zones, and alteration zones. The grids of the acquired magnetic and gravimetric data and associated processed grids (first, second and horizontal derivatives, total gradient amplitude, trend analysis solutions and tilt angle) were analyzed and interpreted together with the mapped bedrock geology and other available geological information (e.g. magnetic susceptibility and rock density).

The survey allowed for a characterization of the gravity and magnetic signatures of the Anahareo pluton and the Strickland pluton and the adjacent greenstone belt units. The Strickland pluton encompasses a large central gravity low which continues into the Pukaskwa batholith to the south with no associated change across the mapped boundary. The gravity low represents either the thickest section of the pluton and batholith and/or the part of the body with the lowest density. Boundaries of the Strickland pluton are defined in both the magnetic and gravity data and are associated with edges of mapped greenstone belts. Large-scale folds were identified within the pluton indicating some degree of deformation. Magnetic anomalies, with corresponding gravity anomalies, have been identified within the Strickland pluton and are interpreted to represent outliers of mafic metavolcanic rocks of the Kabinakagami Lake greenstone belt.

The Anahareo pluton encompasses an irregularly shaped local gravity low within a larger east-west trending regional gravity low and is interpreted to represent either the thickest section of the pluton and Pukaskwa batholith and/or the part of the body with the lowest density. A local magnetic anomaly has been interpreted as due to mafic metavolcanic rocks hosted within the Anahareo pluton.

Preliminary forward modelling was completed on two profile lines covering the main features of the Strickland and Anahareo plutons and adjacent batholiths and greenstone belts within the survey area. The Strickland pluton has been modelled with a roughly constant thickness slightly over 2 km with internal density variations or alternatively with a constant density and variable thickness with a maximum around 4 km in the central part of the pluton.

<b>1</b>	<b>INTRODUCTION.....</b>	<b>6</b>
1.1	Study Objective.....	6
1.2	Geophysical Survey Area.....	6
<b>2</b>	<b>SUMMARY OF GEOLOGY .....</b>	<b>8</b>
2.1	Geological Setting .....	8
2.2	Bedrock Geology .....	8
2.2.1	Strickland Pluton.....	9
2.2.2	Pukaskwa Batholith.....	9
2.2.3	Anahareo Pluton .....	10
2.2.4	Black-Pic Batholith .....	11
2.2.5	Foliated Tonalite Suite.....	12
2.2.6	Mafic Dykes .....	12
2.3	Structural History.....	13
2.3.1	Mapped Structures .....	15
2.4	Metamorphism.....	16
2.5	Quaternary Geology .....	17
<b>3</b>	<b>DATA SOURCE ACQUISITION AND QUALITY.....</b>	<b>18</b>
3.1	Magnetic Data.....	19
3.2	Gravity Data .....	19
3.3	Digital Elevation Data.....	20
3.4	Additional Data Sources.....	21
3.4.1	OGS Mapped Bedrock Geology.....	21
3.4.2	Geological Base Maps.....	21
3.4.3	OGS PETROCH Lithogeochemical Database .....	21
3.4.4	Densities and Magnetic Susceptibilities.....	22
3.4.5	Ontario Precambrian Bedrock Magnetic Susceptibility Geodatabase .....	22
3.4.6	Other Magnetic Susceptibility Measurements.....	22
<b>4</b>	<b>GEOPHYSICAL DATA PROCESSING METHODS.....</b>	<b>23</b>
4.1	Gravity Data Processing.....	23
4.1.1	Bouguer Correction .....	24
4.1.2	Static and Level Corrections .....	24
4.1.3	Gridding and Filtering.....	24

<b>4.2</b>	<b>Magnetic Data Processing .....</b>	<b>25</b>
4.2.1	Levelling.....	25
4.2.2	Micro-Levelling.....	26
4.2.3	Gridding.....	26
<b>4.3</b>	<b>Gravity and Magnetic Derivative Products.....</b>	<b>26</b>
4.3.1	Total Magnetic Intensity Reduced to Pole.....	26
4.3.2	Vertical Derivatives of Total Magnetic Intensity and Bouguer Gravity .....	27
4.3.3	Total Horizontal Gradient of Total Magnetic Intensity and Bouguer Gravity .....	27
4.3.4	Total Gradient Amplitude of Total Magnetic Intensity .....	28
4.3.5	Tilt Angle .....	28
4.3.6	Trend Analysis Method .....	28
<b>5</b>	<b>GEOPHYSICAL INTERPRETATION.....</b>	<b>30</b>
<b>5.1</b>	<b>Results of Qualitative Analysis .....</b>	<b>30</b>
5.1.1	Strickland Pluton.....	30
5.1.2	Anahareo Pluton .....	33
<b>5.2</b>	<b>Preliminary 2.5D Modelling .....</b>	<b>34</b>
5.2.1	Model Descriptions.....	35
5.2.2	Model Results .....	37
<b>6</b>	<b>SUMMARY OF RESULTS .....</b>	<b>46</b>
<b>7</b>	<b>REFERENCES .....</b>	<b>49</b>
<b>8</b>	<b>FIGURES.....</b>	<b>55</b>

# 1 Introduction

This technical report documents the results of the acquisition and interpretation of high-resolution airborne geophysical data (gravity and magnetic) conducted as part of the Phase 2 Geoscientific Preliminary Assessment, to further assess the suitability of the White River area to safely host a deep geological repository (AMEC, 2017). This study followed the successful completion of a Phase 1 Geoscientific Desktop Preliminary Assessment (AECOM, 2014a). The desktop Phase 1 study identified four potentially suitable areas warranting further studies such as high-resolution surveys and geological mapping; two located within the Anahareo pluton, one within the Strickland pluton, and one within the Pukaskwa batholith. Of the potentially suitable areas identified during Phase 1, airborne geophysical data was only acquired for the eastern side of the Anahareo pluton and the Strickland pluton; the interpretation therefore only focuses on two of the four areas identified in Phase 1.

## 1.1 Study Objective

The main purposes of the acquisition and interpretation of magnetic and gravity data are as follows:

- Acquire high-resolution airborne magnetic and gravimetric data within a geophysical survey area that encompasses one of the general potentially suitable areas of the Anahareo pluton and the potentially suitable area in the Strickland pluton identified in the Phase 1 Geoscientific Desktop Preliminary Assessment (AECOM, 2014a).
- Characterize the geophysical response of the bedrock units (e.g. bedrock contacts, intrusive phases, potential natural resources, etc.).
- Characterize the extent of bedrock heterogeneity (e.g. ductile fabric, complexity, etc.).
- Interpret the geophysical character of potential structures (faults, dykes, joints, etc.).
- Develop initial models of bedrock units at depth (2.5D forward modeling).

## 1.2 Geophysical Survey Area

The Township of White River is located northeast of Lake Superior, approximately 295 km east of Thunder Bay, and 240 km north-northwest of Sault Ste. Marie at the intersection of Highway 17 and Highway 631. The White River survey area is located approximately 25 km east of the Township of White River and encompasses an area of more than 1,100 km<sup>2</sup>. The location of the geophysical survey area is shown in Figure 1.1 overlying the bedrock geology, and the full set of survey lines are shown in Figure 1.2. The geophysical survey area is bounded by the coordinates presented in Table 1.1 (NAD-83 datum, UTM zone 16N).

*Table 1.1: Coordinates of the survey area (NAD-83, UTM 16N)*

<b>Easting (m)</b>	<b>Northing (m)</b>
<b>White River block</b>	
650623	5422814
677000	5422861
677000	5379930
657835	5379969
650623	5393782

## **2 Summary of Geology**

Details of the geology of the White River area were described in the Phase 1 Geoscientific Desktop Preliminary Assessment (AECOM, 2014a). The following sections provide brief descriptions of the geologic setting, bedrock geology, structural history and mapped structures, metamorphism and Quaternary geology of the White River area. The focus of the following sections are the bedrock units identified during Phase 1 as being potentially suitable to host a deep geological repository and the important structural features in the area.

### **2.1 Geological Setting**

The White River area is located within the Superior Province of northern Ontario. The Superior Province is a stable craton created from a collage of ancient plates and accreted juvenile arc terranes that were progressively amalgamated over a period of more than 2 Ga (e.g., Percival et al., 2006). The Superior Province covers an area of approximately 1,500,000 km<sup>2</sup> and is divided into subprovinces, including the Wawa Subprovince within which the White River area is located.

The Wawa Subprovince comprises multiple units of volcanic and associated metasedimentary rocks (greenstone belts) separated by extensive granitic plutons and batholiths. These greenstone belts typically occur in elongate, narrow, geometries and represent volumetrically a relatively minor percentage of the rocks. The surrounding granitic bodies are composed primarily of tonalite to granodiorite, and represent the vast majority of the rocks present throughout the White River area.

Several generations of Paleoproterozoic diabase dyke swarms, ranging in age from ca. 2.473 to 2.101 Ga intrude all bedrock units in the White River area (Hamilton et al., 2002; Buchan and Ernst, 2004; Halls et al., 2006).

### **2.2 Bedrock Geology**

The White River area is situated within the Wawa Subprovince, which is a volcano-sedimentary-plutonic terrane bounded to the east by the Kapuskasing structural zone and to the north by the metasedimentary-dominated Quetico Subprovince. The Wawa Subprovince is composed of well-defined greenstone belts of metamorphosed volcanic rocks and associated metasedimentary rocks, separated by granitoid rock units.

There are two semi-linear to arcuate zones of greenstone belts within the Wawa Subprovince, the northern of which includes the Shebandowan, Schreiber-Hemlo, White River-Hornepayne, Dayohessarah, and Kabinakagami greenstone belts (Figure 1.1). The southern zone comprises the Michipicoten, Mishibishu, and Gamitagama greenstone belts, which are located west of the Kapuskasing structural zone, well southeast of the White River area. The Dayohessarah greenstone belt and the western portion of the Kabinakagami belt are within the White River area (Figure 1.1). A small portion of the Schreiber-Hemlo belt is located along the western boundary of the White River area, while the Michipicoten greenstone belt is situated approximately 25 kilometres to the southeast. The Dayohessarah and Kabinakagami greenstone belts have been interpreted by Williams et al. (1991) and Stott (1999) as being part of a once continuous supracrustal belt now represented by the White River-Hornepayne and the Black River assemblage of the Schreiber-Hemlo belts.

The granitoids that separate the greenstone belts comprise 20 to 30 percent of the landmass of the Wawa Subprovince, and consist of massive, foliated and gneissic tonalite-granodiorite, which is cut by massive to foliated granodiorite and granite. The majority of the granitoids were emplaced during or



after the deposition of the greenstone belts with which they are associated (Williams et al., 1991). The granitoids in the White River Phase 2 assessment area include the Strickland and Anahareo plutons, the Pukaskwa batholith and to a lesser extent the Black-Pic batholith.

Several generations of Paleo- and Meso-proterozoic diabase dyke swarms, ranging in age from 2.473 to 1.14 Ga, cut all bedrock units in the White River area. The most prominent of these dyke swarms include the northwest-trending Matachewan swarm, ca. 2.473 Ga (Buchan and Ernst, 2004); the northeast-trending Biscotasing dyke swarm, ca. 2.167 Ga (Hamilton et al., 2002); and the north-trending Marathon dyke swarm ca. 2.121 Ga (Buchan et al., 1996; Hamilton et al., 2002). Less numerous dykes belonging to the west-northwest trending Sudbury (ca. 1.238 Ga; Krogh et al., 1987) and northeast-trending Abitibi (ca. 1.14 Ga; Ernst and Buchan, 1993) dyke swarms also crosscut the area.

The main geological units of interest occurring in the White River area are further described below.

### **2.2.1 Strickland Pluton**

The Strickland pluton occurs in the northern portion of the White River area bordering the Dayohessarah and Kabinakagami greenstone belts. The pluton extends to the northeast of the study area, occupies an area of approximately 600 km<sup>2</sup> and has maximum dimensions (including areas beyond the study area) of 34 kilometres north-south and 55 kilometres east-west (Figure 1.1). Stott (1999) described the Strickland pluton as a relatively homogeneous, quartz porphyritic granodiorite; although, near the outer margin of the pluton, adjacent to the greenstone belt, granodiorite to tonalite and diorite are present. In the area west of the Kabinakagami greenstone belt, Siragusa (1977) noted that massive quartz monzonite (i.e., monzogranite in modern terminology) intrudes the granodioritic and trondhjemitic rocks in the form of medium-grained to pegmatitic dykes and small sills and irregular bodies.

Some degree of post-emplacement deformation and metamorphism of the Strickland pluton is indicated by the observed presence of fine- to medium-grained titanite and the widespread presence of hematite-filled fractures and weak alteration of silicate minerals (Stott, 1999). Stott (1999) noted that the pluton is petrographically similar to the ca. 2.697 Ga Dotted Lake batholith located in the northwestern corner of the White River area and suggested that these plutons are members of an intrusive suite commonly found along the margins of greenstone belts in this part of the Wawa Subprovince.

### **2.2.2 Pukaskwa Batholith**

The Pukaskwa batholith (also referred to as the Pukaskwa gneissic complex) is a large, regionally-extensive intrusion covering an area of at least 5,000 km<sup>2</sup> in the Wawa Subprovince (Figure 1.1). Mapping of the intrusion in the White River area was completed at a reconnaissance scale resulting in crudely defined boundaries of the batholith (Milne et al., 1972; Santaguida, 2001). As mapped by Santaguida (2001), the batholith is bounded to the north by the Strickland pluton, the Danny Lake stock and the Black-Pic batholith. The Pukaskwa batholith surrounds the western extent of the Anahareo pluton.

The Pukaskwa batholith extends over the central portion of the White River area (Figure 1.1) and is described as comprising foliated tonalite and gneissic tonalite suites (Santaguida, 2001). Regionally, the Pukaskwa batholith is a multi-phased intrusion emplaced over an extended time period (Stott, 1999; Beakhouse and Lin, 2006; Beakhouse et al., 2011).

Knowledge of the Pukaskwa batholith is primarily obtained from regional studies conducted to the west, in the vicinity of the Hemlo greenstone belt. An investigation of the batholith by Beakhouse et al. (2011) identified a number of lithologic associations (rock groupings) based on petrological and geochemical characteristics, three of which were volumetrically significant. The oldest association and most abundant of the three are a group of gneissic, well-foliated tonalite to granodioritic rocks. The gneissic nature of these rocks is a composite fabric formed by flattening or transposition of heterogeneities, metamorphic segregation or partial melting, and emplacement of sheet-like intrusive phases controlled by pre-existing anisotropy (Beakhouse et al., 2011). This lithologic association is interpreted to represent rocks derived from melting of a mafic crust and emplaced during the period ca. 2.720 to 2.703 Ga (Corfu and Muir, 1989; Jackson et al., 1998; Stott, 1999; Beakhouse et al., 2011; Lin and Beakhouse, 2013). It is likely that the foliated tonalite and gneissic tonalite suites as described by Santaguida (2001) in the White River area are part of this rock group.

The Pukaskwa batholith's second lithologic association, emplaced in the period between ca. 2.703 and 2.686 Ga, consists of foliated granodiorite to quartz-monzodiorite that is widespread but volumetrically limited (Beakhouse et al., 2011). Corfu and Muir (1989) reported a weakly foliated granodiorite from the Pukaskwa batholith having an inferred magmatic crystallization age of ca. 2.688 Ga. Geochemical analysis indicates that the rocks of the lithological association were derived from, or due to some sort of interaction with, an ultramafic source. These rocks cut the older lithologic association described above and have a weakly to moderate foliation which is generally subparallel to parallel to pre-existing rock units. The geometrical, age and field relationships are interpreted as indicative of a syn-tectonic emplacement of the second lithologic association of the Pukaskwa batholith (Beakhouse et al., 2011). Following the emplacement of the syn-tectonic phases, the Pukaskwa batholith was uplifted as a regional dome structure relative to flanking greenstone belts at approximately 2.680 Ga and synchronous with ongoing regional sinistral transpressive deformation (Beakhouse et al., 2011; Lin and Beakhouse, 2013).

The youngest lithologic association comprises a group of granodioritic to granitic units that form large, homogeneous plutons and small dykes. The geochemical signature of the rocks suggests that they are derived from melting of older intermediate to felsic crust (Beakhouse et al., 2011). The rocks are dated at ca. 2.667 Ga and, therefore, are interpreted as late to post-tectonic (Davis and Lin, 2003; Beakhouse et al., 2011).

### **2.2.3 Anahareo Pluton**

The Anahareo pluton (informal name adopted in this report) is a large felsic intrusion of which approximately 690 km<sup>2</sup> is located within the southern and southeastern parts of the White River area (Figure 1.1). The pluton extends west of the study area and has maximum dimensions (including areas beyond the study area) of over 51 kilometres north-south and 71 kilometres east-west. The intrusion was mapped by Siragusa (1977, 1978) as being dominantly granodiorite and quartz monzonite (i.e., monzogranite in modern terminology). Distal from the contact with the Kabinakagami greenstone belt, these rock types are relatively uniform and appear to represent multi-phase intrusions. Migmatites of trondhjemitic composition, the least dominant granitic rock within the intrusion, are present along the pluton's boundaries and as syntectonic intrusive sheets that locally exhibit a variably developed cataclastic fabric (Siragusa, 1978).

Quartz monzonite is the youngest recognized phase of the Anahareo pluton and commonly intrudes the granodioritic and trondhjemitic rocks in the form of large, coarse-grained pegmatitic dykes, sills and discordant bodies of variable size (Siragusa, 1977; 1978). This phase of the pluton is described

as massive, which prompted Siragusa (1978) to suggest that these young intrusive phases post-date the major period of tectonism in the White River area. However, no geochronological information is currently available to test this interpretation and the age of the pluton is unknown.

No detailed information is available regarding the thickness of the Anahareo pluton.

#### **2.2.4 Black-Pic Batholith**

The Black-Pic batholith is a regionally-extensive intrusion that encompasses roughly 3,000 km<sup>2</sup> within the Wawa Subprovince and underlies only a very small portion along the northern boundary of the White River area (Figure 1.1). It is bounded to the south by the Strickland Pluton, the Pukaskwa batholith, and the Danny Lake stock, and to the east by the Dayohessarah greenstone belt.

The Black-Pic batholith comprises a multi-phase suite that includes hornblende-biotite, monzodiorite, foliated tonalite, and pegmatitic granite with subordinate foliated diorite, granodiorite, granites, and crosscutting aplitic to pegmatitic dykes (Williams and Breaks, 1989; Zaleski and Peterson, 1993). In the White River area, the batholith is described as a gneissic tonalite in a compilation map of Santaguida (2001); however, Fenwick (1967), similarly to Milne (1968), mapped the batholith as uniform, biotite granitic gneiss and biotite granite that becomes gneissic near the boundary with the Dayohessarah greenstone belt (noting that the terminology used was before Streckeisen's (1976) standard classification). Fenwick (1967) also noted the occurrence of migmatites (noting that terminology used was prior to either Mehnert's (1968) or Sawyer's (2008) classifications) composed of highly altered remnants of pre-existing volcanic and sedimentary rocks mixed with variable amounts of granitic material. The migmatites occur as either a breccia type, in which fragments of the older rocks are cemented by dykes; and veins of granitic rock or a banded type, in which layers of the older material alternate with layers of granitic material.

Several generations of intrusions are present within the Black-Pic batholith, yielding geochronological ages ranging from ca. 2.720 Ga (Jackson 1998) for the earliest recognized rock unit to ca. 2.689 Ga for a late-stage monzodioritic unit (Zaleski et al., 1999). In addition, there are also younger granitic phases within the Black-Pic batholith which, despite a lack of geochronological information, are thought to be part of the regional suite of ca. 2.660 Ga, post-tectonic "Algonian granites" (Zaleski et al., 1999). Within the batholith, intrusive relationships are typically destroyed and only metamorphic textures and associated mineral assemblages are preserved. Inclusions of relatively melanocratic members of the suite occur as foliated inclusions within later, leucocratic members (Williams and Breaks, 1989, 1996).

The foliation pattern recognized within the Black-Pic batholith was interpreted to define regional scale domal structures characterized by broad antiforms and tight synforms (Williams and Breaks, 1989; Lin and Beakhouse, 2013). At least one such smaller-scale structure potentially exists to the west of White River Phase 2 assessment area, immediately north of the Danny Lake stock where semi-circular faults outline the position of a possible dome several kilometres in width.

Structurally deeper levels of the tonalite suite in the Black-Pic batholith are strongly foliated with a subhorizontal planar fabric that exhibits a poorly developed, north-trending rodding and mineral-elongation lineation (Williams and Breaks, 1989). Upper structural levels of the tonalite suite are cut by abundant granitic sheets of pegmatite and aplite, and are more massive (Williams and Breaks, 1989; Zaleski and Peterson, 1993). Just to the north of the White River area are zones of migmatized volcanic rocks, and zones of massive granodiorite to granite embodied in the Black-Pic batholith. The contact between these rocks and the tonalitic rocks of the Black-Pic batholith is gradational with

extensive sheeting of the tonalitic unit (Williams and Breaks, 1989; Williams et al., 1991).

No readily available information regarding the thickness of the batholith is available, however, its size and the geological history of the region suggest it may extend to a significant depth.

### **2.2.5 Foliated Tonalite Suite**

On the southeast side of Kabinakagami Lake, Santaguida (2001) outlined two packages of foliated tonalite suite rock, bisected by greenstone, that occur between the Kabinakagami greenstone belt and the Anahareo pluton (Figure 1.1). The tonalite packages extend over a distance of 29 kilometres north-south and 25 kilometres east-west, but only a small amount occurs within the White River area. This suite of rocks is similar to the Anahareo pluton mapped by Siragusa (1977; 1978). Siragusa (1977) described outcrops of the foliated tonalite suite within the White River area as consisting of biotite trondhjemite, trondhjemite, granodiorite, and biotite granodiorite. Biotite trondhjemite is the dominant granitic rock in contact zones between the granitic and supracrustal rocks of the Kabinakagami greenstone belt and also occurs as syntectonic intrusive sheets concordant to the foliations observed in the metavolcanic rocks. The biotite trondhjemite appears as strongly gneissic, grey to brownish grey, medium-grained rock and is locally porphyritic owing to the presence of eye-shaped quartz and feldspar porphyroblasts (Siragusa, 1977).

No absolute age is available for this foliated tonalite suite, although, it may be of the same age as other lithologically similar intrusions in the region. No information is available regarding the thickness of the suite.

### **2.2.6 Mafic Dykes**

Several generations of Paleoproterozoic and Mesoproterozoic diabase dyke swarms crosscut the White River area (Figure 1.1), including:

- Northwest-trending Matachewan Suite dykes (ca. 2.473 Ga; Buchan and Ernst, 2004). This dyke swarm is one of the largest in the Canadian Shield and most predominant of all dyke swarms recognized in the White River area. Individual dykes are generally up to 10 m wide, and have vertical to subvertical dips. The Matachewan dykes comprise mainly quartz diabase dominated by plagioclase, augite and quartz (Osmani, 1991).
- Northeast-trending Biscotasing Suite dykes (ca. 2.167 Ga; Hamilton et al., 2002). These dykes are not considered to be numerous in the White River area.
- North-trending Marathon Suite dykes (ca. 2.121 Ga; Buchan et al., 1996; Hamilton et al., 2002). These form a fan-shaped distribution pattern around the northern, eastern, and western flanks of Lake Superior, and are fairly minor in the White River area. The dykes vary in orientation from northwest to northeast, and occur as steep to subvertical sheets, typically a few m to tens of m thick, but occasionally up to 75 m thick (Hamilton et al., 2002). The Marathon dykes comprise quartz diabase (Osmani, 1991) dominated by equigranular to subophitic clinopyroxene and plagioclase.
- West-northwest-trending Sudbury Suite dykes (ca. 1.238 Ga; Krogh et al., 1987). These dykes are not considered to be numerous in the White River area.

The four dyke swarms in the White River area are generally distinguishable by their unique strike directions, crosscutting relationships and, to a lesser extent, by magnetic amplitude.

## **2.3 Structural History**

Information on the structural history of the White River area is based predominantly on insights derived from structural investigations of the White River and Dayohessarah greenstone belts (Polat, 1998; Zaleski et al., 1994; Peterson and Zaleski, 1999), and the Hemlo gold deposit and surrounding region (Muir, 2003). Additional studies by Lin (2001), Percival et al. (2006), and Williams and Breaks (1996) have also contributed to the structural understanding of the area. The aforementioned studies were performed at various scales and from various perspectives. Consequently, the following summary of the structural history of the White River area should be considered as a best-fit model that incorporates relevant findings from all studies. The structural history of the White River area is described below and summarized in Table 2.1.

On the basis of overprinting relationships between different structures, Polat et al. (1998) suggested that the Schreiber-Hemlo greenstone belt underwent at least two main episodes of deformation. These deformation events can be correlated with observations from Peterson and Zaleski (1999) and Muir (2003), who reported at least five and six generations of structural elements, respectively. Two of these generations of structures account for most of the ductile strain, and although others can be distinguished on the basis of crosscutting relationships, they are likely the products of progressive strain events.

*Table 1.1: Geological and Structural History of the White River Area (adapted from AECOM, 2014a)*

Approximate Time Period (years before present)	Geological Event
2.89 to 2.77Ga	Progressive growth and early evolution of the Wawa-Abitibi terrane by collision, and ultimately accretion, of distinct geologic terranes
2.770 – 2.673 Ga	<ul style="list-style-type: none"> <li>- ca. 2.720 Ga: Onset of volcanism and subordinate sedimentation associated with the formation of the Dayohessarah and Kabinakagami greenstone belts</li> <li>- ca. 2.720 Ga: Emplacement of oldest recognized phase of Black-Pic batholith</li> <li>- ca. 2720-2.703 Ga: Emplacement of oldest lithologic association of Pukaskwa batholith</li> <li>- ca. 2703-2.686 Ga: Emplacement of second lithologic association of Pukaskwa batholith</li> <li>- ca. 2.697 Ga: Intrusion Dotted Lake pluton, and possibly of Strickland pluton</li> <li>- ca. 2.689 Ga: Emplacement of younger recognized phase of Black-Pic batholith</li> <li>- ca. 2.677 Ga: Emplacement of Bremner pluton</li> <li>- ca. 2.719 to 2.673 Ga: Four periods of ductile-brittle deformation (D<sub>1</sub>-D<sub>4</sub>): <ul style="list-style-type: none"> <li>D<sub>1</sub>: ca. 2.719 – 2.691 Ga</li> <li>D<sub>2</sub>: ca. 2.691 – 2.683 Ga → Main phase of coalescence of the Wawa and Quetico subprovinces (Corfu and Stott, 1996)</li> <li>D<sub>3</sub>: ca. 2.682 – 2.679 Ga → Sinistral transpressive deformation, structural domal uplift of Pukaskwa batholith</li> <li>D<sub>4</sub>: ca. 2.679 – 2.673 Ga</li> </ul> </li> <li>- ca.2.688 to 2.675: Regional metamorphism</li> </ul>
2.675 and 2.669 Ga	Peak metamorphism of regional greenstone belts
2.667 Ga	Youngest lithologic association of Pukaskwa batholith
2.5 to 2.1 Ga	<ul style="list-style-type: none"> <li>- ca. 2.5 Ga: Supercontinent fragmentation and rifting in Lake Superior area, development of Southern Province</li> <li>- ca. 2.473 Ga: Emplacement of the Matachewan dyke swarm</li> <li>- ca. 2.167 Ga: Emplacement of Biscotasing dyke swarm</li> <li>- ca. 2.121 Ga: Emplacement of the Marathon dyke swarm</li> </ul>
1.9 to 1.7 Ga	Penokean Orogeny in Lake Superior and Lake Huron areas; possible deposition and subsequent erosion in the White River area
1.238 Ga	- ca. 1.238 Ga emplacement of the Sudbury dyke swarm
1.150 to 1.090 Ga	<ul style="list-style-type: none"> <li>Rifting and formation of the Midcontinent Rift</li> <li>- ca. 1.14 Ga: Emplacement of the Abitibi dyke swarm</li> </ul>
540 to 355 Ma	Possible coverage of the area by marine seas and deposition of carbonate and clastic rocks subsequently removed by erosion
145 to 66 Ma	Possible deposition of marine and terrestrial sediments of Cretaceous age, subsequently removed by erosion
2.6 to 0.01 Ma	Periods of glaciation and deposition of glacial sediments

Integration of the structural histories detailed in Williams and Breaks (1996), Polat et al. (1998), Peterson and Zaleski (1999), Lin (2001), and Muir (2003) suggest that six deformation events occurred within the White River area. The first four deformation events (D<sub>1</sub>-D<sub>4</sub>) are associated with brittle-ductile deformation identified within the greenstone belts. D<sub>5</sub> and D<sub>6</sub> were associated with a combination of brittle deformation and fault propagation through all rock units in the White River area. The main characteristics of each deformation event are summarized below.

The earliest recognizable deformation phase (D<sub>1</sub>) is associated with rarely preserved small-scale isoclinal (F<sub>1</sub>) folds, ductile shear zones that truncate, and a general lack of penetrative foliation development. Peterson and Zaleski (1999) reported that an S<sub>1</sub> foliation is only preserved locally in

outcrop and in thin section. D<sub>1</sub> deformation is poorly constrained to between ca. 2.719 and ca. 2.691 Ga (Muir, 2003).

D<sub>2</sub> structural elements include prevalent open to isoclinal F<sub>2</sub> folds, an axial planar S<sub>2</sub> foliation, and L<sub>2</sub> mineral elongation lineations (Peterson and Zaleski, 1999). Muir (2003) interpreted D<sub>2</sub> to have resulted from progressive north-northeast to northeast directed compression that was coincident with the intrusion of various plutons. The S<sub>2</sub> foliation is the dominant meso- to macro-scale fabric evident regionally. Ductile flow of volcano-sedimentary rocks between more competent batholiths may also have occurred during D<sub>2</sub> deformation. This generation of deformation is constrained to between ca. 2.691 and ca. 2.683 Ga (Muir, 2003).

D<sub>3</sub> deformation was the result of northwest-southeast shortening during regional dextral transpression. D<sub>3</sub> structural elements include macroscale F<sub>3</sub> folds, including the regional scale isoclinal fold developed within the Manitouwadge greenstone belt, and local shear fabrics that exhibit a dextral sense of motion and overprint D<sub>2</sub> structures (Peterson and Zaleski, 1999; Muir, 2003). D<sub>3</sub> deformation did not develop an extensive penetrative axial planar and (or) crenulation cleavage. D<sub>3</sub> deformation is constrained to between ca. 2.682 and ca. 2.679 Ga (Muir, 2003).

D<sub>4</sub> structural elements include isolated northeast-plunging F<sub>4</sub> kink folds with a Z-asymmetry, and associated small-scale fractures and faults overprinting D<sub>3</sub> structures. D<sub>3</sub>-D<sub>4</sub> interference relationships are best developed in the Manitouwadge greenstone belt and in rocks of the Quetico Subprovince. D<sub>4</sub> deformation is roughly constrained to between ca. 2.679 and ca. 2.673 Ga (Muir, 2003).

Details of structural features associated with the D<sub>5</sub> and D<sub>6</sub> deformation events are limited in the literature to brittle and brittle-ductile faults of various scales and orientations (Lin, 2001; Muir, 2003). Within the Hemlo greenstone belt, Muir (2003) suggested that local D<sub>5</sub> and D<sub>6</sub> faults offset the Marathon and Biscotasing dyke swarms (all ca. 2.2 Ga), and as such, suggested that in the Hemlo region D<sub>5</sub> and D<sub>6</sub> faults propagated after ca. 2.2 Ga. However, since there are no absolute age constraints on specific events, the entire D<sub>5</sub>-D<sub>6</sub> interval of brittle deformation can only be constrained to a post-2.673 Ga timeframe that may include many periods of post-Archean tectonic re-activation.

### **2.3.1 Mapped Structures**

In the White River area five unnamed faults are indicated on public domain geological maps (Fenwick, 1966; Siragusa, 1977, 1978; Stott, 1995a, b, c; Santaguida, 2001; OGS, 2011; Figure 1.1). The longest unnamed fault parallels the axis of Esnagi Lake in the southeast corner of the area (Siragusa, 1978). A northeast-trending mapped fault is located crossing the western margin of the White River area and is mapped as juxtaposing the Pukaskwa batholith against the Strickland pluton. A northwest-trending mapped brittle fault is located at the southern extent of Nameigos Lake that is shown offsetting the Kabinakagami Lake greenstone belt with a dextral strike-separation. A northwest-trending mapped fault is located within the Anahareo pluton, southwest of Anahareo Lake. A mapped west-northwest trending fault is located at the northern extent of Nameigos Lake that is shown as truncating the Pukaskwa batholith against the Strickland pluton and the Kabinakagami Lake greenstone belt.

In the Kabinakagami Lake greenstone belt, Siragusa (1977) reported that it is likely that a northeast-trending strike-slip fault with horizontal displacement of 240 m is present in a narrow valley, to the north of the inlet of the Kabinakagami River.

Fenwick (1967) and Siragusa (1977) noted that lineaments parallel the trend of two sets of diabase dykes, which strike either northeast or northwest, and assumed that the lineaments formed from the weathering of diabase dykes or from vertical joints.

## **2.4 Metamorphism**

Studies on metamorphism in Precambrian rocks across the Canadian Shield have been summarized in a few publications since the 1970s (e.g., Fraser and Heywood, 1978; Kraus and Menard, 1997; Menard and Gordon, 1997; Berman et al., 2000; Easton, 2000a; 2000b; and Berman et al., 2005) and the thermochronological record for large parts of the Canadian Shield is documented in a number of studies (Berman et al., 2005; Bleeker and Hall, 2007; Corrigan et al., 2007; and Pease et al., 2008).

The Superior Province of the Canadian Shield largely preserves low-pressure–high-temperature Neoarchean (ca. 2.710–2.640 Ga) metamorphic rocks. The relative timing and grade of regional metamorphism in the Superior Province corresponds to the lithological composition of the subprovinces (Easton, 2000a; Percival et al., 2006). Subprovinces comprising volcano-sedimentary assemblages and synvolcanic to syntectonic plutons (i.e., granite-greenstone terranes) are affected by relatively early lower greenschist to amphibolite facies metamorphism. Subprovinces comprising both metasedimentary- and migmatite-dominated lithologies, such as English River and Quetico, and dominantly plutonic and orthogneissic domains, such as Winnipeg River, are affected by relatively late middle amphibolite to granulite facies metamorphism (Breaks and Bond, 1993; Corfu et al., 1995). Subgreenschist facies metamorphism in the Superior Province is restricted to limited areas, notably within the central Abitibi greenstone belt (e.g., Jolly, 1978; Powell et al., 1993).

In general, most of the Canadian Shield preserves a complex episodic history of Neoarchean metamorphism overprinted by Paleoproterozoic tectonothermal events culminating at the end of the Grenville orogeny ca. 950 Ma. The distribution of contrasting metamorphic domains in the Canadian Shield is a consequence of relative uplift, block rotation, and erosion resulting from Neoarchean orogenesis, subsequent local Proterozoic orogenic events and broader epeirogeny during later Proterozoic and Phanerozoic eons.

All Precambrian rocks of the White River area display some degree of metamorphism. The Dayohessarah greenstone belt is typically characterized by amphibolite facies metamorphism (Stott, 1999). This amphibolite facies metamorphic grade may be a manifestation of an amphibolite grade contact metamorphic aureole bordering the Strickland pluton (Stott, 1999). Little information regarding the metamorphic grade of the exposed rocks of the Kabinakagami greenstone belt is available in the reviewed literature. Based on ages obtained from metamorphic monazites, Zaleski et al. (1995; 1999) suggested that near-peak metamorphism of the White River-Hornepayne greenstone belt occurred between 2.675 and 2.669 Ga. It can be inferred that the Dayohessarah and Kabinakagami belts may have been subjected to metamorphism during this period, as the age constraints given by Zaleski et al. (1994; 1999) correspond well with the  $2.675 \pm 1$  and  $2.661 \pm 1$  Ga periods of regional metamorphism recognized by Schandl et al. (1991).

Typical metamorphic grades in plutonic rocks within the White River area are variable from non-metamorphosed to amphibolite grade in metamorphic contact aureoles. No evidence to date suggests that rocks in the White River area were affected by thermal overprints related to post-Archean events.



## 2.5 Quaternary Geology

Quaternary geology of the White River area is described in detail in the remote sensing and terrain evaluation completed as part of the Phase 1 Desktop Preliminary Assessment (AECOM, 2014b). An overview of the relevant Quaternary features is summarized below.

The Quaternary sediments, commonly referred to as drift, soil, or overburden, in the White River area comprise glacial and post-glacial materials that overlie the bedrock. All glacial landforms and related materials are associated with the Wisconsinan glaciation, which began approximately 115,000 years ago (Barnett, 1992). Geddes et al. (1985) and Geddes and Kristjansson (1986) reported that glacial striae in the White River area reveal an early north to south ice movement that was followed by a strong, regional flow oriented approximately 220 degrees (°). Bedrock erosional features indicate that ice flow, likely in the waning stage of glacial cover, was influenced by local topographic conditions as demonstrated by striae measurements ranging from 180° to 245°.

Till thickness is variable and while depths of several m are present locally, thicknesses are typically less than 3 m (A. Bajc, pers. comm., 2013). Gartner and McQuay (1980a, 1980b) reported that the till is seldom more than 1 metre thick on the crests of the hills, but can thicken to 5 m or more on the flanks and in the valleys between the bedrock hills. For large parts of the White River area drift thickness over bedrock is limited and the ground surface reflects the bedrock topography (Geddes and Kristjansson, 1986). Over the majority of the area bedrock outcrops are common and the terrain is classified, for surficial purposes, as a bedrock-drift complex, i.e., thin drift cover that only locally achieves thicknesses that mask or subdue the bedrock topography. Valleys and lowland areas typically have extensive and thicker surficial deposits that frequently have a linear outline.

Glaciofluvial outwash deposits in the White River area occur as northeast trending areas of limited relief along the esker-kame complexes and within the larger modern drainage systems, such as the Gum, Kwinkwaga, Shabotik, and White rivers to the west of the study area. Smaller deposits, occupying topographic lows and bedrock valleys, are scattered across the area. The thickness of the outwash deposits are likely to be variable, but may be substantial where they are proximal to ice-contact stratified drift (ICSD) features. Deposits are generally well-sorted and consist predominantly of stratified sand with a low clast content; however, locally they are coarser-grained and gravel-rich (Geddes and Kristjansson, 1986).

Glaciolacustrine sediments in the area consist of fine sand, silt, and minor clay deposited in shallow lakes within bedrock controlled basins. The largest of these deposits is located proximal to Nameigos Lake (Gartner and McQuay, 1980a, 1980b). Other small deposits, typically occur towards the northeast of the area (Geddes and Kristjansson, 2009).

Bogs and organic-rich alluvial deposits, consisting of sand, silt and organic debris, are present along several of the water courses in the White River area. These deposits tend to be relatively narrow (<200 m), although their width can increase notably proximal to lakes. Larger expanses of organic terrain, some of several square kilometres in size, are present in the northeast and northwestern parts of the White River area near Nameigos and Gourlay lakes, respectively. These deposits may be developed on finer-grained glaciolacustrine deposits and/or outwash that occupy lowland areas. Smaller occurrences of organic terrain exist in bedrock-controlled basins throughout the White River area.

### 3 Data Source Acquisition and Quality

Sander Geophysics Limited (SGL) completed a fixed-wing high-resolution airborne magnetic and gravity survey in the White River area between July 31 and October 6, 2015. The survey area comprised one block 25 km east of the Township of White River. The survey block was designed to cover two potentially suitable areas in the Anahareo and Strickland plutons identified in the Phase 1 preliminary assessment (AECOM, 2014a) and capture relevant geological features.

The survey included a total of 14,383 km flight lines covering a surface area over 1,100 km<sup>2</sup>. Flight operations were conducted out of the Manitouwadge Municipal Airport, in Manitouwadge, Ontario using a Cessna 208B Grand Caravan. Data were acquired along traverse lines flown in a north-south direction spaced at 100 m, and control lines flown east-west spaced at 500 m. The survey was flown at an approximate altitude of 80 m above ground level, with an average ground speed of 100 knots (approximately 185 km/h or 50 m/s). Airborne magnetic and gravity data were acquired using equipment with very high sensitivity and accuracy. The airborne magnetic data was recorded using a magnetometer sensor mounted in a fibreglass stinger extending from the tail of the aircraft. The airborne gravity data was recorded using a gravimeter, which includes three orthogonal accelerometers that are mounted on a stabilized platform inside the cabin of the aircraft. Table 3.1 gives a quick reference of the details of the survey.

*Table 3.1: Survey Details*

Survey Particulars	
Survey Start Date:	July 31, 2015
Survey End Date:	October 6, 2015
Field Office Location:	Manitouwadge
Airport Used:	Manitouwadge Municipal Airport (CYMG)
Aircraft Type:	Cessna 208B Grand Caravan
Total line kilometers:	14,383
Traverse Line numbers:	6390 - 6653
Traverse Line direction:	North – South
Traverse Line spacing:	100 m
Control Line numbers:	629 – 732, 801 – 805
Control Line direction:	East – West
Control Line spacing:	500 m
Survey Altitude:	Smoothed drape with target height of 80 m above ground
Digital Terrain Source:	SRTM
Number of Flights (numbers):	23 (2008, 2012, 2014, 2016, 2024, 2027 – 2029, 2031 – 2038, 2040 – 2042, 2044, 2045, 2058, 2063)
Aircraft Target Ground Speed:	100 knots
Magnetic Field Reference location	(NAD83 UTM 16N): 545,105 m E, 5,427,638 m N
Magnetic Field Inclination (+ve down):	74.3388°
Magnetic Field Declination (+ve east):	-6.9914°
Approximate total field value:	56,669.4 nT
Magnetic Reference Field Model:	World Magnetic Model (2015) interpolated to date and location of acquisition

Fundamental Gravity Network Ties:	Referenced to the local gravity value established by Sander Geophysics at the Ottawa Airport
Survey Base Gravity Value:	980854.00 mGal
Survey Base Parking Location (NAD83):	583,674.60 m E 5,437,649.6 m N Height: 331.306 m (above WGS-84 ellipsoid)
Base Station Locations (NAD83):	REF1: 587,100.5 m E, 5,442,586.9 m N Height: 290.93 m (above WGS-84 ellipsoid) REF2: 587,097.4 m E, 5,442,600.3 m N Height: 292.54 m (above WGS-84 ellipsoid) REF3: 584,501.4 m E, 5,441,099.0 m N Height: 307.26 m (above WGS-84 ellipsoid)
Field Acquisition Datum:	WGS-84
UTM Projection:	UTM 16N

### 3.1 Magnetic Data

Total magnetic field measurements were recorded with a single cesium magnetometer mounted in a fibreglass stinger extending from the tail of the survey aircraft. SGL's hardware and software system, AIRComp, was used to remove the effects of the aircraft and its manoeuvres from the recorded magnetic data. Coefficients to be used for compensation were derived by processing the calibration flight data, based on principles presented by Leliak (1961). The compensation coefficients were applied to data recorded during normal survey operations to produce compensated magnetic data.

Low-pass filtered reference station diurnal was subtracted from the airborne data on a reading by reading basis. As more than one reference station was used, the reference station value could be interpolated, based on the relative distance of the reading from each reference station.

Both the ground and airborne systems used the Geometrics G-822A cesium magnetic sensor. Total magnetic field measurements were recorded at 160 Hz in the aircraft, and then later down sampled to 10 Hz in the processing. A second order Butterworth 0.9 Hz low pass filter is utilised in the process for compensation and anti-aliasing. The ground systems recorded magnetic data at 11 Hz.

A pre-planned drape surface was prepared for the survey to guide the aircraft over the topography in a consistent manner, as close to the minimum clearance as possible. The drape surface was prepared with digital elevation model (DEM) data obtained from the Shuttle Radar Topography Mission (SRTM) (<http://srtm.usgs.gov/>) for the area. The DEM included an extension beyond the survey boundary to allow the aircraft to achieve the drape clearance before coming on line.

Details of the processing of the magnetic data are provided in Section 4.2 of this report.

### 3.2 Gravity Data

Gravity data were acquired with SGL's propriety AIRGrav (*Airborne Inertially Referenced Gravimeter*) system, which uses a Schuler tuned inertial platform supporting three orthogonal accelerometers, which remain fixed in inertial space, independent of the manoeuvres of the aircraft, allowing precise isolation from the effects of the movement of the aircraft. The gravity sensor used in AIRGrav is a very accurate accelerometer with a wide dynamic range. The system is not affected by the strong vertical motions of the aircraft, allowing the final gravity data to be almost completely unaffected by in-flight

conditions classified as “moderate turbulence” or better. The instrument is also considered to be an inertial navigator and as such, the platform levelling was essentially unaffected by horizontal accelerations.

In typical survey flying, accelerations in an aircraft can reach 0.1 G, equivalent to 100,000 milligal. Data processing must extract gravity data from this very noisy environment. This was achieved by modelling the gravity due to movements of the aircraft in flight as measured by extremely accurate Global Positioning System (GPS) measurement. These measurements are affected by noisy conditions in the ionosphere, and by the variable conditions (e.g. temperature, pressure and humidity) within the troposphere. SGL has developed a full suite of programs to carry out all the necessary corrections.

The GPS data are extracted from the airborne and reference station acquisition system and reformatted. Differential corrections to correct the airborne ranges for variations calculated from the base station GPS data were performed. Each recorded position was recalculated based on these ranges. The original reference system for all GPS data was the WGS-84 datum. Positions were then converted to the local datum, reference system and desired projection. Each line was then checked for data continuity and quality.

An extremely accurate location of the base station GPS receiver is determined using an IGS permanent GPS Reference Station to apply differential corrections (<http://igs.org/network>). This technique provides a final base station receiver location with an accuracy of better than a few decimetres. The entire airborne data set is then reprocessed differentially using the recalculated base station location.

Gravity data were recorded at 128 Hz. Accelerations were filtered and resampled to 10 Hz to match the GPS, using specially designed filters to avoid biasing the data. Gravity was calculated by subtracting the GPS derived accelerations from the inertial accelerations. The calculated gravity was corrected for the Eötvös effect and latitude corrected (i.e. normal gravity), and the sample interval was then reduced to 2 Hz. These operations were all performed by SGL's proprietary GravGPS software. A detailed description of gravity processing is provided in Section 4.1 of this report.

### **3.3 Digital Elevation Data**

Digital elevation data were collected during the survey using a laser altimeter (Riegl LD90-31K-HiP) mounted to the base of the aircraft. The elevation data were sampled at a rate of 3.3 Hz, which is consistent with a sample roughly every 16 m along the profile line. Even though the laser altimeter can record returns from more than 700 m above the ground with a high degree of certainty, some laser data dropouts occurred while flying over the areas of poor reflectivity. The laser data shows the effects of the dense tree cover; variable penetration of the canopy results in a high-frequency variation of recorded altitude. The raw laser data were processed with an iterative de-spiking routine designed to remove many of the early laser returns from trees.

Digital elevation data were also collected using a King radar altimeter mounted to the base of the aircraft. Elevation data were sampled at a rate of 10 Hz, which is consistent with a sample roughly every 6m. The radar data penetrates the canopy less as it records the first return within the footprint of its signal. The radar altimeter data were filtered to remove high-frequency noise using a 67-point low pass filter.

A digital elevation model (DEM) was derived by subtracting the laser altimeter data from the

differentially corrected DGPS altitude with respect to the Canadian Geodetic Vertical Datum 2013 (CGVD2013). Short sections of poor laser data due to locally weak reflectivity were replaced using King radar data. The DEM reflects the presence of vegetation (for example trees) and buildings and thus is not considered to be a digital terrain model (DTM).

The digital elevation data were gridded to form a DEM grid using a cell size of 25 m over the White River survey area. The 25 m gridding cell was applied to present the highest resolution of the digital elevation model within the boundaries of the survey block comprising the principal survey area (Figure 3.1).

### **3.4 Additional Data Sources**

In addition to the acquired data, a number of other publically available data sources were used. These are detailed below.

#### **3.4.1 OGS Mapped Bedrock Geology**

The Precambrian Geoscience Section of the Ontario Geological Survey has compiled a 1:250,000 scale map of the bedrock geology of Ontario (OGS, 2011). This compilation was recently revised and issued as 'Miscellaneous Release – Data 126 – Revision 1'. The data is publically available as a seamless GIS data set and includes such details as bedrock units, major faults, dyke swarms, iron formations and kimberlites. The Ontario Geological Survey bedrock geology map has been further updated based on information from the Precambrian geology compilation map series (M2666; Santaguida, 2001). This resource was of fundamental importance in assisting with the geophysical interpretation of the acquired potential field data. The mapped bedrock geology was used for both qualitative and quantitative aspects of the interpretation. In the case of the qualitative interpretation, the mapped bedrock geology gave the overall context for the magnetic and gravity data. For the 2.5D modelling, the mapped bedrock geology provided initial surface constraints.

#### **3.4.2 Geological Base Maps**

Several additional geological maps are available (M2129, M2355, M2382, P3309, P3310 and P3311) in and around the White River survey area (Fenwick, 1967; Siragusa, 1977; 1978; Stott et al 1995a; 1995b; 1995c). These bedrock geologic maps were georeferenced and incorporated into the project geodatabase where applicable. Structural measurements including foliations and bedding planes, folds and faults provided structural constraints and were incorporated into the qualitative and quantitative interpretations.

#### **3.4.3 OGS PETROCH Lithogeochemical Database**

The Ontario Geological Survey has a publicly available PETROCH Lithogeochemical Database (Haus and Pauk, 2010). The database contains detailed rock chemical data collected by OGS geoscientists, which includes information about rock type, chemical composition, age, stratigraphy, major oxide values, sample location and specific gravity. Sixty data points are located within the survey area, including samples taken from the Anahareo and Strickland plutons, and the Kabinakagami Lake greenstone belt. No samples were available within the Dayohessarah greenstone belt. This information was used in the interpretation to: 1) obtain further information on the composition of major mapped rock units where samples have been taken; and 2) constrain the density of rock units used in the 2.5D modelling.

#### **3.4.4 Densities and Magnetic Susceptibilities**

Bedrock densities and magnetic susceptibilities in the White River survey area were gathered from a database maintained by the Geological Survey of Canada (GSC, 2015). The database includes classification of rock type, and measured densities and magnetic susceptibilities. Only one data point occurs within the survey area, however 9 additional samples occur directly adjacent to the survey area within the Strickland and Anahareo plutons, Black-Pic batholith, and Dayohessarah greenstone belt. No samples were available within the Kabinakagami Lake greenstone belt. No magnetic susceptibility values were given for any of these rock units and only the density information was used in the modelling.

#### **3.4.5 Ontario Precambrian Bedrock Magnetic Susceptibility Geodatabase**

The Ontario Geological Survey has a publicly available Ontario Precambrian Bedrock Magnetic Susceptibility Geodatabase for 2001 to 2012 (Muir, 2013), which is known as Miscellaneous Release – Data 273 (MRD 273-Rev). This GIS database contains measurements of magnetic susceptibilities and rock classifications for points across Ontario. No data points occur directly within the White River area, but 61 samples are located approximately 75 km to the northwest, in the Manitouwadge Area.

#### **3.4.6 Other Magnetic Susceptibility Measurements**

Additional magnetic susceptibility data was obtained from Miles (1998) for several lithologies in the region of the Manitouwadge greenstone belt, approximately 75 km northwest of the White River area. Statistics (minimum, maximum, mean, standard deviation) were presented. The lithologies and unit numbers/name were simplified from Zaleski and Peterson (1995).

## 4 Geophysical Data Processing Methods

### 4.1 Gravity Data Processing

Advanced gravity processing allows for the generation of high-resolution gravity data. These processes involve the use of GPS phase angle corrections, the integration of GPS processing with inertial data from the gravimeter and the advanced analysis of system states and uncertainties. This processing helps reduce system noise and allows for the generation of high quality, low noise raw gravity data through a wider range of survey conditions than was previously possible. The following standard corrections were applied to the gravity data (Telford et al 1990; Blakely, 1996):

- a. Eötvös correction,

$$\delta g_{Eötvös} = -2 W_s v_x \cos \Phi - \frac{v_x^2}{\frac{r}{(1 - e^2 \sin^2 \Phi)^{1/2}} + h} - \frac{v_y^2}{\frac{r(1 - e_2)}{(1 - e^2 \sin^2 \Phi)^{3/2}} + h}$$

where  $\Phi$  is the latitude of the aircraft,  $v_x$  and  $v_y$  are the velocities of the aircraft in the  $x$  (east) and  $y$  (north) direction,  $r$  is the Earth's radius at the equator (6,378,137 m),  $e$  is a correction for Earth's flattening towards the poles (0.0818191908426),  $W_s$  is the angular velocity of Earth's rotation ( $7.2921158553 \times 10^{-5}$  rad/s), and  $h$  is the altitude of the plane above the ellipsoid;

- b. Normal gravity,

$$g_{Normal} = \frac{9.7803267715 (1 + 0.0019318513353 \sin^2 \Phi)}{\sqrt{1 - 0.0066943800229 \sin^2 \Phi}}$$

where  $\Phi$  is the latitude of the aircraft;

- c. Free air correction,

$$g_{fa} = - (0.3087691 - 0.0004398 \sin^2 \Phi) h + 7.2125 \times 10^{-8} h^2$$

where  $h$  is the height of the aircraft in metres above the ellipsoid;

- d. Full 3D Bouguer correction,  $g_b$ . See below for a description of the Bouguer correction technique;  
e. Static correction,  $g_{sc}$ , based on static ground recordings and repeat lines;  
f. Level correction,  $g_{lc}$ , based on line intersections.

Thus, the Bouguer anomaly in mGal is determined:

$$BouguerAnomaly = G - g_{fa} - g_b - g_{sc} - g_{lc}$$

where  $G$  is the calculated gravity in mGal adjusted for Eötvös effect and normal gravity.

#### **4.1.1 Bouguer Correction**

Shuttle Radar Topography Mission (SRTM) digital elevation model data were used to calculate the Bouguer corrections for gravity processing. The SRTM data contains information in a grid with a 3 arcsecond spacing, approximately equal to 100 m cell spacing, which has a higher density than the line spacing for this survey, and therefore provides terrain data at a better resolution between the survey lines than the SRTM data. Coverage up to 160 km from the survey block was kept for accurate regional corrections.

Terrain corrections were computed using software developed by SGL. The algorithm calculates the topographic attraction of the terrain using a mass prism model with a constant density. The difference between the topographic attraction and the simple Bouguer correction is the terrain correction. The terrain and Bouguer corrections were calculated for the bedrock at the height of the aircraft using a density of 2.67 g/cm<sup>3</sup>.

Terrain corrections were filtered to match the degree of filtering applied to the gravity data as described below.

#### **4.1.2 Static and Level Corrections**

The gravimetric data were levelled to compensate for instrument variations in two steps. A single constant shift determined from ground static recordings was applied on a flight-by-flight basis. The pre- and post-flight readings were averaged for each flight and the difference between the average value and the local gravity value was removed. This acts as a simple but effective coarse levelling of the data.

Intersection statistics were then used to adjust individual survey lines. Unlike magnetic levelling, individual intersections were not used to make corrections. Instead, intersection differences from whole lines were averaged and a single adjustment was applied to each survey line and each control line. Minor adjustments were calculated for sections of each line based on statistics from groups of intersections. The adjustments were smoothed and applied to line data that was filtered as described below. Grids of adjusted data were inspected to determine that the adjustments were appropriate.

#### **4.1.3 Gridding and Filtering**

Statistical noise in the data was reduced by applying a cosine tapered low-pass filter to the time series line data. For this survey, a 20 second (1000 m) half-wavelength filter was employed. The data were gridded using a minimum curvature algorithm that averages all values within any given grid cell and interpolates the data between survey lines to produce a smooth grid. The algorithm produces a smooth grid by iteratively solving a set of difference equations by minimizing the total second horizontal derivative while attempting to honour the input data (Briggs, 1974). Grids were generated using a 25 m grid cell size.

Low-pass spatial filtering is applied to the grid for noise reduction. Essentially, the survey area is over-sampled as the line spacing is smaller than the grid filter used. A range of grid filters were used and evaluated for noise levels and signal content. Final data for this survey was filtered with a 1.0 km half-wavelength grid filter.

The gravity data were gridded using a cell size of 25 m and 250 m over the White River area. The 25 m gridding cell was applied to present the highest resolution of data within the boundary of the survey block, comprising the principal survey area. The 250 m gridding cell was applied to include the



extensions of the flight lines beyond the survey block, comprising the extended survey area. The Bouguer gravity with a terrain correction of 2.67 g/cm<sup>3</sup> is displayed in Figures 4.1 (principal survey area, grid cell size of 25 m) and Figure 4.2 (extended survey area, grid cell size of 250 m). The Free Air gravity is displayed in Figures 4.3 (principal survey area, grid cell size of 25 m) and Figure 4.4 (extended survey area, grid cell size of 250 m).

## 4.2 Magnetic Data Processing

The airborne magnetometer data were recorded at 160 Hz, and down sampled to 10 Hz for processing. A second order Butterworth 0.9 Hz low pass filter is utilized in the process for compensation and anti-aliasing. All magnetic data were plotted and checked for any spikes or noise. A 0.244 second static lag correction due to signal processing, plus a dynamic lag correction which varies between 0.04 s and 0.06 s, depending on the instantaneous velocity of the aircraft, was determined on a line-by-line basis using SGL's Dynlag software.

Ground magnetometer data were inspected for cultural interference and edited where necessary. All reference station magnetometer data were filtered using a 121-point low-pass filter to remove any high-frequency noise, but retain the low-frequency diurnal variations.

A correction for the International Geomagnetic Reference Field (IGRF) year 2015 model was applied to all ground magnetometer data using the fixed ground station location and the recorded date for each flight. The mean residual value of the reference station was calculated (173.141 nT) and subtracted to remove any bias when correcting the local anomalous field on the survey grid. Diurnal variations in the airborne magnetometer data were removed by subtracting the reference station data after subtraction of the mean residual.

The airborne magnetometer data were also corrected for the IGRF using the location, altitude, and date of each point. IGRF values were calculated using the year 2015 IGRF model. The altitude data used for the IGRF corrections are DGPS heights above the WGS-84 datum.

### 4.2.1 Levelling

Intersections between control and traverse lines were determined by a program which extracts the magnetic, altitude, and x and y values of the traverse and control lines at each intersection point. Each control line was adjusted by a constant value to minimize the intersection differences, calculated as follows:

$\sum |i - a|$  summed over all traverse lines, where:

$i$  = (individual intersection difference)

$a$  = (average intersection difference for that traverse line)

Adjusted control lines were further corrected locally to minimize any residual differences. Traverse line levelling was carried out by a program called CLEVEL that interpolates and extrapolates levelling values for each point based on the two closest differences at intersections. After traverse lines were levelled, the control lines are matched to them. This ensured that all intersections tie very closely and permitted the use of all data in the final products.

CLEVEL provides a curved correction using a function similar to spline interpolation. A third degree polynomial was used to interpolate between two intersections. CLEVEL allows intersection points to be preserved with no mismatch and interpolation is smooth with the first derivative continuously

approaching the same value from both sides of the intersection points.

The levelling procedure was verified through inspection of the magnetic anomaly and vertical derivative grids, by plotting profiles of corrections along lines, and by examination of levelling statistics to check for steep correction gradients.

#### **4.2.2 Micro-Levelling**

Micro-levelling is occasionally applied to magnetic data to remove any residual diurnal effects by using directional filters to identify and remove artifacts that are long wavelengths parallel to survey lines and short wavelengths perpendicular to survey lines. In this case, no micro-levelling was required for the White River magnetic data.

#### **4.2.3 Gridding**

The grid of the total magnetic intensity was made using a minimum curvature algorithm to create a two-dimensional grid equally sampled in the x and y directions following Briggs (1974). The final grids of the magnetic data were created with 25 m grid cell size appropriate for survey lines spaced at 100 m. Grids were also made that included the 1000 m spaced lines that extend out from the main block area. These were gridded with a cell size of 250 m. The magnetic data were gridded using a cell size of 25 m and 250 m over the White River area. The 25 m gridding cell was applied to present the highest resolution of data within the boundary of the survey block, comprising the principal survey area. The 250 m gridding cell was applied to include the extensions of the flight lines beyond the survey block, comprising the extended survey area. The total magnetic intensity (or more correctly, the magnetic anomaly) is displayed in Figures 4.5 (principal survey area, grid cell size of 25 m) and Figure 4.6 (extended survey area, grid cell size of 250 m).

### **4.3 Gravity and Magnetic Derivative Products**

Filters may be applied to the data to enhance different wavelength information that arises from different sources. In many cases, filtering is best achieved by transforming the data from the space domain to the frequency domain by Fourier transform since frequency characteristics of the filter to be applied are more precisely defined in the frequency domain. The filtered derivatives created to assist with interpretation are described below.

#### **4.3.1 Total Magnetic Intensity Reduced to Pole**

Reduction to the pole (RTP) transforms anomalies as if they were at the north magnetic pole. The basic assumption is that magnetic anomalies arise from induced magnetization. This assumption may not always be true where significant magnetic remanence occurs. The method allows direct comparison of anomaly shapes from different magnetic latitudes, and if the assumptions hold true, the anomaly will be symmetrically disposed about the causative body. Reduction to pole is essentially a phase shift filter applied in the frequency domain, and is described by Baranov and Naudy (1964):

$$F(k_x, k_y) = \frac{1}{[\sin I + i \cos I \cos(D - \theta)]^2}$$

where

- $\theta$  is the angle in the  $k_x$   $k_y$  plane
- $I$  is the local magnetic inclination
- $D$  is the local magnetic declination

For ease of calculation, this transformation was performed through filtering in the frequency domain using a constant (average/central) inclination and declination which was considered valid throughout the entire grid. The inclination used was 74.092°, and the corresponding declination used was -7.836° representing a station approximately at the centre of the survey. The total magnetic intensity reduced to the pole is shown in Figure 4.7 (principal survey area, grid cell size of 25 m) and Figure 4.8 (extended survey area, grid cell size of 250 m).

#### **4.3.2 Vertical Derivatives of Total Magnetic Intensity and Bouguer Gravity**

If  $k_x$  and  $k_y$  are the wave numbers of the potential field in the two-dimensional frequency domain, the  $n^{\text{th}}$  vertical derivative of a potential field is easily derived in the Fourier domain by applying the following filter:

$$F(k_x, k_y) = (-k)^n \quad \text{where } k = \sqrt{(k_x^2 + k_y^2)}$$

Vertical derivatives act as high-pass filters that enhance high-frequency data and suppress low-frequency data. The first vertical derivative ( $n=1$ ) enhances the rapid changes in gravity or magnetic field at the edges of anomalies and is therefore useful for delimiting the extents of causative bodies. The second vertical derivative ( $n=2$ ) enhances high-frequency signal variations even more, such that textural variations in the character of the potential field (especially for magnetic data) can be used to delimit domains of a specific geophysical response.

The first vertical derivative of the reduced to pole total magnetic intensity is shown in Figure 4.9 (principal survey area, grid cell size of 25 m) and Figure 4.10 (extended survey area, grid cell size of 250 m). The first vertical derivative of the Bouguer gravity with a terrain correction using a density of 2.67 g/cm<sup>3</sup> is shown in Figure 4.11 (principal survey area, grid cell size of 25 m) and Figure 4.12 (extended survey area, grid cell size of 250 m). The first vertical derivative of the free air gravity is shown in Figure 4.13 (principal survey area, grid cell size of 25 m) and Figure 4.14 (extended survey area, grid cell size of 250 m). The second vertical derivative of the pole reduced total magnetic intensity is shown in Figure 4.15 (principal survey area, grid cell size of 25 m) and Figure 4.16 (extended survey area, grid cell size of 250 m). The gravity data do not contain high-frequency information to render its second vertical derivative useful for interpretation.

#### **4.3.3 Total Horizontal Gradient of Total Magnetic Intensity and Bouguer Gravity**

Horizontal gradients are most conveniently calculated in the space domain. Total horizontal gradient of a potential field ( $T$ ) is from the gradients in the horizontal  $x$  and  $y$  planes as follows (Nabighian, 1972):

$$\text{Total horizontal derivative} = \sqrt{(\partial T / \partial x)^2 + (\partial T / \partial y)^2}$$

Horizontal gradient grids are used primarily for edge detection of causative bodies (contacts, faults with large vertical displacement), and the data may also be employed for trend analysis and depth to source calculations.

Total horizontal derivatives of the pole reduced total magnetic intensity, Bouguer gravity (2.67g/cm<sup>3</sup> terrain corrections) and free air gravity are shown in Figures 4.17, 4.19, 4.21 (principal survey area, grid cell size of 25 m) and Figures 4.18, 4.20, 4.22 (extended survey area, grid cell size of 250 m).

#### **4.3.4 Total Gradient Amplitude of Total Magnetic Intensity**

The total gradient amplitude, otherwise known as the 3D analytic signal amplitude, of a potential field ( $T$ ) is defined as:

$$|A(x, y)| = \sqrt{(\partial T / \partial x)^2 + (\partial T / \partial y)^2 + (\partial T / \partial z)^2}$$

$|A(x, y)|$  is the amplitude of the analytic signal and  $T$  is the magnetic intensity at a point  $(x, y)$ . The horizontal derivatives are easily calculated in the space domain, whilst the vertical derivative is calculated in the frequency domains. The analytic signal is independent of field direction and direction of magnetization, and is mostly independent of the type of magnetization (induced or remanent). This means that all similar bodies have a similar analytic signal response, and that peaks in the analytic signal are symmetric and centred over the middle of narrow bodies and the edges of wide bodies. The amplitude however is affected by the strike of a body such that north-south oriented bodies at low latitudes are relatively weak for magnetic data. The analytic signal highlights areas where the field varies quickly in any direction, such as for contacts. The total gradient amplitude of the total magnetic intensity is shown in Figure 4.23 (principal survey area, grid cell size of 25 m) and Figure 4.24 (extended survey area, grid cell size of 250 m).

#### **4.3.5 Tilt Angle**

The tilt angle can be applied to the pole reduced total magnetic intensity to preferentially enhance the weaker magnetic signals. This is particularly useful for mapping texture, structure, and edge contacts of weakly magnetic sources. The arctan operator restricts the tilt angle to within the range of -90° to +90°, irrespective of the amplitude and wavelength of the field and enhances weak anomalies compared to the stronger anomalies. The tilt angle (Miller and Singh, 1994; Verduzco et al., 2004; Salem et al., 2007) is defined as:

$$\Theta = \tan^{-1} \frac{\text{vertical component of gradient}}{\text{horizontal component of gradient}} = \tan^{-1} \left[ \frac{\partial T / \partial z}{\partial T / \partial h} \right]$$

The vertical and horizontal gradients of the reduced to pole total magnetic intensity calculations are described above in subsections 4.3.2 and 4.3.3. The tilt angle grid for the reduced to pole total magnetic intensity is displayed in Figure 4.25 (principal survey area, grid cell size of 25 m) and Figure 4.26 (extended survey area, grid cell size of 250 m).

#### **4.3.6 Trend Analysis Method**

Depth trend as implemented by Phillips (1997) can be utilized for the depth estimation using the horizontal gradient grid (HG). It uses the horizontal gradient of the reduced to pole total magnetic intensity and gravity grids to estimate strikes of and depths to thick and thin edges, respectively (Phillips, 2000). The method relies on the general principle that shallow sources produce anomalies with steep gradients, whereas deep sources produce anomalies with broad gradients. Depth estimates

from the RTP magnetic and gravity data estimate the minimum and maximum depths to the top edge of the layer, respectively (Phillips, 2000).

The program uses a 5 by 5 window to both locate the crests of maxima and determine their strike direction. Once a crest is located and the strike direction is known, data within the window and within a belt perpendicular to the strike can be used to determine the depth of the contact by performing a least squares fit to the theoretical shape of the  $HG$  over a contact. If " $h$ " is the horizontal distance to the contact, " $d$ " is the depth to the top of the contact and " $K$ " is a constant, then the theoretical curve is given by (Roest and Pilkington, 1993):

$$HG(h) = K/(h^2 + d^2)$$

The least-squares fit gives an estimate of both the depth and its standard error, which can be expressed as a percentage of the depth. Only depth estimates with standard errors of 20% or better are retained in this interpretation.

Due to the assumption of thick sources, the depth estimates obtained using the above procedure represent minimum depths. It is also possible to assume very thin sources and use a standard "pseudogravity" transformation instead of reduction to the pole (Roest and Pilkington, 1993). In this case the same analysis is done on the  $HG$  of the pseudogravity field, and the depth estimates represent maximum depths. Figures 4.27 and 4.28 show the depth results from the trend analysis solutions for the Bouguer gravity and the reduced to pole total magnetic intensity, respectively. Solutions depths from Bouguer gravity data are provided as depth below the topographic surface while solution depths from magnetic data are provided as depths from the sensor.

## 5 Geophysical Interpretation

The geophysical interpretation of the acquired gravity and magnetic data in the White River area involved qualitative analysis of the various products derived from the magnetic and gravity grids (described in Section 4), and 2.5D forward modelling of the gravitational and magnetic data along two profile lines covering the main features of the Strickland and Anahareo plutons and adjacent batholiths and greenstone belts within the survey area.

### 5.1 Results of Qualitative Analysis

Qualitative analysis of the gravity derivative products was used to provide general indications about the contact relationships and general geometry of the Strickland and Anahareo plutons and their bounding geological units; including the variation in depth to bottom across the plutons; internal variation; and the presence of major or deep seated structures. Qualitative analysis of the magnetic derivative products was used to: identify the presence of potential features within the plutons, such as faults and dykes (documented in SRK, 2016); and evaluate variation in the magnetic character of the plutons that may indicate changing composition of the rock or other potential heterogeneities.

For the qualitative geophysical interpretation, the Bouguer gravity (Figure 5.1), its first vertical derivative (Figure 5.2) and its total horizontal derivative (Figure 5.3), as well as the total magnetic intensity reduced to the pole (Figure 5.4), its first vertical derivative (Figure 5.5), and its total horizontal derivative (Figure 5.6), were primarily utilized. In addition, the total gradient amplitude was used for interpretation of the magnetic data (Figures 4.23 and 4.24) because: (a) it has a maxima over vertical magnetic contacts regardless of the direction of magnetization; and (b) the magnetic intensity reduced to pole requires the assumption of only induced magnetization with the result that anomalies from remanently and anisotropically magnetized bodies can be severely distorted. Unlike the RTP, the total gradient amplitude will produce maxima over the edges of vertical magnetic contacts regardless of the presence of remanent magnetism (MacLeod, 1993).

#### 5.1.1 *Strickland Pluton*

- The Bouguer gravity data shows a broad low response located centrally within the Strickland pluton (Figure 5.1). The magnitude of the gravity response gradually increases in all directions. High magnitude gravity responses correspond well to the mapped boundaries of the Dayohessarah greenstone belt and the Kabinakagami Lake greenstone belt along the western and eastern sides of the Strickland pluton, respectively.
- In general, the reduced to pole total magnetic intensity over the Strickland pluton shows a moderate to strong magnetic response that locally shows internal variations in magnetic fabric intensity and dyke overprinting (Figure 5.4). Interpreted dykes are evident within the pluton and surrounding area as linear features with high magnetic responses. Similar to the gravimetric response, the magnetic data corresponds well to the mapped boundaries of the Dayohessarah greenstone belt and the Kabinakagami Lake greenstone belt.

Specific features identified in Strickland pluton and surrounding area during the qualitative interpretation are discussed below.

- The central portion of the Strickland pluton is characterized by a broad low response in the Bouguer gravity (labelled G-A1 in Figure 5.1). The edges of G-A1 were interpreted from a textural change in the first vertical derivative of the Bouguer gravity (Figure 5.2) and peaks in total

horizontal derivative of the Bouguer gravity (Figure 5.3). The gravity low coincides with both granitoid rocks of the Strickland pluton and gneissic tonalites of the Black-Pic batholith to the south, but does not align directly with the mapped geologic boundaries. Because the gravity anomaly is not consistent with surface bedrock mapping may suggest either the surface mapping is incorrect or that the lower density batholith may extend under the gneissic tonalites at depth. The position of the low gravity response may suggest either the thickest section of the pluton and batholith and/or the lowest density bedrock. The southern to southeastern boundary of the gravity low is marked by a prominent gradient associated with the mapped Kabinakagami greenstone belt. Within G-A1 there seems to be fewer cross cutting dykes than the surrounding area, but there is no other obvious correlation to the magnetic fabric.

- A gradient in the gravity data was identified using peaks in the total horizontal derivative of the Bouguer gravity (Figure 5.3) and a textural change in the first vertical derivative of the Bouguer gravity (labelled G-D1 in Figure 5.2). This boundary separates the central gravity low G-A1 from the surrounding gravity high of the Dayohessarah greenstone belt and its location is primarily within the western margin of Strickland pluton. Where G-D1 extends into tonalitic gneisses in the south, it becomes less evident in the data. Stott (1995a, 1995b, 1995c and 1999) describes the western margin of the Strickland pluton, adjacent to the Dayohessarah greenstone belt, as comprising a complex mix of intrusive to metamorphosed units that range in composition from granodiorite to tonalite and diorite, generally associated with a gneissic fabric. This interpretation is consistent with historic mapping of the same area that identified gneissic rocks between the western boundary of the Strickland pluton and the adjacent Dayohessarah greenstone belt (Fenwick, 1967; see M2129). The interpreted boundary (G-D1) may therefore reflect a lithological variation between gneissic rocks of variable composition adjacent to the greenstone belt and a more homogeneous granitic unit characteristic of the central portion of the Strickland pluton.
- Within the Strickland pluton, north of the Kabinakagami Lake greenstone belt, tightly spaced high and low magnetic intensity layering, and a number of tight folds, are evident in the magnetic data (labelled M-F1 to M-F5 in Figures 5.4 - 5.6). The layering, and the fold structures that it defines, highlight features consistent with macroscopic, ductile deformation within what was previously mapped as the marginal zone of the Strickland pluton. Historic mapping suggests that these areas are, in fact, dominated by foliated granitic bedrock (see M2355; Siragusa, 1977), in particular in proximity to the Kabinakagami Lake greenstone belt. Elsewhere the bedrock is largely mapped as undifferentiated granites, or to the west of the interpreted tight folds, mapped as a relatively uniform granodiorite.
- Matachewan dykes with NW-SE strike cross-cut these folds with no horizontal offset, implying no reactivation of the ductile layering after the ca. 2.473 Ga emplacement age (Buchan and Ernst, 2004) of these dykes.
- The linear magnetic boundary labelled M-D1 in Figures 5.4 to 5.6 approximates the mapped contact between the Black-Pic batholith and the Strickland pluton. The anomaly defines a boundary where there is a discrete change in the orientation and character of the magnetic fabric. South of the boundary the magnetic fabric has a higher magnetic intensity and is oriented predominantly east-west. North of M-D1 the magnetic fabric has a lower intensity and is principally northeast trending and parallel to a narrow band of rock with a reduced magnetic intensity defined in the Hornepayne area (M-D12 in SGL, 2016a). This narrow band in the Hornepayne area is interpreted to represent a northeastern extension of the Dayohessarah greenstone belt which may

be continuous with the mapped mafic metavolcanic sliver within the Black-Pic batholith (SGL, 2016a).

- A distinct curvilinear magnetic low anomaly, labelled M-L1 in Figures 5.4 to 5.6, is identified in the Strickland pluton. The curved nature of this feature is different from most magnetic low features identified within the pluton, which are usually linear (SRK, 2016). The magnetic signature of this anomaly tends to show some asymmetry in the reduced to pole magnetic intensity (Figure 5.6), with higher values predominantly located on the southwestern side of the anomaly, and weaker values on the northeastern side. The asymmetry of this curvilinear anomaly may be interpreted as a potential fracture zone dipping towards the northeast. At the point where this curvilinear anomaly intersects a northeast trending Biscotasing dyke there is an interpreted sinistral offset of approximately 400 m. However, it is not clear if the offset is due to horizontal or oblique displacement across M-L1, or if the dyke simply side stepped during intrusion. Northwest of where M-L1 crosses the Biscotasing dyke the anomaly becomes more difficult to trace but it may branch into northwest and northeast trending arms.
- On the western side of the Strickland pluton the Dayohessarah greenstone belt produces a prominent crescent shaped gravity high defined by G-A2 (Figures 5.1 to 5.3). The high gravity response is associated with the presence of high density mafic metavolcanic bedrock associated with the greenstone belt. The greenstone belt also has an associated magnetic anomaly, although the greenstone belt only occurs in the area of coarse survey coverage. The magnetic anomaly produced by the Dayohessarah greenstone belt is labelled M-A1 in Figures 5.4 to 5.6. Both gravity and magnetic anomalies show good correlation to the mapped extent and geometry of the greenstone belt, though the gravity anomaly associated with the greenstone belt extends slightly farther east (~ 700 m) and the magnetic anomaly extends slightly farther west (~1 km). Stott (1999) described the structure of the Dayohessarah greenstone belt as a steeply east-dipping and southerly plunging syncline. The greenstone belt is primarily strongly magnetic in its core and is surrounded by non- to low magnetic mafic metavolcanics. The crescent shaped greenstone belt tapers into thin zones of anomalous magnetic lows which extend beyond both ends of the crescent.
- The Kabinakagami Lake greenstone belt coincides with a prominent gravity high located on the eastern side of the survey area and labelled G-A3 in Figures 5.1 to 5.3. This gravity high correlates fairly well with the mapped geologic extent of the greenstone belt. Areas with the highest gravity response are interpreted to arise from dense and/or thick areas of mafic metavolcanic rocks within the belt. Areas of relatively lower gravity response within the greenstone belt, such as the anomaly labelled G-A4 (Figures 5.1-5.3), have also been mapped as mafic metavolcanics, but may only have a thin veneer of dense rock close to surface with more extensive amounts of less dense felsic to intermediate metavolcanic rocks and metasedimentary rocks at depth. The magnetic anomaly associated with the Kabinakagami greenstone belt is labelled M-A2 in Figures 5.4 to 5.6. This anomaly is well defined by an intense magnetic fabric in the derivative grids of the magnetic data and encompasses an inner area of banded, curvilinear magnetic highs reflecting intermediate to mafic horizons and an outer zone of magnetic lows, likely reflecting intermediate to felsic metavolcanic rocks and/or metasedimentary rocks. Previous magnetic data interpretations by Siragusa (1977) suggested that the magnetic anomalies may correspond to iron formation, but also noted that the most magnetic areas are covered by water. Some areas of the Kabinakagami greenstone belt appear to have strong negative magnetic intensity suggesting remanent magnetization, such as the near ellipsoidal magnetic low near the western end of the belt (labelled



M-A3 in Figures 5.4 to 5.6). Areas of remanent magnetization were interpreted by comparing the pole reduced magnetic intensity grid to the analytic signal (Figure 4.23).

- Several anomalies within the Strickland pluton proximal to the Kabinakagami Lake greenstone belt are identified as prominent magnetic highs (labelled M-A4 and M-A5 in Figures 5.3-5.6). Anomaly M-A4 has a corresponding gravity anomaly (labelled G-A5 in Figures 5.1-5.3) and occurs in the nose of the fold labelled M-F1 (Figures 5.4 to 5.6). These anomalies likely represent outliers of mafic metavolcanic of the Kabinakagami Lake greenstone belt. Localized outliers of mafic metavolcanics have been observed in previous mapping in proximity to the Kabinakagami Lake greenstone belt (see M2355 and M2382; Siragusa, 1977; 1978).
- South of the Strickland pluton, within an area mapped as gneissic tonalite, a zone with a well-defined internal magnetic fabric has been interpreted and labelled M-A6 (Figures 5.4 to 5.6). This zone has a sinusoidal shape and extends from the western side of the Kabinakagami Lake greenstone belt and is interpreted to connect to the Dayohessarah greenstone belt. Within this zone the magnetic character consists of several subparallel magnetic lineations visible in the magnetic derivative grids (Figures 4.9 and 4.15). This arcuate anomaly does not correlate to any mapped geologic structure or contact, however historic bedrock mapping in the area identified several small bodies of mafic metavolcanic rocks in granitic gneiss within the same zone (see M2129; Fenwick, 1967). Based on this association, anomaly M-A6 is interpreted as a deeply eroded remnant of a previously continuous or semi-continuous sliver of greenstone belt. The northern edge of this anomaly may also correspond to the southern boundary zone of the Strickland pluton.
- A strongly negative linear feature is observed in the magnetic data (labelled M-L2 in Figures 5.4 to 5.6) extending from the southwestern edge of the survey area northeast through the Strickland pluton. This feature in the data terminates shortly after crossing the curvilinear magnetic anomaly M-L1. The intensity and character of this negative feature suggests that it represents a reversely magnetized dyke, rather than a fault causing demagnetization. In all but one instance this dyke overprints the magnetic anomaly of the ca. 2.473 Ga Matachewan dykes where they intersect, suggesting that the reversely magnetized dyke has a younger age of emplacement. Based on the bedrock geology map (OGS, 2011) this dyke is not affiliated to any swarm, however it strikes in the same northeasterly direction as both normally magnetized younger Abitibi (1.14 Ga) and Biscotasing (2.17 Ga) dykes (Ernst and Buchan, 1993, Hamilton et al., 2002). Reversely magnetized northeast trending dykes have also been identified in the Manitouwadge area (SGL, 2016b).

### **5.1.2 Anahareo Pluton**

- The Bouguer gravity data over the Anahareo pluton shows a broad low response located near its northern mapped boundary (Figure 5.1). The magnitude of the gravity response increases towards the northeast and northwest approaching the Kabinakagami Lake and Dayohessarah greenstone belts and also increases towards the south.
- In general, the reduced to pole total magnetic intensity over the surveyed portion of the Anahareo pluton shows a moderate to strong magnetic response, with local internal variations in magnetic fabric intensity (Figure 5.4). The magnetic intensity abruptly increases towards the south and southeast. Interpreted dykes are evident transecting the pluton and surrounding area as linear features with high magnetic responses. Similar to the gravimetric response, the magnetic data

corresponds well to the mapped boundaries of the Kabinakagami Lake greenstone belt along the northeastern margin of the Anahareo pluton.

Specific features identified in the Anahareo pluton during the qualitative interpretation are discussed below.

- The gravity low that occurs in the south-central portion of the survey area falls predominantly within the Anahareo pluton and partly within the gneissic tonalites mapped immediately northwest of the pluton (G-A6 in Figures 5.1 to 5.3). The edges of G-A6 were defined from peaks in the total horizontal derivative of the Bouguer gravity and a subtle change in the coherence of the first vertical derivative of the Bouguer gravity. G-A6 represents a local gravity low within a generally east-west trending regional gravity low that correlates to the granite-granodiorite phase of the Anahareo pluton (PGW, 2014). As suggested by PGW (2014), regionally this gravity low may represent a thickening of the Anahareo pluton, but may also be explained by density variation due to mineralogical variations. The northern boundary of G-A6 appears to coincide with a subtle transition from a higher coincident magnetic response to a lower magnetic response to the north.
- Along the southern edge of the Anahareo pluton, M-A7 defines an area of increased magnetic background (Figures 5.4 to 5.6). The magnetic intensity increases slightly towards the southeast through this area, with the entire area abruptly bounded by a zone of lower magnetic intensity. It is possible to extend area M-A7 farther northeast, past the interpreted boundary of M-A7, but with a reduced anomaly amplitude. Though the cause of this anomaly is unknown, its character is similar to the region of increased magnetic background within the Strickland pluton west of M-A4 (Figure 5.4), which in both cases may simply reflect increased magnetic mineral content.
- The northern to northwestern side of the mapped boundary of the Anahareo pluton is bound by an area mapped as gneissic tonalite suite. As discussed above, this area has a unique magnetic fabric (labelled M-A6 in Figures 5.4-5.6) which extends from the western side of the Kabinakagami Lake greenstone belt and is interpreted to connect to the Dayohessarah greenstone belt. This zone may represent the remnant of a larger greenstone belt that has since been eroded. The southern edge of M-A6 is less well defined than its northern edge and the interpreted boundary is based on the disappearance of the magnetic fabric.
- A teardrop shaped magnetic anomaly (labelled M-A8 in Figures 5.4-5.6) has been identified, extending southwest from the magnetic anomaly associated with the Kabinakagami greenstone belt (M-A2). M-A8 is interpreted as a body of mafic metavolcanic rock hosted within the Anahareo pluton in a similar style to M-A4 and M-A5 in the Strickland pluton. Several small bodies of mafic metavolcanic rocks have been mapped within the bounds of M-A8 (see M2382; Siragusa, 1978) therefore the larger extent of M-A8 may suggest a greater abundance of mafic metavolcanics at depth.

## 5.2 Preliminary 2.5D Modelling

The purpose of the 2.5D modelling is to develop an idea of the approximate depth to the base of the Strickland and Anahareo plutons and surrounding rocks. The preliminary 2.5D modelling used the gravity, magnetic and digital elevation data sets, accompanied with constraints from the qualitative interpretation of the geophysical data and the mapped bedrock geology to provide a preliminary image of the subsurface along the two profile lines shown in Figures 5.7 and 5.8.

For the purpose of this initial modelling attempt, density and magnetic susceptibility values were assigned to the bedrock units mapped on the surface (Figure 1.1) and to the bedrock units at depth based on readily available information. In the White River area, several surface bedrock density and magnetic susceptibility values have been compiled from available literature (data sources discussed in Section 3) and incorporated as constraints into the models. These assumed density and magnetic susceptibility values should be considered as approximate values.

Alternative models were considered in order to assess the sensitivity of the assigned density and magnetic susceptibilities on the modelled geometry and thickness of the bedrock units. The initial models assumed a relatively flat, tabular structure for the Anahareo and Strickland. The plutons are both surrounded by gneissic tonalite rock of the Black-Pic and Pukaskwa batholiths which are in turn underlain by undifferentiated basement bedrock along a flat boundary for the initial models. Densities for the Black-Pic batholith and undifferentiated basement were kept constant where possible and only varied within the plutons in order to fit the model to the observed data. For the alternative models each pluton is assigned a uniform density and the geometry of the base of the intrusions is varied to fit the model to the observed data. Both model approaches provide a good fit to the data. As we have an idea of the range of likely density values, the resulting 2.5D models can give an idea of the upper and lower bounds on total depth to the base of the plutons.

It is important to emphasize that the accuracy of these preliminary models is limited at this early stage of the assessment due to limited availability of bedrock densities and magnetic susceptibilities, which are key for constraining the model. It is anticipated that the preliminary 2.5D models would be revised and refined if more field data is collected in the future.

### 5.2.1 Model Descriptions

The preliminary 2.5D forward modelling of gravity and magnetic data was carried out using GMSYS Software (copyright Northwest Geophysical Associates Inc. 2006) running under Geosoft Oasis Montaj (Geosoft, 2015). The modelling considered two profile lines. The locations of the profile lines are shown in Figure 5.7 superimposed on the Bouguer gravity, and in Figure 5.8 superimposed on the total magnetic intensity. The coordinates of the start and end points for each of the profile lines are listed in Table 5.1.

*Table 5.1: Coordinates of 2.5D Model Profiles (UTM 16N, NAD83)*

Profile Line	Start		End	
	UTM X	UTM Y	UTM X	UTM Y
1	639000	5412805	689000	5412805
2	663460	5371665	663460	5428467

The process for constructing the models was as follows:

- The location and extent of profile models was taken into consideration during survey planning. A group of control lines were extended past the eastern and western edges of the White River survey block to capture relevant regional features outside the area of high resolution coverage. Control lines were also designed to join with the Hornepayne area traverse lines (SGL, 2016a) to allow for a single long profile line between adjacent survey blocks.

- The profiles were modelled from Bouguer gravity and the total magnetic intensity data. It is possible to model either Free-Air or Bouguer gravity. Both approaches are valid, the difference is that topographic effects have been corrected in the Bouguer gravity, assuming a single density within the range of relief ( $2.67 \text{ g/cm}^3$  in this instance). Some terrain effects will still occur in the Bouguer gravity where density varies from the assumed value within the range of relief. The best choice depends on the degree to which the single density terrain corrections are applied and correctly handled. The model results should be essentially the same with either approach.
- Large bodies were modelled as 2D (i.e. extending to infinity perpendicular to the profile line), while small bodies were modelled as 2.5D (i.e. extending to a finite distance perpendicular to the profile line).
- Generally speaking, gravity data were modelled first to determine the broad large scale features and the magnetic data were used to refine the model and to help model the overall shape of smaller geological units. Long wavelength magnetic trends associated with large rock units were modelled as opposed to individual discrete anomalies and, as such, only a subset of dykes and faults; that produce to large amplitude, discrete anomalies were included to fit the observed data.
- Densities for individual greenstone belts were assumed to be uniform throughout unless there were additional data that suggested the contrary (e.g. well logs, density measurements, etc.). This assumption was only violated if it was impossible to model the gravity using uniform densities. Thus the gravity anomalies were generally accounted for by varying the shapes of the rock units after initial density assumptions were made, rather than by varying the densities within the rock units.
- Depth trend, tilt angle and extended Euler solutions of the Bouguer gravity and magnetic data were used for determining locations and dips of faults and lithological contacts.
- Available geologic mapping (OGS, 2011) and qualitative interpretation of the geophysical data were used to determine the location of the points at which geological boundaries occur along the surface of the models.
- Density information has been obtained and incorporated into the models from the OGS PETROCH database (Haus and Pauk, 2011) and the GSC rock property database (GSC, 2015), as discussed in Section 3. The density ranges used in the models are listed in Table 5.2.
- In determining the magnetic susceptibilities, measured values from the OGS Precambrian Bedrock Magnetic Susceptibility Geodatabase (Muir, 2013) and Miles (1998) were used as initial values for modelling, but were adjusted so as to (a) best match the amplitude of the magnetic variations that were obviously associated with terrain, (b) best reproduce the overall long wavelength trend associated with the larger rock units. This approach was employed due to the variability of the measured susceptibilities, in some cases over several orders of magnitude.
- In seeking to model magnetic variations within individual rock units, steeply dipping to vertical boundaries were generally used in the absence of other indications. Where possible these boundaries were set to be coincident with the gravity defined boundaries. Trend analysis

solutions for the magnetic field reduced to the pole were also used to model the dip of magnetic contacts. Trend analysis solutions are shown in the 2.5D model figures for both gravity and magnetic data. The solutions shown are those which occur no more than 0.5 km away from the model line.

- The overburden has not been included in the modelling. It is deemed to be sufficiently thin that its effect on the gravity and magnetic anomalies is negligibly small for modelling purposes.
- Where the 2.5D model lines intersect, the geological boundaries, densities, and magnetic susceptibilities have been made to coincide at the model intersection points.

*Table 5.2: Densities and magnetic susceptibilities used in the 2.5D models*

<b>Layer</b>	<b>Density (g/cm<sup>3</sup>)</b>	<b>Magnetic Susceptibility (S. I.)</b>
<i>Mafic metavolcanics (2)</i>	2.75 – 2.95	0 – 0.126
<i>Metasediments (5)</i>	2.72	0 – 0.01
<i>Gneissic tonalite (9)</i>	2.60 – 2.70	0 – 0.014
<i>Foliated tonalite (10)</i>	2.66	0
<i>Granite-granodiorite (13)</i>	2.58 – 2.70	0 – 0.010
<i>Dyke</i>	2.61 – 2.70	0.009 – 0.039
<i>Undifferentiated basement</i>	2.69	0

### **5.2.2 Model Results**

This section discusses the results of the 2.5D modelling for the two profile lines considered. It is assumed that a uniformly dense unit defined as undifferentiated basement (density of 2.69 g/cm<sup>3</sup>) lies below the gneissic tonalite rock which surrounds and underlies the Anahareo and Strickland plutons. Distances along profiles are listed relative to the profiles western and southern origin for Lines 1 and 2, respectively.

The 2.5D modeling results for the White River area are shown on Figures 5.9 to 5.12. The figures show a plan view along the profile line (e.g. top panel Figure 5.9) in order to show the distribution of bedrock units that are included in the model calculations perpendicular to the strike of the profile line. The gravity view (i.e. second panel Figure 5.9) shows the observed gravity data along the profile line, as well as the calculated gravity data, the misfit and the RMS error (i.e. root mean square error). The RMS error is used as a measure of the difference between the observed gravity data and the modelled gravity results. The next gravity view (e.g. third panel Figure 5.9) shows the assignment of the rock density values to each of the bedrock units in the model. The magnetic view (e.g. fourth panel Figure 5.9) shows the observed and calculated magnetic data, as well as the misfit and RMS error between the two data sets. The next magnetic view (e.g. fifth panel Figure 5.9) shows the assignment of the magnetic susceptibility values to each of the bedrock units in the model. The structural view provides the overall interpretation of the modelled results, which are coloured based on geological unit (e.g. sixth panel on Figure 5.9). Each of these model views shows the depth on the y-axis in kilometers below MSL.

### 5.2.2.1 Initial Model Line 1 (Figure 5.9)

As shown in Figures 5.7 and 5.8, Line 1 runs from west to east starting just west of the Dayohessarah greenstone belt, extending across the Strickland pluton, and ending in the Kabinakagami Lake greenstone belt (Figure 5.9).

- On the western side of the profile, the Dayohessarah greenstone belt has been modelled as an upright synform with its contacts dipping eastward and a maximum depth of approximately 3 km below MSL. The eastern limb of the synform, in contact with the Strickland pluton, has been modelled as steeper than the western limb which contacts the Black-Pic batholith, though the gravity data does not fully cover the western side of the belt. The overall model geometry of the greenstone belt is in agreement with Stott (1999) and the modelled depth conforms to estimated depths for the belt of between 2 and 3 km (SRK, 2014); however, in order to match this depth, the belt was assigned a higher density than the Kabinakagami Lake greenstone belt ( $2.95 \text{ g/cm}^3$  vs.  $2.85 \text{ g/cm}^3$ ). A density of  $2.85 \text{ g/cm}^3$  for the Dayohessarah greenstone belt would increase its depth to base to over 6 km below MSL. Density differences between the Dayohessarah and Kabinakagami Lake greenstone belts could be explained by relative differences in the proportion of denser mafic metavolcanics to less dense felsic and intermediate metavolcanic rocks and metasedimentary rocks within the belt. Both assigned densities ( $2.85 \text{ g/cm}^3$  and  $2.95 \text{ g/cm}^3$ ) fall within the range of densities measured regionally on mafic metavolcanic bedrock samples.
- A single strongly magnetic, near-vertical zone was modelled to fit the prominent short wavelength, high amplitude magnetic anomaly at the centre of the Dayohessarah greenstone belt (located approximately 4 km from the west end of the profile). The remainder of the greenstone belt was modelled as non-magnetic and is typically less magnetic than the regional background of the Strickland pluton across the profile. Remanent magnetization could be introduced within the belt to model the magnetic signal. Alternatively, the magnetic low of the Dayohessarah greenstone belt could be modelled by assigning a non-zero magnetic susceptibility to all other rocks along the profile while assigning zero magnetic susceptibility to rocks within the Dayohessarah greenstone belt.
- The Strickland pluton has been modelled as a relatively flat, tabular body with depth extent of approximately 2.3 km below MSL. This model maintains the tabular structure of the Strickland pluton by assigning a variable density to near-vertical blocks within the pluton. An alternative model with a constant density throughout the Strickland pluton is explored in Section 5.2.2.2.
- An approximately 2 km wide block at the western end of the Strickland pluton was modelled with a density of  $2.64 \text{ g/cm}^3$  equal to the density determined for a single trondhjemite sample taken 7 km south of the center of the profile line. The next block, stretching from 7.5 km to 12 km from the west end of the profile has an increased density of  $2.68 \text{ g/cc}$ . The eastern edge of this higher density block corresponds to the G-D1 edge defined during the qualitative interpretation. There is an approximately 2 mGal amplitude, 2 km wide gravity anomaly centered at approximately 8 km from the west end of the profile which is not modelled. Previous mapping along the western boundary of the Strickland pluton shows the presence of gneissic rocks in this area (P0288; P0227; M2129, Stott et al., 1995a; Stott et al., 1995b; Fenwick, 1967). The inclusion of a higher density unit here may reflect the presence of a gneissic tonalite suite of rocks between the margin of the greenstone belt and the more homogeneous granitic units of the Strickland pluton.

- The Strickland pluton, from 12 km to 26 km from the west end of the profile, is modelled by a series of blocks of decreasing density followed by blocks of increasing density up to 31 km. A density of 2.62 g/cm<sup>3</sup> is used from 12 km to 16 km, 2.60 g/cm<sup>3</sup> from 16 km to 19 km, 2.58 g/cm<sup>3</sup> from 19 km to 26 km, 2.59 g/cm<sup>3</sup> from 26 km to 28 km, and 2.62 g/cm<sup>3</sup> from 28 km to 31 km. The density changes reflect the variation in gravity across the pluton, which is lowest between 19 km and 26 km. The depth to base of the pluton is kept relatively constant across the pluton at 2.3 km below MSL. Below the pluton, gneissic tonalite rocks extend to 6.7 km below MSL to the contact with undifferentiated basement. Gneissic tonalite rocks across the whole profile line were modelled with a constant density of 2.66 g/cm<sup>3</sup>.
- The background magnetic anomaly within the Strickland pluton has fairly low amplitude. There are a number of short-wavelength anomalies with amplitudes around 100 nT which correspond to mafic dykes which cross-cut the Strickland pluton, particularly on the western side of the pluton. One prominent short wavelength, high amplitude magnetic anomaly associated with a Biscotasing dyke was included in the model at 18.75 km. There are also some subtle longer wavelength variations of the magnetic data from 25.5 km to 31 km along the profile. An area of Strickland pluton was modelled with an increased magnetic susceptibility between 25.5 km and 28 km adjacent to another more magnetic block between 28 km and 30 km along the profile. These areas correspond to a broad increase in the magnetic anomaly visible in the data on the eastern side of the Strickland pluton.
- Gneissic tonalites have been mapped at the surface at 32 km from the west end of the profile (OGS, 2011). A small body of gneissic tonalite was included in the model as a shallow inlier with a maximum depth of approximately 0.4 km below MSL, surrounded by granitoid bedrock of the Strickland pluton. There are no obvious magnetic or gravity anomalies associated with this gneissic tonalite body except for a subtle magnetic fabric, perhaps representing gneissic layering, paralleling the boundary of the greenstone belt. The body is modelled with a density of 2.66 g/cm<sup>3</sup> which is slightly denser than that assigned to the Strickland pluton on its western side (2.62 g/cm<sup>3</sup>) and eastern side (2.64 g/cm<sup>3</sup>) and the same density assigned to the gneissic tonalite modelled below the Strickland pluton. Both the gneissic tonalite and the Strickland pluton have been modelled as non-magnetic, which appears to fit the general trend of the background magnetic anomaly. As there is little physical property contrast between gneissic tonalite unit and the Strickland pluton, as well as an absence of structural measurements from historic base maps, the geometry and structure of the gneissic tonalite body is essentially unconstrained by the geophysical data. An alternate geometry is presented in “Alternative Model Line 1” in Section 5.2.2.2.
- On the eastern edge of the profile, the Kabinakagami Lake greenstone belt has been modelled as a relatively wide synform extending to a depth of approximately 2.2 km below MSL using a density of 2.85 g/cm<sup>3</sup>. Density measurement taken on 8 samples of mafic rocks within the belt ranged from 2.86 g/cm<sup>3</sup> to 2.99 g/cm<sup>3</sup> (Haus and Pauk, 2010). When modelled with a density of 2.99 g/cm<sup>3</sup> the greenstone belt has a maximum depth of approximately only 1 km below MSL, however the profile transects the greenstone belt at a non-orthogonal angle to its mapped boundary and does not intersect the most intense gravity anomaly associated with it. The mapped western edge of the greenstone belt does not coincide with the edge of the gravity high anomaly and so the model includes a thin wedge of the greenstone with a lower density (2.75 g/cm<sup>3</sup>) in this region. Siragusa (1977) noted that the contact between the metavolcanic rocks of the greenstone belt and the granitic rocks of the Strickland pluton is

largely unexposed, which could explain the mismatch.

- The Kabinakagami Lake greenstone belt locally produces several high amplitude, short wavelength magnetic anomalies which have been modelled as a series of thin, near-vertical zones near the centre of the belt. The majority of the greenstone belt was modelled as non-magnetic. Two wedges of mafic metavolcanic rock were mapped at 46 km and 48.5 km, and are modelled as encapsulated by metasediments that fold into the centre of the belt on its eastern side. These bodies produce subtle magnetic anomalies but are located farther east than the gravity data.
- At the eastern end of the profile line, west of approximately 49 km, a zone of foliated tonalite bedrock was mapped east of the Kabinakagami Lake greenstone belt (OGS, 2011). The model has incorporated this zone as dipping under the core of the Kabinakagami Lake greenstone belt. Siragusa (1977) identified moderately to steeply west dipping schistosity and gneissosity, similar to adjacent metasedimentary rocks, but the relationship between this unit and the Kabinakagami greenstone belt at depth is unclear. This unit is similar to the Anahareo pluton mapped by Siragusa (1977; 1978) immediately to the west (AECOM, 2014a). No petrophysical measurements were available for the unit.

#### **5.2.2.2 Alternative Model Line 1 (Figure 5.10)**

For this alternative model for Line 1 a constant density is assigned to the Strickland pluton. The model makes the assumption that the relief at the base of the pluton, rather than internal density variations, is the controlling factor in producing the Bouguer gravity anomalies along the profile.

- The structure and density of the Dayohessarah and Kabinakagami Lake greenstone belts is generally the same in this model as in the initial model. The key difference between this model and the initial model is the depth to base of the Strickland pluton. In the initial model the pluton was modelled as a relatively flat tabular body with maximum depth to base of approximately 2.3 km below MSL and the density of the pluton varied in order to produce the gravity anomaly. The alternative model uses a constant density of 2.60 g/cm<sup>3</sup> for the Strickland pluton, with relief at its base to produce the gravity anomaly. This changes the structure of the pluton in a number of ways.
- The depth to the base of the Strickland pluton from the contact with the Dayohessarah greenstone belt at 5 km to approximately 12 km is modelled as very shallow, with a minimum total thickness of about 100 m. Where the pluton is thin the reduction in the thickness of the pluton alone is not sufficient to create a gravity anomaly to fit the Bouguer gravity data and therefore a 2 km thick body of denser gneissic tonalite (2.69 g/cm<sup>3</sup>) was included below. If the Strickland plutonic rock is completely removed from this area and gneissic tonalitic rock with a density of 2.66 g/cm<sup>3</sup> is exposed at surface, the gravity anomaly produced is still insufficient without the inclusion of an additional body whose density is greater than 2.66 g/cm<sup>3</sup>.
- The broad gravity low that extends from approximately 12 km to 31 km is explained in this model by a convex shape for the Strickland pluton with a maximum depth to base of approximately 4 km below MSL at 23 km from the western side of the profile. A density of 2.60 g/cm<sup>3</sup> was used throughout the pluton. Density measurements on granitoid samples taken within this pluton range from 2.64 g/cm<sup>3</sup> to 2.71 g/cm<sup>3</sup>. A higher density has the effect of increasing the depth to base of the pluton. If 2.64 g/cm<sup>3</sup> is used, the maximum depth to base of



the pluton increases to over 15 km below MSL. If the minimum density value measured in the Anahareo pluton ( $2.52 \text{ g/cm}^3$ ) is also considered for the Strickland pluton, the base of the pluton shallows to a maximum depth of approximately 1.2 km below MSL.

- A second change introduced into the alternative model relates to the structural relationship between the Strickland pluton and the gneissic tonalite at 32 km. In the initial model, this zone of gneissic tonalite was mapped as an inlier surrounded and underlain by the Strickland pluton. In the alternative model, the Strickland pluton pinches out eastwards and the top of the gneissic tonalite, which underlays all of the Strickland pluton, comes up to surface. On the eastern side of the gneissic tonalite, east of 33 km, the Strickland pluton reappears and dips eastward under the Kabinakagami greenstone belt. As was previously mentioned, there is no gravity or magnetic anomaly associated with this contact and as such this relationship is poorly constrained by the data.

### **5.2.2.3 Initial Model Line 2 (Figure 5.11)**

As shown in Figures 5.7 and 5.8, Line 2 runs south to north and begins at the southern edge of the Anahareo pluton, extending north across the gneissic tonalite suite and into the Strickland pluton (Figure 5.11). The line continues north into the Hornepayne area (SGL, 2016a); however only the portion of the profile within the White River area is described below.

- The Anahareo pluton covers the southern half of the profile. The pluton has been modelled extending to approximately 2 km below MSL at its southern end, deepening to approximately 2.3 km at the northern side. The northern and southern boundaries of the pluton are modeled to dip steeply where it is mapped in contact with gneissic tonalite bedrock of the Pukaskwa batholith at the surface (Santaguida, 2001; OGS, 2011). The Anahareo pluton is modelled as underlain by gneissic tonalites of the Pukaskwa batholith, which are in turn underlain by undifferentiated basement at approximately 6.7 km below MSL. The gravity over the pluton is a broad low with a number of superimposed low amplitude ( $<1 \text{ mGal}$ ), short wavelength (2 km) near surface anomalies which were not accounted for in the model. The pluton was modelled as a series of vertical sided blocks with different densities ranging from  $2.58 \text{ g/cm}^3$  to  $2.70 \text{ g/cm}^3$  so as to minimize relief of the base of the pluton. The south side of the pluton has been modelled with a density of  $2.61 \text{ g/cm}^3$ . A 4 mGal gravity anomaly is recorded at approximately 5 km. To model this anomaly, a block with density of  $2.70 \text{ g/cm}^3$  was used. This block does not correlate to any mapped structure, but does correlate to a group of Matachewan dykes which could locally increase the bulk density of the bedrock. North of 12 km from the south end of the profile to approximately 22 km, the Anahareo pluton was modelled with a density of  $2.58 \text{ g/cm}^3$ . This area correlates to the gravity anomaly defined by G-A6 of the qualitative interpretation. At 22 km, a 3 mGal gravity anomaly is encountered which was modelled with a density increase within the Anahareo pluton to  $2.64 \text{ g/cm}^3$ ,  $0.06 \text{ g/cm}^3$  higher than the rocks on either side. The width of the denser zone was determined by the Bouguer gravity trend analysis solutions. A thinner body than the one defined by trend analysis solutions with proportionately higher density would slightly improve the model fit. There is no obvious long wavelength magnetic signature in this area and no structural measurements are locally available.
- A number of density measurements are available from granitoid samples (granite, granodiorite, trondhjemite, quartz diorite) within the Anahareo pluton, with density values ranging from  $2.52 \text{ g/cm}^3$  to  $2.72 \text{ g/cm}^3$  (GSC, 2015; Haus and Pauk, 2010). Samples identified as tuff/chert were

also measured close to the profile line (within the Anahareo pluton, Pukaskwa batholith and Kabinakagami greenstone belt) and had densities ranging from 2.76 g/cm<sup>3</sup> to 3.06 g/cm<sup>3</sup>. Though the density values showed no obvious spatial correlation to the observed gravity data, the range of densities encountered suggests that lithological variations may be a contributing factor in the variable gravity signature within the pluton; samples within a small area on the Anahareo pluton often have a wide range of lithologies and associated density values.

- In order to approximate the general trend of the magnetic anomaly for the Anahareo pluton it was modelled as non-magnetic. No measured magnetic susceptibility values are available for this unit. Despite the pluton unit being modeled as non-magnetic, the measured magnetic anomaly tends to have a lower magnitude compared to the model. This may indicate some degree of magnetic remanence preserved in the bedrock that has not been accounted for in the model. Two prominent linear magnetic anomalies associated with diabase dykes were included within the model, though many more similar but lower amplitude magnetic anomalies occur in the area of the pluton.
- The contact between the Pukaskwa batholith and the Anahareo pluton occurs at approximately 26 km from the south end of the profile. Immediately to the north of the contact is a 6 mGal, 2 km wide gravity anomaly which can be modelled with a 2 km wide denser block. On the northern side of this dense block is the western tip of the Kabinakagami Lake greenstone belt, which by itself is too small to model the gravity anomaly. A number of greenstone bodies have been mapped adjacent to this area at surface (see M2129, M2392; Fenwick, 1967; Siragusa, 1978) and the presence of more mafic metavolcanic rocks, either at the surface or at depth, is likely the cause of this anomaly. This anomaly has been modelled by a near-vertical block with a density 2.68 g/cm<sup>3</sup> extending to appropriately 6.7 km to the undifferentiated basement. A small sliver of the mapped volcanics is included in the model although it is not required by the geophysical data. The anomaly may also be modelled with a slightly higher density, with a reduced depth. For example, if the body is assigned a density of 2.70 g/cm<sup>3</sup> the anomaly can be modelled with a block extending to approximately 1 km below MSL underlain by gneissic tonalite with a density of 2.66 g/cm<sup>3</sup> (the same density assigned to the gneissic tonalite just to the south). The total depth of the tonalite of the Pukaskwa batholith to the top of the undifferentiated basement is approximately 6.7 km and is not affected by these changes.
- Magnetic data at approximately 26 km shows some short-wavelength anomalies related to cross-cutting Matachewan dykes and there is no obvious magnetic signature along the profile line associated with the Anahareo pluton, Pukaskwa batholith and Kabinakagami Lake greenstone units.
- A broad Bouguer gravity low occurs from approximately 28 km from the south end of the profile to about 42 km. The gravity low corresponds to the anomaly G-A1 identified in the qualitative interpretation and transects both gneissic tonalites of the Pukaskwa batholith and granite-granodiorites of the Strickland pluton without an associated gravity anomaly at the geologic contact. For the initial model this anomaly within the Pukaskwa batholith has been modelled as a vertical sided body that extends to approximately 6.7 km below MSL using a density of 2.60 g/cm<sup>3</sup>. It is possible to raise the depth to undifferentiated basement by lowering the density of the gneissic tonalite rock between 28 km and 33 km. A density of 2.58 g/cm<sup>3</sup> would raise the base of the Pukaskwa batholith to approximately 4.5 km below MSL. On the other hand, a density for the Pukaskwa batholith higher than 2.60 g/cm<sup>3</sup> for this area would increase the

depth to undifferentiated basement. No density measurements were available immediately adjacent to the profile line, however a sample of gneiss approximately 16 km to the west, within the Pukaskwa batholith, yielded a density of 2.67 g/cm<sup>3</sup>. The magnetic background data within this section of the Pukaskwa batholith is slightly elevated relative to the denser block of Pukaskwa batholith between 26 and 28 km. Generally the magnetic background increases from 28 km northwards into the Strickland pluton, which is modelled by increasing the magnetic susceptibility of the bedrock units northwards.

- The Strickland pluton produces no distinguishing gravity or magnetic anomaly at its southern contact with the Pukaskwa batholith at approximately 33 km and is a continuum of the gravity low beginning in the Pukaskwa batholith to the south. Gravity generally increases northwards with some minor (<1 mGal) short wavelength variations. The magnetic background within the pluton is generally higher than in the adjacent Pukaskwa batholith to the south and Black-Pic batholith to the north, and also higher than the Anahareo pluton. A number of short-wavelength anomalies are visible within the pluton that correspond to cross-cutting dykes. The Strickland pluton has been modelled to a depth of approximately 2.3 km below MSL and is underlain by gneissic tonalite rock which extends to approximately 6.7 km below MSL. The pluton is modelled with a density of 2.58 g/cm<sup>3</sup> from 33 km to 44 km which is the northern boundary of the anomaly G-A1 (Figures 5.1-5.3). The density of the pluton increases to 2.60 g/cm<sup>3</sup> between 44 km to 46 km, 2.62 g/cm<sup>3</sup> between 46 km to 50 km, and 2.66 g/cm<sup>3</sup> between 50 km to 52 km at the northern contact of the Strickland pluton and Black-Pic batholith. A variable density across the pluton allows for the base of the pluton to remain relatively flat around 2.3 km below MSL. If the density of the pluton is increased or decreased, the thickness of the pluton increases or decreases correspondingly. For example, if the density of the pluton is increased from 2.58 g/cm<sup>3</sup> to 2.60 g/cm<sup>3</sup> between 33 km to 45 km, the depth to gneissic tonalite increases to approximately 4 km below MSL. A similar increase in density on the northern side of the pluton (from 45 km to 52 km) is required if the flat tabular structure is to be retained.
- The Strickland pluton is modelled as underlain by a uniformly dense layer of gneissic tonalite rock (2.66 g/cm<sup>3</sup>) which has a constant depth to undifferentiated basement of approximately 6.7 km. The depth to base of the gneissic tonalite is relatively constant throughout the entire profile line and because it is flat and has a mostly constant density, its depth is not well constrained. The depth to undifferentiated basement has been modelled to be consistent with the depth to undifferentiated basement elsewhere (SGL, 2016a; SGL, 2016b) and is principally controlled by the density of gneissic tonalite bodies modelled between 25 km and 33 km and north of 52 km when have been assigned a densities of 2.68 g/cm<sup>3</sup> from 26 km to 28 km, 2.60 g/cm<sup>3</sup> from 28 km and 33 km, and 2.67 g/cm<sup>3</sup> north of 52 km. If the depth to undifferentiated base is increased, or decreased (i.e. the layer of gneissic tonalite is thickened or thinned) the density of these blocks would have to be decreased or increased respectively.
- North of 52 km from the south end of the profile, gneissic tonalites of the Black-Pic batholith have been mapped at surface north of the Strickland pluton (OGS, 2011). The Bouguer gravity continues to increase from this point north to end of the profile. The Black-Pic batholith has been modelled with a density of 2.67 g/cm<sup>3</sup> which increases to 2.70 g/cm<sup>3</sup> north of 55 km. A small wedge of mafic metavolcanics has been mapped at surface and included in the model at approximately 56 km. The mafic metavolcanic body produces a small magnetic anomaly but no disenable gravity anomaly. The profile from this point continues into the Hornepayne area to the north and is discussed in a separate report (SGL, 2016a).

#### 5.2.2.4 *Alternative Model Line 2 (Figure 5.12)*

For this alternative model for Line 2 a constant density is assigned to the Anahareo and Strickland plutons. The model makes the assumption that the Bouguer gravity anomalies are caused solely by the structure and relief at the base of the plutons. The density of gneissic tonalites of the Pukaskwa batholith is kept constant from the south end of the profile until at approximately 52 km; density within the Black-Pic batholith increases. The depth to undifferentiated basement is constant at approximately 6.7 km below MSL across the entire profile line.

- Both the Anahareo and Strickland plutons were modelled with a constant density of  $2.60 \text{ g/cm}^3$ . With this density, the southern portion of the Anahareo pluton between 0 km and 5 km is modelled down to a maximum depth to base of 1.5 km; the depth to base increases to a maximum of 3.6 km below MSL in the northern portion of the pluton, between 5 km and 26 km. At 5 km there is a 4 mGal gravity anomaly, in an area where the Anahareo pluton is modelled to thin to approximately 300 m; however, the model does not produce a gravity anomaly with an amplitude large enough to completely match the Bouguer gravity data. Even reducing the thickness of Anahareo pluton to zero at this location so that the gneissic tonalite occurs at the surface, the model does not produce a fit to the data; to achieve that a small zone with a density higher than  $2.66 \text{ g/cm}^3$  is required, though not included in this alternative model. Another gravity anomaly within the Anahareo pluton at 22 km, which was modelled using a more dense area in the initial model, could not be fit by varying the relief at the base of Anahareo pluton alone; a zone of increased density beneath the pluton is also required in the alternative model. A number of density measurements are available close to the profile line within the Anahareo pluton. These samples range in density from  $2.52 \text{ g/cm}^3$  to  $2.72 \text{ g/cm}^3$  for granitoid samples (GSC, 2015; Haus and Pauk, 2010). If the model is changed to use the lowest measured density value (i.e.  $2.52 \text{ g/cm}^3$ ) the depth to base of the Anahareo pluton would decrease to approximately 1.1 km below MSL. Conversely, if a density value greater than  $2.60 \text{ g/cm}^3$  is used, the depth to base will be greater than 3.6 km.
- The Strickland pluton is modelled with a constant density of  $2.60 \text{ g/cm}^3$  and is assumed to be the sole cause of the gravity low measured between 28 km and 42 km. As a result, the southern boundary of the Strickland pluton incorporated into the model is based on the position of the edge of the gravity low anomaly and is located approximately 3 km further to the south compared to the initial model. With this assumption the pluton is modelled as being thickest in its southern portion corresponding to the lowest gravity response, with a maximum depth to base of approximately 5.5 km below MSL at 30 km from the south end of the profile. The modelled thickness of the Strickland pluton in this alternative profile decreases northwards towards its contact with the Black-Pic batholith. The south side of the pluton is modelled to be consistent with the mapped geologic contacts (OGS, 2011) and therefore a very thin (approximately 100 m total thickness) wedge of gneissic tonalite is required above the pluton between 29 km and 33 km. Removing this wedge would slightly decrease the depth to base of the Strickland pluton. Fewer density samples were available for the Strickland pluton than the Anahareo pluton. Density values range from  $2.64 \text{ g/cm}^3$  to  $2.70 \text{ g/cm}^3$  for granitoid samples. A larger density value has the effect of extending the depth to base of the Strickland pluton. If a density of  $2.64 \text{ g/cm}^3$  is used for the pluton, the maximum depth of the pluton is extended to approximately 15 km below MSL, and by doing so, the depth to undifferentiated basement below the gneissic tonalite unit is also extended. If a density of  $2.52 \text{ g/cm}^3$  is used (i.e. the

minimum density values measured within the Anahareo pluton) the depth to base of the Strickland pluton is reduced to approximately 1.6 km below MSL.

## 6 SUMMARY OF RESULTS

The following provides a summary of the qualitative observations and the preliminary 2.5D modeling of the geophysical data, with a focus on two of the areas identified during Phase 1 as being potentially suitable located within the Strickland and Anahareo plutons.

### ***Strickland Pluton***

- The Strickland pluton encompasses a large central gravity low which continues into the Pukaskwa batholith to the south with no associated change across the mapped boundary. The gravity low represents either the thickest section of the pluton and batholith and/or the lowest density. Magnetic anomalies through the pluton are due to a number of distinct dyke swarms trending northwest and northeast with little horizontal offset since emplacement. Locally, several large-scale folds were identified within the pluton highlighting some degree of deformation.
- Boundaries of the Strickland pluton are defined in both the magnetic and gravity data. The southern to southeastern boundary is defined by a prominent magnetic and gravity gradient associated with the edge of the mapped Kabinakagami greenstone belt. Within the western margin of Strickland pluton similar gradients are associated with the edge of the Dayohessarah greenstone belt and is interpreted as a lithological variation between gneissic rocks adjacent to the greenstone belt and the granitic rock of the central portion of the Strickland pluton.
- The southern boundary of the Strickland pluton is marked by a zone with a well-defined internal magnetic fabric. This zone extends from the western side of the Kabinakagami Lake greenstone belt and is interpreted to connect to the Dayohessarah greenstone belt. This anomaly does not correlate to any mapped geologic structure or contact, however historic bedrock mapping in the area did identified several small bodies of mafic metavolcanic rocks in granitic gneiss within the same zone.
- Within the Strickland pluton two magnetic anomalies, with corresponding gravity anomalies, have been identified near to the Kabinakagami Lake greenstone belt. These anomalies likely represent outliers of mafic metavolcanic of the Kabinakagami Lake greenstone belt. Localized outliers of mafic metavolcanics have been observed from historic mapping in proximity to the Kabinakagami Lake greenstone belt.
- The Strickland pluton has been modelled with a depth of approximately 2.3 km below MSL when modelled with internal density variations. Internal density variations are used to limit the relief at the base of the pluton and maintain the structure of the pluton as a relatively flat, tabular body. By contrast if a constant density is used, the pluton is modelled as very thin on its western side where it is in contact with the Dayohessarah greenstone belt (approximately 100 m minimum total thickness) and deep in the central part of the pluton (approximately 4 km below MSL). If a constant density is used, the depth to base of the pluton is highly dependent upon the density value chosen. On the eastern side of the Strickland pluton, its structure and thickness are not well constrained as there is very little physical property contrast between the granite-granodiorite of the pluton and gneissic tonalite rocks mapped at surface.
- The Strickland pluton is underlain by a layer of gneissic tonalite rock that overlies undifferentiated basement at approximately 6.7 km below MSL. This depth of the relatively flat basement is not well constrained by the modelling.

## **Anahareo Pluton**

- The Anahareo pluton generates an irregularly shaped local gravity low within a larger east-west trending regional gravity low. The local gravity low continues into the Pukaskwa batholith to the north with no discernible change in the observed gravity associated with the transition. The gravity low represents either the thickest section of the pluton and batholith and/or the lowest density. Magnetic data in the area of the pluton includes linear anomalies due to distinct dyke swarms that trend northwest and northeast with little horizontal offset since emplacement. The background magnetic anomaly of the pluton varies but generally increases towards the southwest.
- Southwest of the Kabinakagami greenstone belt a magnetic anomaly has been interpreted as a body of mafic metavolcanic rock hosted within the Anahareo pluton. Several small bodies of mafic metavolcanic rocks have been mapped in this area and may suggest a presence of mafic metavolcanics at surface or at depth.
- The Anahareo pluton has been modelled with a maximum depth to base of approximately 2.3 km by allowing the internal density to vary. A constant density model for the Anahareo pluton was also created; in this alternative model the Anahareo pluton has a maximum depth to base of approximately 3.6 km below MSL in the northern portion of the pluton along the profile line. If a constant density is used for the Anahareo pluton, the amplitude and frequency of the short wavelength gravity anomalies cannot be accommodated by structure and relief at the base of the pluton alone. Additional high density blocks beneath the pluton are required.
- The Anahareo pluton was modelled as underlain by a layer of gneissic tonalite which extends to a nearly flat basement at approximately 6.7 km below MSL, but as with the Strickland pluton, the depth estimates for the contact between the gneissic tonalite and undifferentiated basement is not well defined.

For the modelling results, it is important to emphasize that the accuracy of these preliminary models is limited at this early stage of the assessment due to limited availability of bedrock densities and magnetic susceptibilities that are key for constraining the model. It is anticipated that the preliminary 2.5D models would be revised and refined if more field data is collected in the future.





## 7 REFERENCES

- AMEC, 2017. Phase 2 Geoscientific Preliminary Assessment, Initial Findings, Township of White River and Area, Ontario. Report prepared for NWMO, APM-REP-01332-0212.
- AECOM, 2014a: Phase 1 Geoscientific Desktop Preliminary Assessment of Potential Suitability for Siting a Deep Geological Repository for Canada's Used Nuclear Fuel. Township of White River, Ontario. Report prepared for NWMO, November 2014. APM-REP-06144-0083. Report available at [www.nwmo.ca](http://www.nwmo.ca)
- AECOM, 2014b: Phase 1 Geoscientific Desktop Preliminary Assessment Terrain and Remote Sensing Study. Township of White River, Ontario. Report prepared for NWMO, November 2014. APM-REP-06144-0084. Report available at [www.nwmo.ca](http://www.nwmo.ca)
- Baranov, V., and Naudy, H. 1964. Numerical Calculation of the Formula of Reduction to the Magnetic Pole. *Geophysics*, **29**: 67-79.
- Barnett, P.J. 1992. Quaternary Geology of Ontario; In: *Geology of Ontario*, Ontario Geological Survey, Special Volume 4, Part 2, 1010–1088.
- Beakhouse, G.P. and Lin, S. 2006. Tectonic significance of the Pukaskwa batholith with the Hemlo and Mishibishu greenstone belts; Ontario Geological Survey, Open File Report 6192, 7-1 to 7-7.
- Beakhouse, G.P., Lin, S. and Kamo, S.L. 2011. Magnetic and tectonic emplacement of the Pukaskwa batholith, Superior Province, Ontario, Canada. *Canadian Journal of Earth Science*, **48**: 187-204.
- Berman, R.G., Easton, R.M. and Nadeau, L. 2000. A New Tectonometamorphic Map of the Canadian Shield: Introduction; *The Canadian Mineralogist*, **38**: 277-285.
- Berman, R.G., Sanborn-Barrie, M., Stern, R.A. and Carson, C.J. 2005. Tectonometamorphism at ca. 2.35 and 1.85 Ga: In: the Rae Domain, western Churchill Province, Nunavut, Canada: Insights from structural, metamorphic and in situ geochronological analysis of the southwestern Committee Bay Belt; *The Canadian Mineralogist*, **43**: 409-442.
- Blakely, R.J. 1996. *Potential Theory in Gravity and Magnetic Applications*. Cambridge University Press.
- Bleeker, W. and Hall, B. 2007. The Slave Craton: Geology and metallogenic evolution; In Goodfellow, W.D., ed., *Mineral Deposits of Canada: A Synthesis of Major Deposit-Types, District Metallogeny, the Evolution of Geological Provinces, and Exploration Methods*: Geological Association of Canada, Mineral Deposits Division, Special Publication No. 5, 849-879
- Breaks, F.W. and Bond, W.D. 1993. The English River Subprovince – An Archean Gneiss Belt: Geology, geochemistry and associated mineralization; Ontario Geological Survey, Open File Report 5846, **1**: 483.
- Briggs, I.C. 1974. Machine contouring using minimum curvature, *Geophysics*, **39**: no. 1, 39-48.
- Buchan K.L., Halls, H.C., and Mortensen, J.K. 1996. Paleomagnetism, U-Pb geochronology, and geochemistry of Marathon dykes, Superior Province, and comparison with the Fort Frances swarm; *Canadian Journal of Earth Sciences*, **33**: 1583-1595.

- Buchan, K.L., and Ernst, R.E. 2004. Diabase dyke swarms and related units in Canada and adjacent regions; Geological Survey of Canada, Map 2022A, scale 1:5,000,000.
- Corfu, F. and Muir, T.L. 1989. The Hemlo-Heron Bay greenstone belt and Hemlo Au-Mo deposit, Superior Province, Ontario, Canada: 1. Sequence of igneous activity determined by zircon U-Pb geochronology; *Chemical Geology*, **79**: 183-200.
- Corfu, F. and Stott, G.M. 1996. Hf isotopic composition and age constraints on the evolution of the Archean central Uchi Subprovince, Ontario, Canada. *Precambrian Research*, **78**: 53-63
- Corfu, F., Stott, G.M. and Breaks, F.W. 1995. U-Pb geochronology and evolution of the English River subprovince, an Archean low P – high T metasedimentary belt in the Superior Province. *Tectonics*, **14**: 1220-1233
- Corrigan, D., Galley, A.G. and Pehrsson, S. 2007. Tectonic evolution and metallogeny of the southwestern Trans-Hudson Orogen, in Goodfellow, W.D., ed., *Mineral Deposits of Canada: A Synthesis of Major Deposit-Types, District Metallogeny, the Evolution of Geological Provinces, and Exploration Methods*: Geological Association of Canada, Mineral Deposits Division, Special Publication No. 5, 881-902.
- Davis, D.W., and Lin, S. 2003. Unraveling the geologic history of the Hemlo Archean gold deposit, Superior Province, Canada; a U-Pb geochronological study; *Economic Geology and the Bulletin of the Society of Economic Geologists*, **98**, 51–67.
- Easton, R.M. 2000a. Metamorphism of the Canadian Shield, Ontario, Canada. I. The Superior Province; *The Canadian Mineralogist*, **38**: 287-317.
- Easton, R.M. 2000b. Metamorphism of the Canadian Shield, Ontario, Canada. II. Proterozoic metamorphic history; *The Canadian Mineralogist*, **38**: 319-344.
- Ernst, R.E., and Buchan, K.L. 1993. Paleomagnetism of the Abitibi dyke swarm, southern Superior Province, and implications for the Logan Loop. *Canadian Journal of Earth Sciences*, **30**: 1886-1897.
- Fenwick, K.G. 1966. Dayohessarah Lake area, Algoma District; Ontario Department of Mines, Map 2129, scale 1:26,720
- Fenwick, K.G. 1967. Geology of the Dayohessarah Lake Area, Ontario Department of Mines, Geological Report 49. Accompanied by Map 2129, Dayohessarah Lake area, District of Algoma, scale 1 inch to 2 miles.
- Fraser, J.A. and Heywood, W.W. (editors) 1978. *Metamorphism in the Canadian Shield*; Geological Survey of Canada, Paper 78-10.
- Gartner, J.F. and McQuay, D.F. 1980a. Obakamiga Lake Area (NTS 42F/SW). Districts of Algoma and Thunder Bay; Ontario Geological Survey, Northern Ontario Engineering Geology Terrain Study 45, 16p., Accompanied by Map 5084, scale 1:100,000.
- Gartner, J.F. and McQuay, D.F. 1980b. Kabinakagami Lake Area (NTS 42C/NE), District Algoma; Ontario Geological Survey, Northern Ontario Engineering Geology Terrain Study 62, Accompanied by Map 5095, scale 1:100,000.
- Geddes R.S. and Kristjansson, F.J. 1986. Quaternary geology of the White River area, Districts of Thunder Bay and Algoma; Ontario Geological Survey, Map P.2988, Geological Series-

Preliminary Map. scale 1:50,000.

- Geddes R.S. and Kristjansson. F.J. 2009. Quaternary Geology of the White River Area, northern Ontario; Ontario Geological Survey, Map 2682, scale 1:50,000.
- Geddes. R.S., Bajc, A.F. and Kristjansson, F.J. 1985. Quaternary Geology of the Hemlo Region, District of Thunder Bay; In: Summary of Field Work, 1985, Ontario Geological Survey, Ontario Geological Survey, Miscellaneous Paper 126, 151-154.
- Geosoft. 2015. Oasis montaj geophysical processing system, v 8.5.1, Geosoft Inc.
- GSC (Geological Survey of Canada). 2015. Bedrock densities and magnetic susceptibilities. Geoscience Data Repository for Geophysical and Geochemical Data, gdr.nrcan.gc.ca. (data accessed December 2015).
- Halls, H.C., Stott, G.M., Ernst, R.E. and Davis, D.W., 2006. A Paleoproterozoic mantle plume beneath the Lake Superior region; p.23-24 In: Institute on Lake Superior Geology, 52nd Annual Meeting Sault Ste Marie, Ontario, Part 1, Program and Abstracts.
- Hamilton M.A., David, D.W., Buchan, K.L., and Halls, H.C. 2002. Precise U-Pb dating of reversely magnetized Marathon diabase dykes and implications for emplacement of giant dyke swarms along the southern margin of the Superior Province, Ontario. Geological Survey of Canada, Current Research 2002-F6.
- Haus, M., and Pauk, T. 2010. Data from the PETROCH Lithogeochemical database, Ontario Geological Survey, Miscellaneous Release – Data 250, ISBN 978-1-4435-3732-2 [CD] ISBN 978-1-4435-3731-5 [zip file].
- Jackson, S.L. 1998. Stratigraphy, structure and metamorphism; Part 1, p.1--58, in S.L. Jackson, G.P. Beakhouse and D.W. Davis, Geological Setting of the Hemlo Gold Deposit; an Interim Progress Report, Ontario Geological Survey, Open File Report 5977.
- Jolly, W.T. 1978. Metamorphic history of the Archean Abitibi Belt; In: Metamorphism in the Canadian Shield; Geological Survey of Canada, Paper 78-10, 63-78.
- Kraus, J. and Menard, T. 1997. A thermal gradient at constant pressure: Implications for low- to medium-pressure metamorphism in a compressional tectonic setting, Flin Flon and Kisseynew domains, Trans-Hudson Orogen, Central Canada; The Canadian Mineralogist, **35**:, 1117-1136.
- Krogh, T.E., Corfu, F., Davis, D.W., Dunning, G.R., Heaman, L.M., Kamo, S.L., Machado, N., Greenough, J.D., and Nakamura, E. 1987. Precise U -Pb isotopic ages of diabase dykes and mafic to ultra mafic rocks using trace amounts of baddeleyite and zircon. In Mafic dyke swarms. Edited by H.C. Halls and W .F. Fahrig. Geological Association of Canada, Special Paper 34, 147-152.
- Leliak, P. 1961. Identification and evaluation of magnetic field sources of magnetic airborne detector equipped aircraft. IRE Transactions on Aerospace and Navigational Electronics, **8(3)**: 95-105.
- Lin, S. 2001. Stratigraphic and Structural Setting of the Hemlo Gold Deposit, Ontario, Canada. Economic Geology, **96**: 477–507.
- Lin, S., and Beakhouse, G.P. 2013. Synchronous vertical and horizontal tectonism at late stages of Archean cratonization and genesis of Hemlo gold deposit, Superior craton, Ontario, Canada, Geology, **41**: 359-362.

- MacLeod, I.N. 1993. 3-D Analytic Signal in the Interpretation of Total Magnetic Field Data at Low Magnetic Latitudes, *Exploration Geophysics*, **24**: 679-688.
- Mehnert, K.R. 1968. *Migmatites and the origin of granitic rocks*; Elsevier, Amsterdam.
- Menard, T. and Gordon, T.M. 1997. Metamorphic P-T paths from the Eastern Flin Flon Belt and Kiseeynew Domain, Snow Lake, Manitoba; *The Canadian Mineralogist*, **35**: 1093-1115.
- Miles, W.F. 1998. An Interpretation of high resolution aeromagnetic data over the Manitouwadge greenstone belt, Ontario, Canada; MSc Thesis, Ottawa-Carleton Geoscience Centre and University of Ottawa, Ottawa, Canada.
- Miller, H.G., and Singh, V. 1994. Potential field tilt – a new concept for location of potential field sources, *Journal of Applied Geophysics*, **32**: 213-217.
- Milne, V.G., 1968. Geology of the Black River area, District of Thunder Bay; Ontario Department of Mines, Geological Report 72.
- Milne, V.G., Giblin, P.E., Bennett, G., Thurston, P.C., Wolfe, W.J., Giguere, J.F., Leahy, E.J. and Rupert, R.J. 1972. Manitouwadge-Wawa sheet, geological compilation series, Algoma, Cochrane, Sudbury and Thunder Bay districts; Ontario Geological Survey, M2220, scale 1:253,440 or 1 inch to 4 miles.
- Muir, T.L. 2013. Ontario Precambrian Bedrock Magnetic Susceptibility Geodatabase for 2001 to 2012, Ontario Geological Survey, Miscellaneous Release – Data 273 – Revised.
- Muir, T.L. 2003. Structural evolution of the Hemlo greenstone belt in the vicinity of the world-class Hemlo gold deposit. *Canadian Journal of Earth Sciences*, **40**: 395-430.
- Muir, T.L., 2000. Geologic compilation of the eastern half of the Schreiber-Hemlo greenstone belt; Ontario Geological Survey, Map 2614, scale 1:50,000.
- Nabighian, M.N. 1972. The analytic signal of two-dimensional magnetic bodies with polygonal cross-section: Its properties and use for automated anomaly interpretation. *Geophysics*, **37**: 507-517.
- Nuclear Waste Management Organization (NWMO). 2014. Preliminary Assessment for Siting a Deep Geological Repository for Canada's Used Nuclear Fuel - Township of White River, Ontario - Findings from Phase One Studies. NWMO Report Number: APM-REP-06144-0081.
- OGS (Ontario Geological Survey). 2011. 1:250 000 Scale Bedrock Geology of Ontario, Ontario Geological Survey, Miscellaneous Release – Data 126 – Revision 1.
- Osmani, I.A. 1991. Proterozoic mafic dyke swarms in the Superior Province of Ontario. in *Geology of Ontario*, Ontario Geological Survey, Special Volume 4, Part 1, 661-681
- Pease, V., Percival, J., Smithies, H., Stevens, G. and Van Kranendonk, M. 2008. When did plate tectonics begin? Evidence from the orogenic record; In: Condie, K.C. and Pease, V., eds., *When Did Plate Tectonics Begin on Earth?*; Geological Society of America Special Paper 440, 199-228.
- Percival, J.A., Sanborn-Barrie, M., Skulski, T., Stott, G.M., Helmstaedt, H. and White, D.J. 2006. Tectonic evolution of the western Superior Province from NATMAP and Lithoprobe studies; *Can. J. Earth Sciences* **43**: 1085-1117.
- Peterson, V.L., and Zaleski, E. 1999. Structural history of the Manitouwadge greenstone belt and its

- volcanogenic Cu-Zn massive sulphide deposits, Wawa Subprovince, south-central Superior Province; *Can. Jour. of Earth Sciences*, **36**: 605-625.
- PGW (Paterson, Grant & Watson Ltd.). 2014. Phase 1 Geoscientific Desktop Preliminary Assessment, Processing and Interpretation of Geophysical Data. Township of White River, Ontario. Prepared for Nuclear Waste Management Organization (NWMO). NWMO Report APM-REP-06144-0085. Toronto, Canada.
- Phillips, J.D. 1997. Potential-field geophysical software for the PC, version 2.2, U.S. Geological Survey Open-File Report 97-725.
- Phillips, J.D. 2000. Locating magnetic contacts: a comparison of the horizontal gradient, analytic signal, and local wavenumber methods, *Society of Exploration Geophysics, Expanded Abstracts with Biographies, 2000 Technical Program*, **1**: 402-405.
- Polat, A. 1998. Geodynamics of the Late Archean Wawa Subprovince greenstone belts, Superior Province, Canada. PhD Thesis, Department of Geological Sciences, University of Saskatchewan, Saskatoon.
- Powell, W.G., Carmichael, D.M. and Hodgson, C.J. 1993. Thermobarometry in a subgreenschist to greenschist transition in metabasites of the Abitibi greenstone belt, Superior Province, Canada; *J. Metamorphic Geology*, **11**: 165-178.
- Roest, W., and Pilkington, M., 1993. Identifying Remanent Magnetization Effects in Magnetic Data, *Geophysics*, **58**: no. 5, 653-659.
- Salem, A., Williams, S., Fairhead, J. D., Ravat, D., and Smith, R. 2007. Tilt-depth method: A Simple depth estimation method using first-order magnetic derivatives, *The Leading Edge*, **26**: 1502-1505.
- Santaguida, F. 2001. Precambrian geology compilation series - White River sheet; Ontario Geological Survey, Map 2666, Scale 1:250,000.
- Sawyer, E.W. 2008. Atlas of Migmatites; The Canadian Mineralogist Special Publication 9; Mineralogical Association of Canada, NRC Research Press, Ottawa.
- Schandl, E.S., Davis, D.W., Gorton, M.P., and Wasteneys, I.A. 1991. Geochronology of hydrothermal alteration around volcanic-hosted massive sulphide deposits in the Superior Province; Ontario Geological Survey, Miscellaneous Paper 156, 105-120.
- SGL (Sander Geophysics Limited). 2016a. Phase 2 Geoscientific Preliminary Assessment, Acquisition, Processing and Interpretation of High-Resolution Airborne Geophysical Data, Township of Hornepayne and Area, Ontario. Prepared for Nuclear Waste Management Organization (NWMO). NWMO Report Number: APM-REP-01332-0205.
- SGL (Sander Geophysics Limited). 2016b. Phase 2 Geoscientific Preliminary Assessment, Acquisition, Processing and Interpretation of High-Resolution Airborne Geophysical Data, Township of Manitouwadge and Area, Ontario. Prepared for Nuclear Waste Management Organization (NWMO). NWMO Report Number: APM-REP-01332-0213.
- Siragusa, G.M. 1977. Geology of the Kabinakagami Lake area, District of Algoma; Ontario Division of Mines, Geoscience Report 159, including Map 2355, scale 1:63 360.
- Siragusa, G.M. 1978. Geology of the Esnagi Lake area, District of Algoma; Ontario Division of Mines,

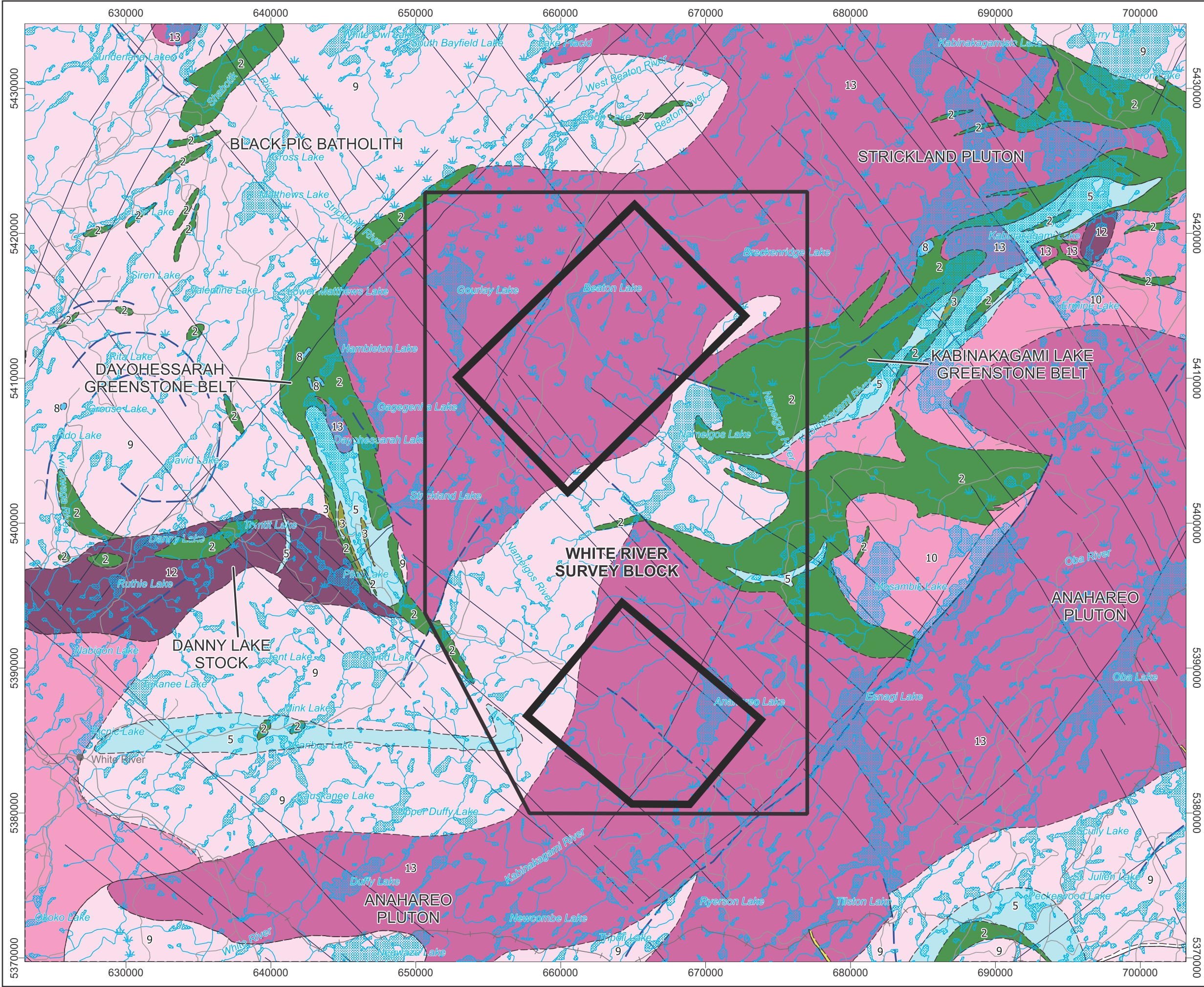
- Geoscience Report 176, including Map 2382, scale 1:63 360.
- SRK Consulting Inc., 2014. Phase 1 Geoscientific Desktop Preliminary Assessment, Lineament Interpretation, Township of White River, Ontario. Prepared for Nuclear Waste Management Organization (NWMO). NWMO Report Number: APM-REP-06144-0086.
- SRK Consulting Inc. 2017a. Phase 2 Geoscientific Preliminary Assessment Lineament Interpretation, Township of White River and Area, Ontario. Prepared for Nuclear Waste Management Organization (NWMO). NWMO Report Number: APM-REP-01332-0210
- Stott, G., Mahoney, K.L., and Zwiers, W.G. 1995a. Precambrian Geology, Dayohessarah Lake Area (North); Ontario Geological Survey, Preliminary Map P.3309, scale 1:20 000.
- Stott, G., Mahoney, K.L., and Zwiers, W.G. 1995b. Precambrian Geology, Dayohessarah Lake Area (Central); Ontario Geological Survey, Preliminary Map P.3310, scale 1:20 000.
- Stott, G., Mahoney, K.L., and Zwiers, W.G. 1995c. Precambrian Geology, Dayohessarah Lake Area (South); Ontario Geological Survey, Preliminary Map P.3311, scale 1:20 000.
- Stott, G.M. 1999. Precambrian geology of the Dayohessarah Lake area, White River, Ontario. Ontario Geological Survey, Open File Report 5984. Sudbury, Canada.
- Streckeisen, A. L., 1976. Classification of the common igneous rocks by means of their chemical composition: a provisional attempt; Neues Jahrbuch fr Mineralogie, Monatshefte, 1976 H. 1, p.1-15.
- Telford, W.M.; Geldart, L.P.; and Sheriff, R.E. 1990. Applied geophysics. 2nd edition. Cambridge University Press.
- Verduzco B., Fairhead J.D., Green C.M. and MacKenzie C. 2004. New insights into magnetic derivatives for structural mapping, The Leading Edge, 116-119.
- Williams, H.R. and Breaks, F.W. 1989. Geological studies in the Manitouwadge-Hornepayne area; Ontario Geological Survey, Miscellaneous Paper 146, 79-91.
- Williams, H.R. and F.W. Breaks, 1996. Geology of the Manitouwadge-Hornepayne region, Ontario; Ontario Geological Survey, Open File Report 5953.
- Williams, H.R., Stott, G.M., Heather, K.B., Muir, T.L., and Sage, R.P. 1991. Wawa Subprovince; In: The Geology of Ontario, Ontario Geological Survey, Special Volume 4, Part 1, 485-539.
- Zaleski E., and Peterson, V.L. 1995. Depositional setting and deformation of massive sulfide deposits, iron-formation, and associated alteration in the Manitouwadge greenstone belt, Superior Province, Ontario; Economic Geology, **90(8)**: 2244-2261.
- Zaleski, E. and Peterson, V.L. 1993. Geology of the Manitouwadge greenstone belt, Ontario; Geological Survey of Canada, Open File 2753, scale 1:25,000
- Zaleski, E., Peterson, V.L., and van Breemen, O., 1994. Structure and tectonics of the Manitouwadge greenstone belt and the Wawa-Quetico subprovince boundary, Superior province, northwestern Ontario; In: Current Research 1994-C; Geological Survey of Canada, 237-247.
- Zaleski, E., van Breemen O. and Peterson, V.L. 1999. Geological evolution of the Manitouwadge greenstone belt and the Wawa-Quetico subprovince boundary, Superior Province, Ontario, constrained by U-Pb zircon dates of supracrustal and plutonic rocks; Canadian Journal of

## **8 FIGURES**

- 1.1 Survey Area
- 1.2 Flight Lines
- 3.1 Digital Elevation Model (25 m cell)
- 4.1 Bouguer Gravity (Density:  $2.67\text{g/cm}^3$ ) (25 m cell)
- 4.2 Bouguer Gravity (Density:  $2.67\text{g/cm}^3$ ) (250 m cell)
- 4.3 Free Air Gravity (25 m cell)
- 4.4 Free Air Gravity (250 m cell)
- 4.5 Total Magnetic Intensity (25 m cell)
- 4.6 Total Magnetic Intensity (250 m cell)
- 4.7 Reduction to the Pole of the Magnetic Field (25 m cell)
- 4.8 Reduction to the Pole of the Magnetic Field (250 m cell)
- 4.9 First Vertical Derivative of the Reduction to the Pole of the Total Magnetic Intensity (25 m cell)
- 4.10 First Vertical Derivative of the Reduction to the Pole of the Total Magnetic Intensity (250 m cell)
- 4.11 First Vertical Derivative of the Bouguer Gravity (Density:  $2.67\text{g/cm}^3$ ) (25 m cell)
- 4.12 First Vertical Derivative of the Bouguer Gravity (Density:  $2.67\text{g/cm}^3$ ) (250 m cell)
- 4.13 First Vertical Derivative of the Free Air Gravity (25 m cell)
- 4.14 First Vertical Derivative of the Free Air Gravity (250 m cell)
- 4.15 Second Vertical Derivative of the Reduction to the Pole of the Total Magnetic Intensity (25 m cell)
- 4.16 Second Vertical Derivative of the Reduction to the Pole of the Total Magnetic Intensity (250 m cell)
- 4.17 Total Horizontal Derivative of the Reduction to the Pole of the Total Magnetic Intensity (25 m cell)
- 4.18 Total Horizontal Derivative of the Reduction to the Pole of the Total Magnetic Intensity (250 m cell)
- 4.19 Total Horizontal Derivative of the Bouguer Gravity (Density:  $2.67\text{g/cm}^3$ ) (25 m cell)
- 4.20 Total Horizontal Derivative of the Bouguer Gravity (Density:  $2.67\text{g/cm}^3$ ) (250 m cell)
- 4.21 Total Horizontal Derivative of the Free Air Gravity (25 m cell)
- 4.22 Total Horizontal Derivative of the Free Air Gravity (250 m cell)
- 4.23 Analytic Signal of the Total Magnetic Intensity (25 m cell)

- 4.24 Analytic Signal of the Total Magnetic Intensity (250 m cell)
- 4.25 Tilt Angle of the Reduction to the Pole of the Total Magnetic Intensity (25 m cell)
- 4.26 Tilt Angle of the Reduction to the Pole of the Total Magnetic Intensity (250 m cell)
  
- 4.27 Trend Analysis Solutions of Bouguer Gravity (terrain correction density = 2.67 g/ cm<sup>3</sup>)
- 4.28 Trend Analysis Solutions of Reduction to the Pole of the Total Magnetic Intensity
- 5.1 Bouguer Gravity (terrain correction density = 2.67 g/cm<sup>3</sup>) with Selected Interpretation Features
- 5.2 First Vertical Derivative of the Bouguer Gravity (terrain correction density = 2.67 g/cm<sup>3</sup>) with Selected Interpretation Features
- 5.3 Total Horizontal Derivative of the Bouguer Gravity (terrain correction density = 2.67 g/cm<sup>3</sup>) with Selected Interpreted Features
- 5.4 Reduction to the Pole of the Total Magnetic Intensity with Selected Interpretation Features
- 5.5 First Vertical Derivative of the Reduction to the Pole of the Total Magnetic Intensity with Selected Interpretation Features
- 5.6 Total Horizontal Derivative of the Reduction to the Pole of the Total Magnetic Intensity with Selected Interpretation Features
- 5.7 Location of 2.5D Model Lines shown with Bouguer Gravity (terrain correction density = 2.67 g/cm<sup>3</sup>)
- 5.8 Location of 2D Model Lines shown with Total Magnetic Intensity
- 5.9 Forward Modeling Results: Line 1 – Initial Model, White River, Ontario
- 5.10 Forward Modeling Results: Line 1 – Alternative Model, White River, Ontario
- 5.11 Forward Modeling Results: Line 2 – Initial Model, White River Ontario
- 5.12 Forward Modeling Results: Line 2 – Alternative Model, White River, Ontario





Legend

Hydrography

Roads

Railway

Mine

Geology

Fault

Dyke

2: Mafic metavolcanics

3: Felsic and intermediate metavolcanics

5: Metasedimentary rocks

8: Gabbroic rocks

9: Gneissic tonalite suite

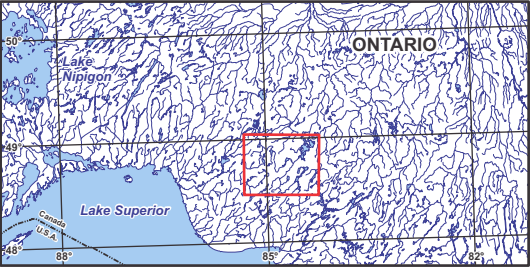
10: Foliate tonalite suite

12: Diorite-monzonite-granodiorite

13: Granite-granodiorite

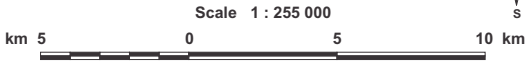
Survey Area

Withdrawal Area



Survey Location

BASE DATA: National Topographic Database - NRCAN  
GEOLOGY DATA: OGS M-Series maps: M2666 & MRD126-rev1  
DATUM: NAD83  
PROJECTION: Universe Transverse Mercator (UTM Zone 16N)

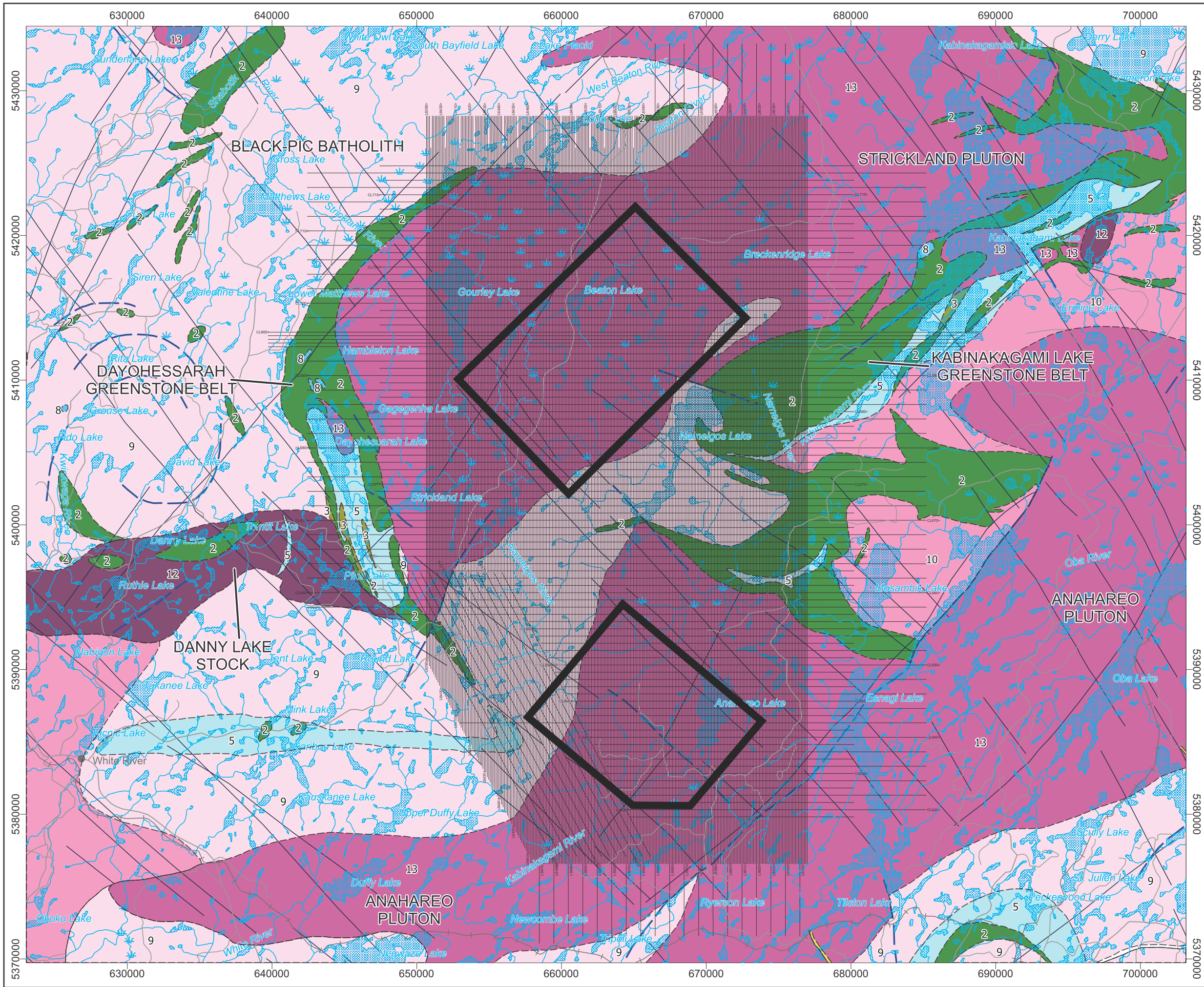


Airborne Geophysics  
Acquisition and Interpretation  
White River Area, Ontario 2016

Survey Area

	DESIGN	JK, MP	14/07/2016	REV. 1.2
	GIS	YC, PT	14/07/2016	FIGURE: 1.1
	DATA	MP, PT, MM	14/07/2016	
	QC	MB	15/07/2016	





**Legend**

Hydrography .....

Roads .....

Railway .....

Mine .....

**Geology**

Fault .....

Dyke .....

2: Mafic metavolcanics

3: Felsic and intermediate metavolcanics

5: Metasedimentary rocks

8: Gabbroic rocks

9: Gneissic tonalite suite

10: Foliate tonalite suite

12: Diorite-monzonite-granodiorite

13: Granite-granodiorite

**Flight Lines**

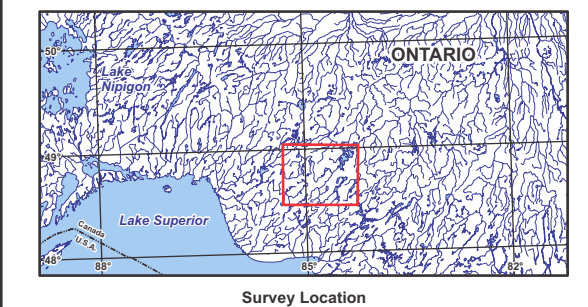
L14100> 41250

Fiducial

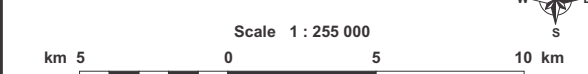
Line direction

Line number

Withdrawal Area .....



BASE DATA: National Topographic Database - NRCAN  
GEOLOGY DATA: OGS M-Series maps: M2666 & MRD126-rev1  
DATUM: NAD83  
PROJECTION: Universe Transverse Mercator (UTM Zone 16N)

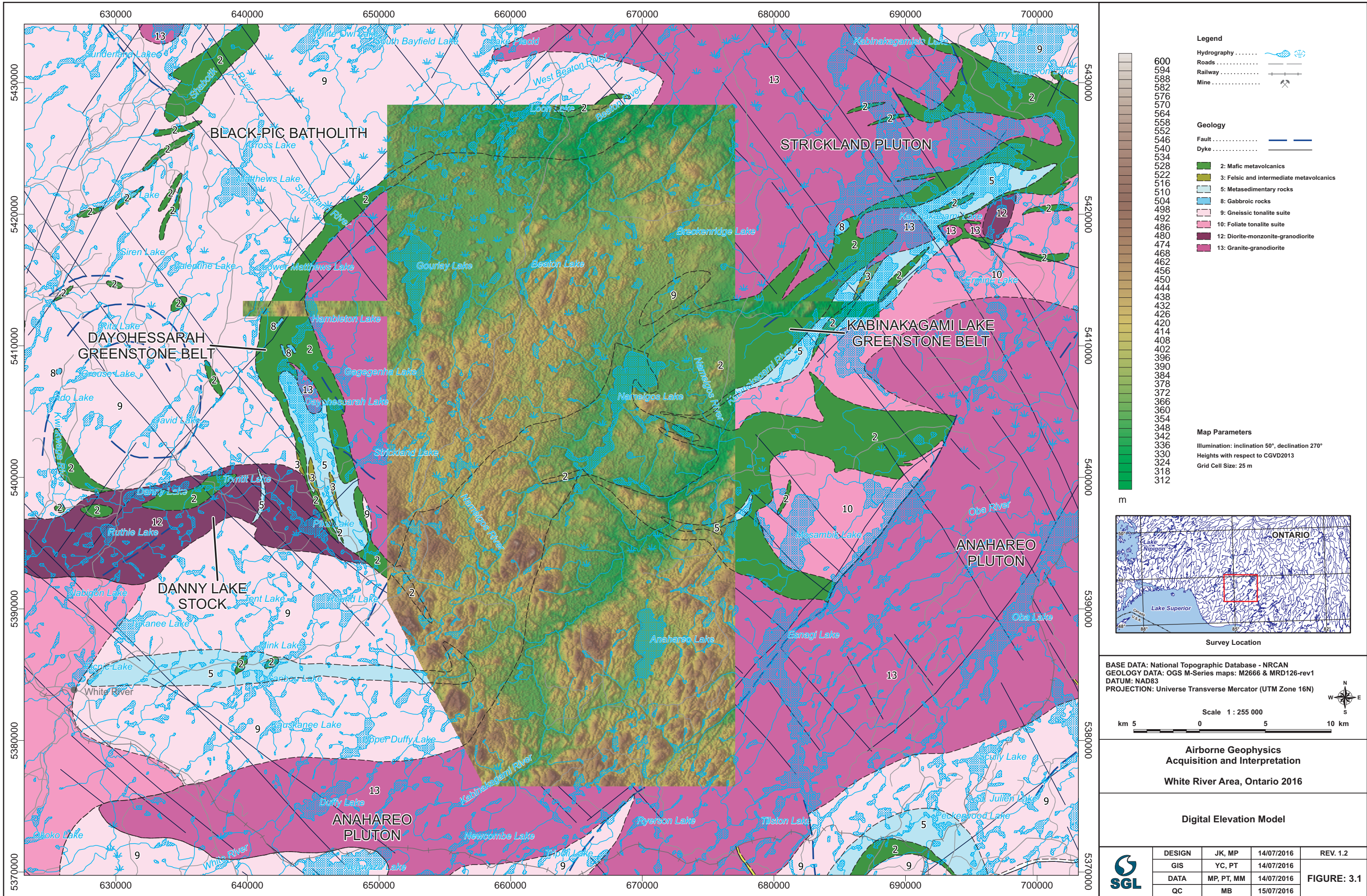


**Airborne Geophysics  
Acquisition and Interpretation**

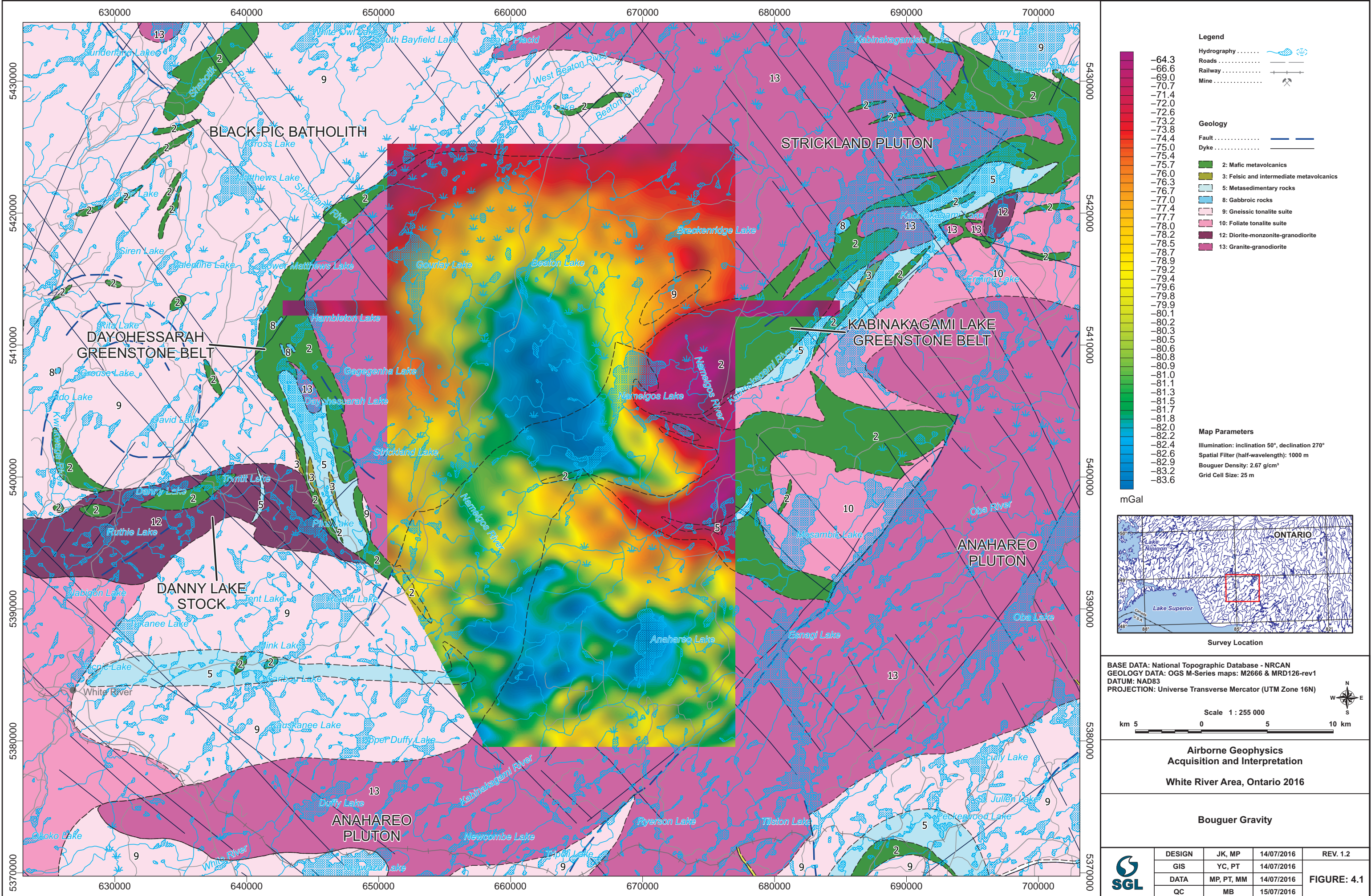
**White River Area, Ontario 2016**

Flight Lines			
DESIGN	JK, MP	14/07/2016	REV. 1.2
GIS	YC, PT	14/07/2016	FIGURE: 1.2
DATA	MP, PT, MM	14/07/2016	
QC	MB	15/07/2016	

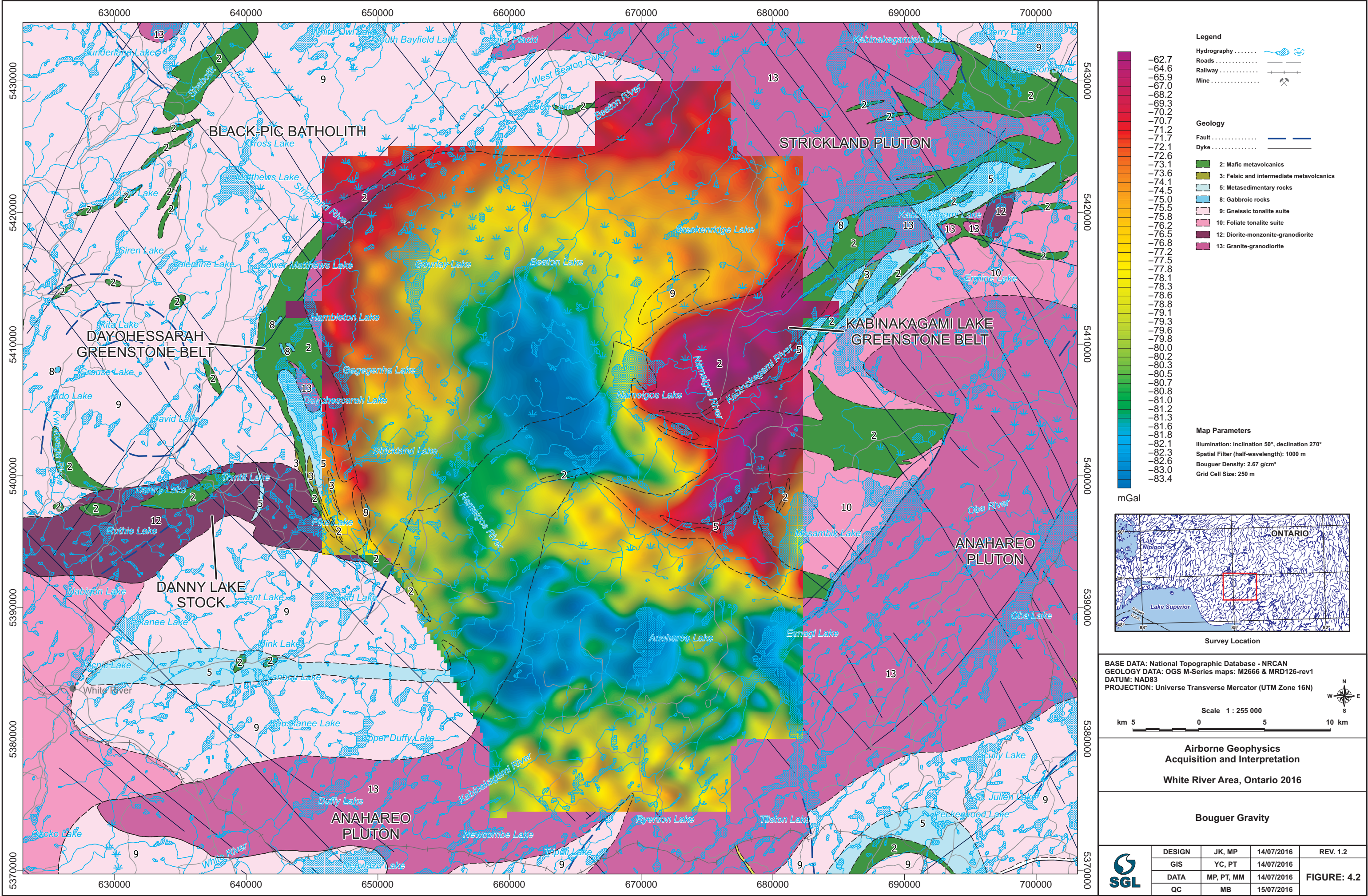




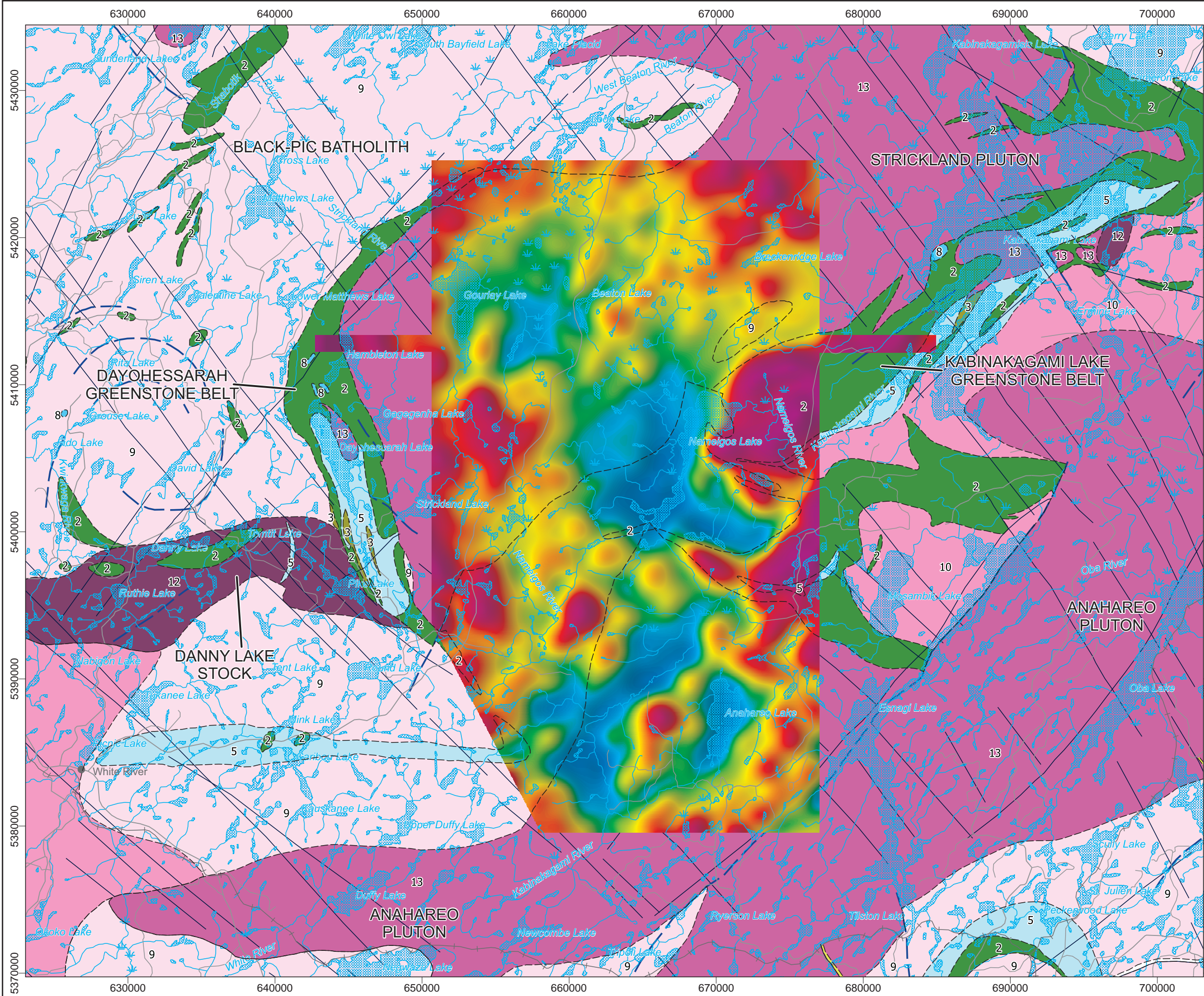












**Legend**

Hydrography .....  
Roads .....  
Railway .....  
Mine .....  
Fault .....  
Dyke .....

**Geology**

2: Mafic metavolcanics  
3: Felsic and intermediate metavolcanics  
5: Metasedimentary rocks  
8: Gabbroic rocks  
9: Gneissic tonalite suite  
10: Foliate tonalite suite  
12: Diorite-monzonite-granodiorite  
13: Granite-granodiorite

**Map Parameters**

Illumination: inclination 50°, declination 270°  
Spatial Filter (half-wavelength): 1000 m  
Grid Cell Size: 25 m

mGal

5370000  
5380000  
5390000  
5400000  
5410000  
5420000  
5430000

630000 640000 650000 660000 670000 680000 690000 700000

**Survey Location**

BASE DATA: National Topographic Database - NRCAN  
GEOLOGY DATA: OGS M-Series maps: M2666 & MRD126-rev1  
DATUM: NAD83  
PROJECTION: Universe Transverse Mercator (UTM Zone 16N)

Scale 1 : 255 000

km 5 0 5 10 km

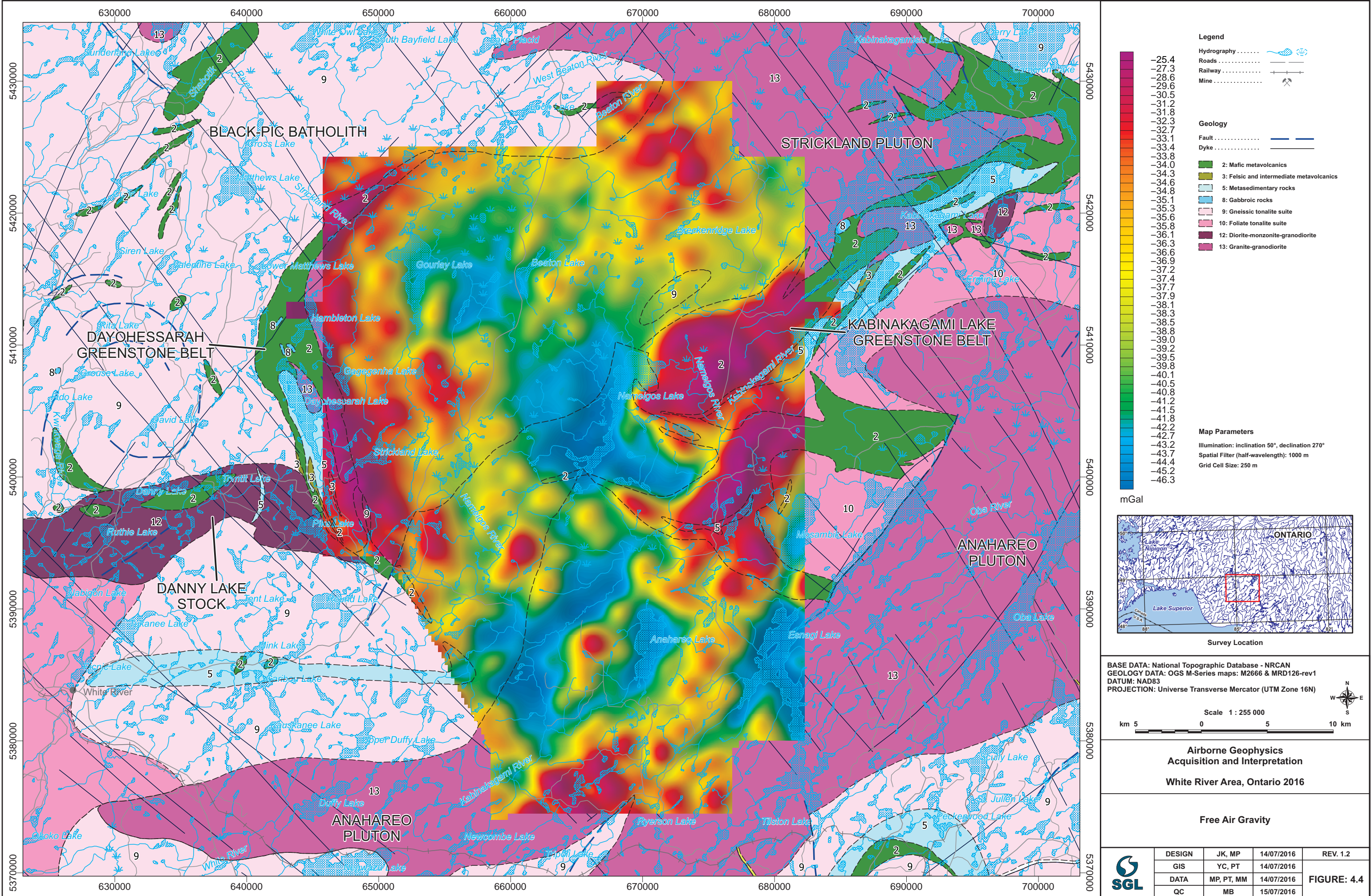
**Airborne Geophysics  
Acquisition and Interpretation**

**White River Area, Ontario 2016**

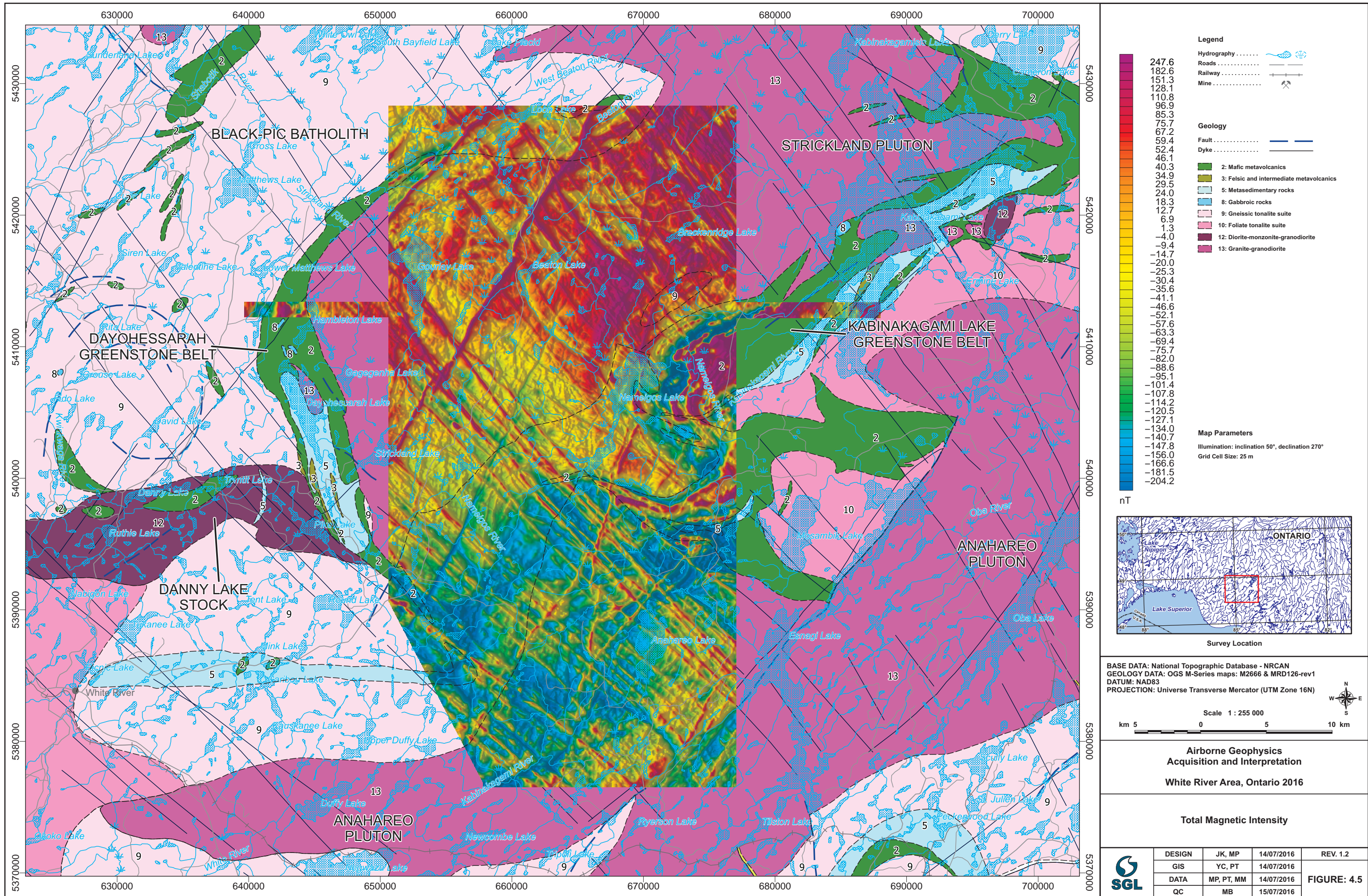
**Free Air Gravity**

	DESIGN	JK, MP	14/07/2016	REV. 1.2
	GIS	YC, PT	14/07/2016	
	DATA	MP, PT, MM	14/07/2016	FIGURE: 4.3
	QC	MB	15/07/2016	

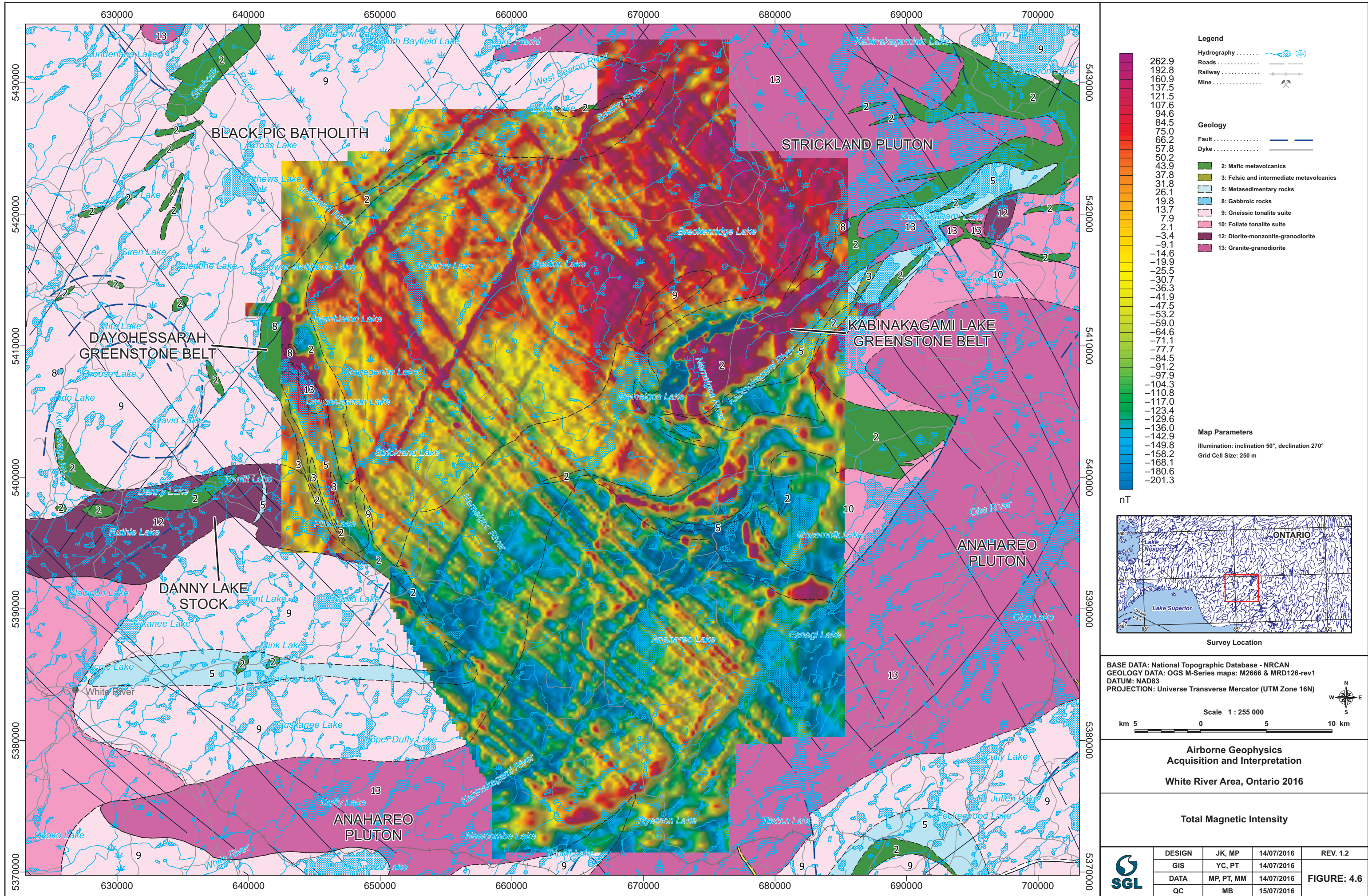








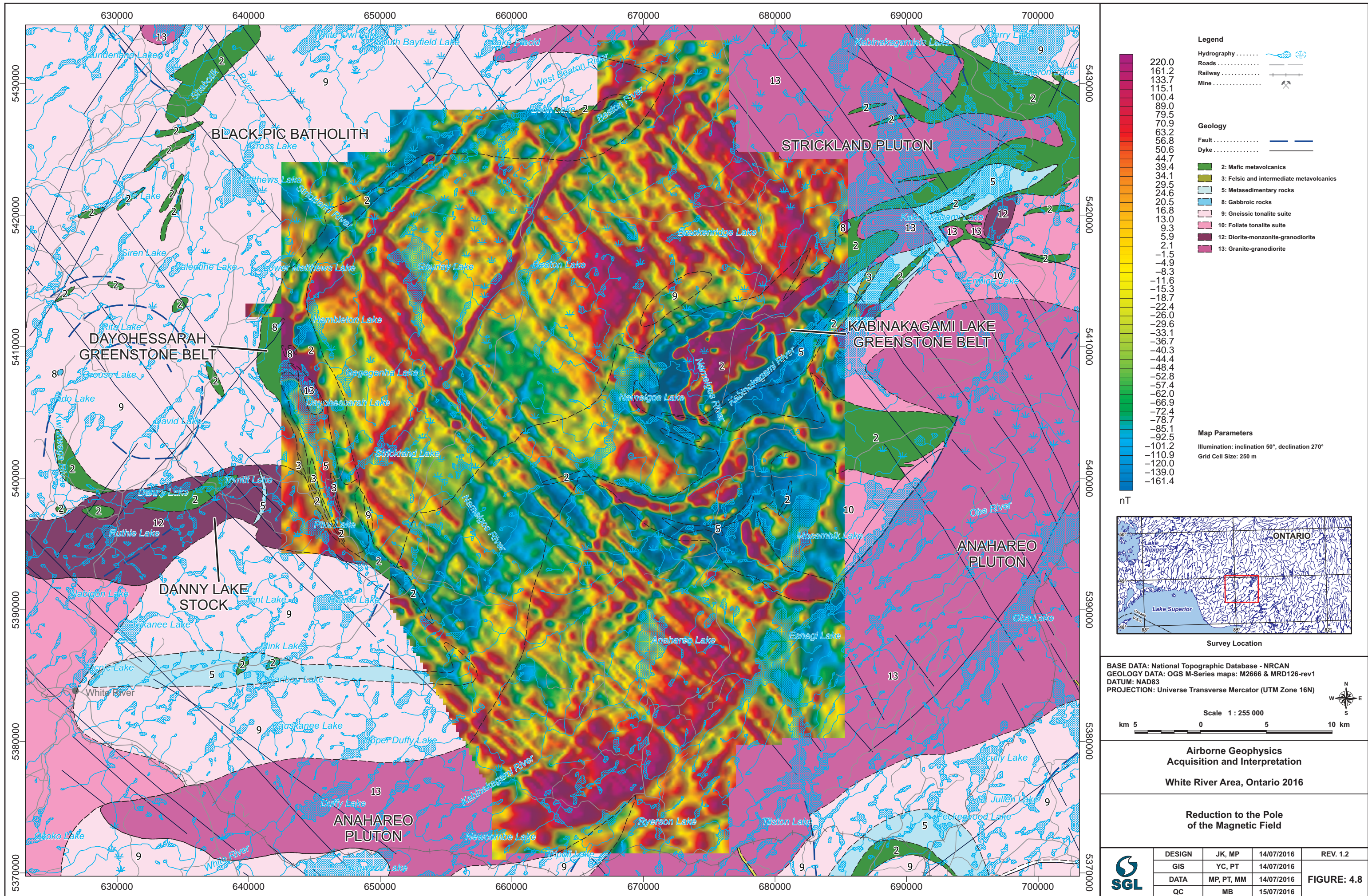




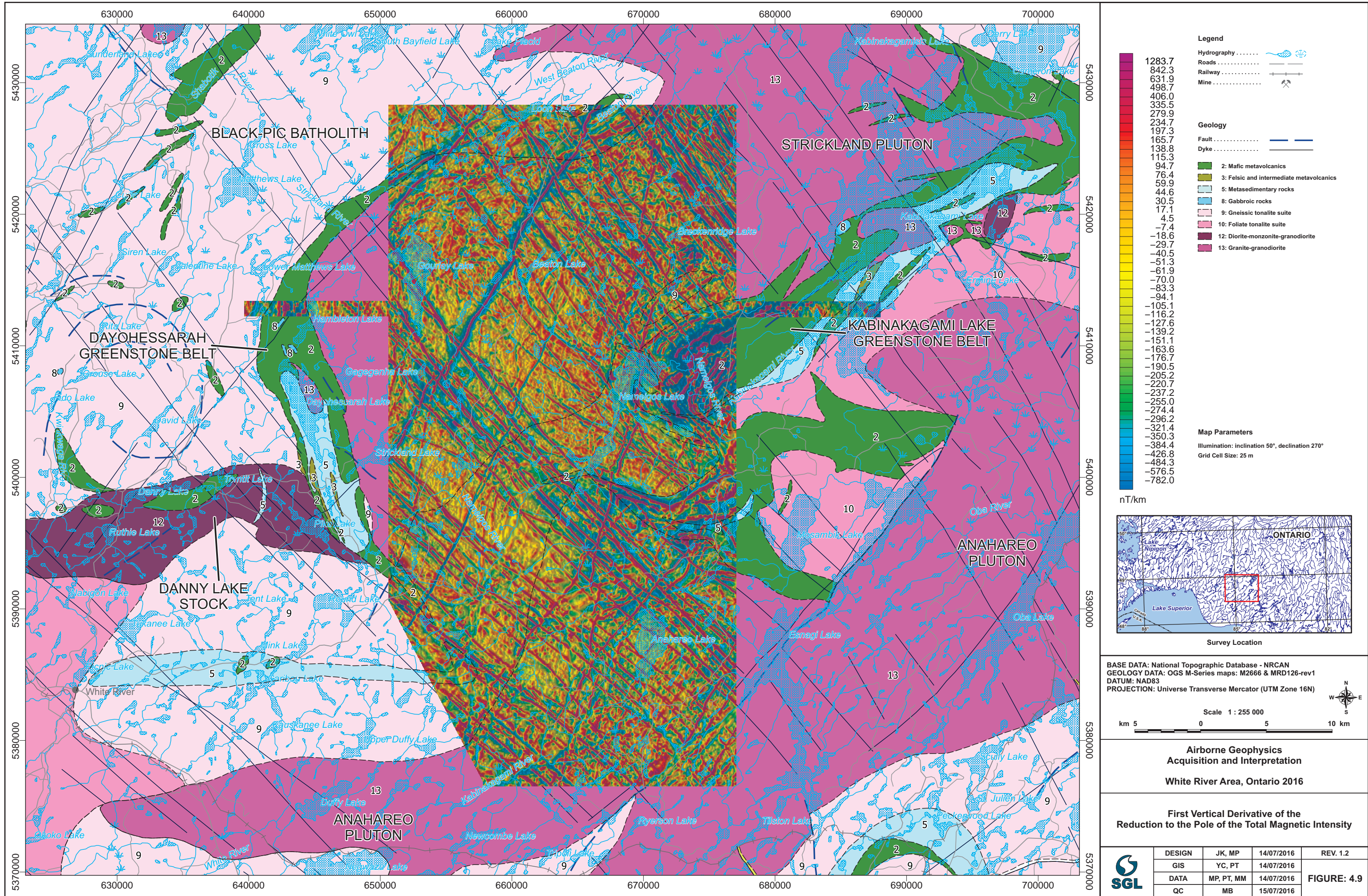








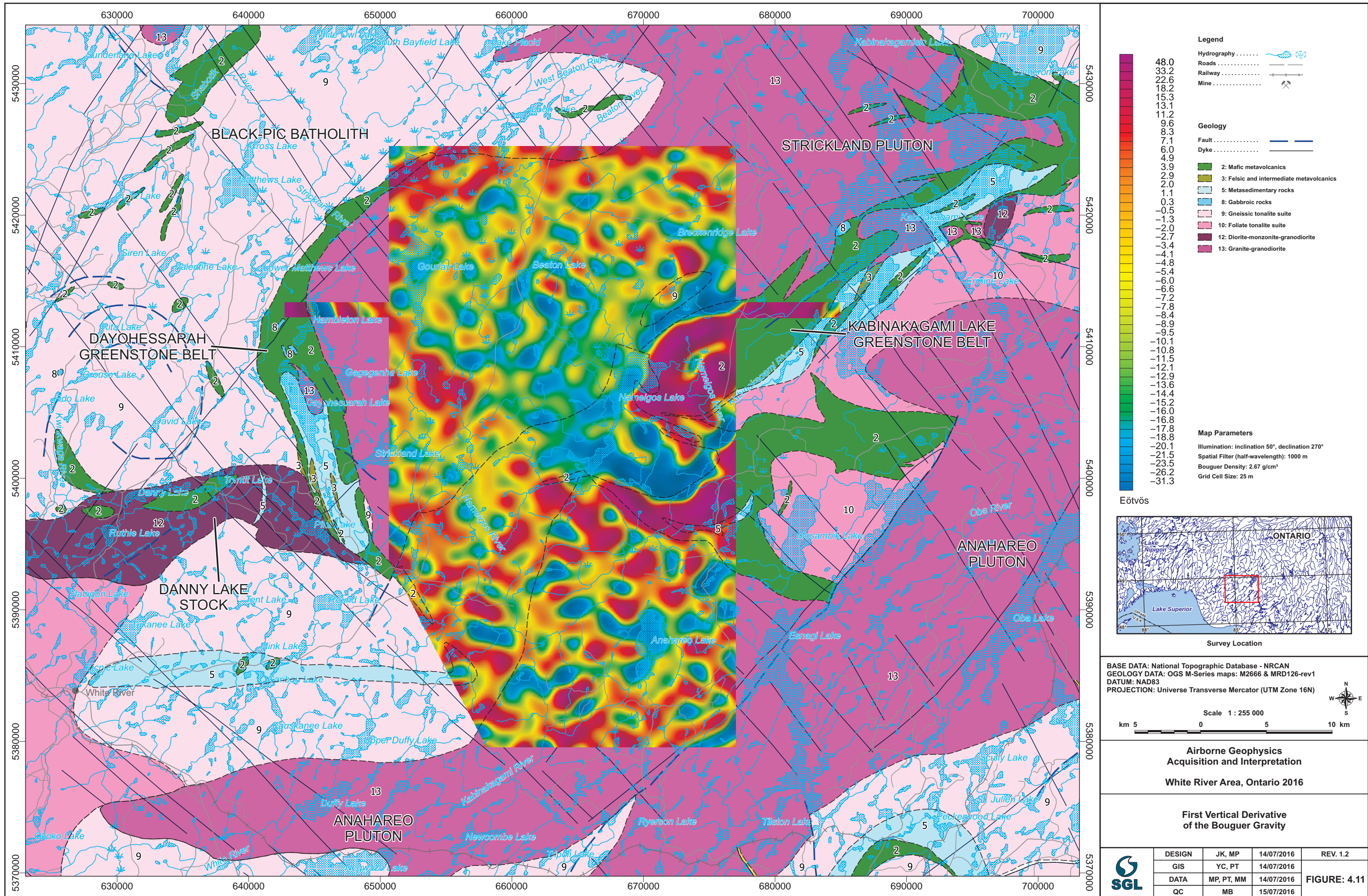




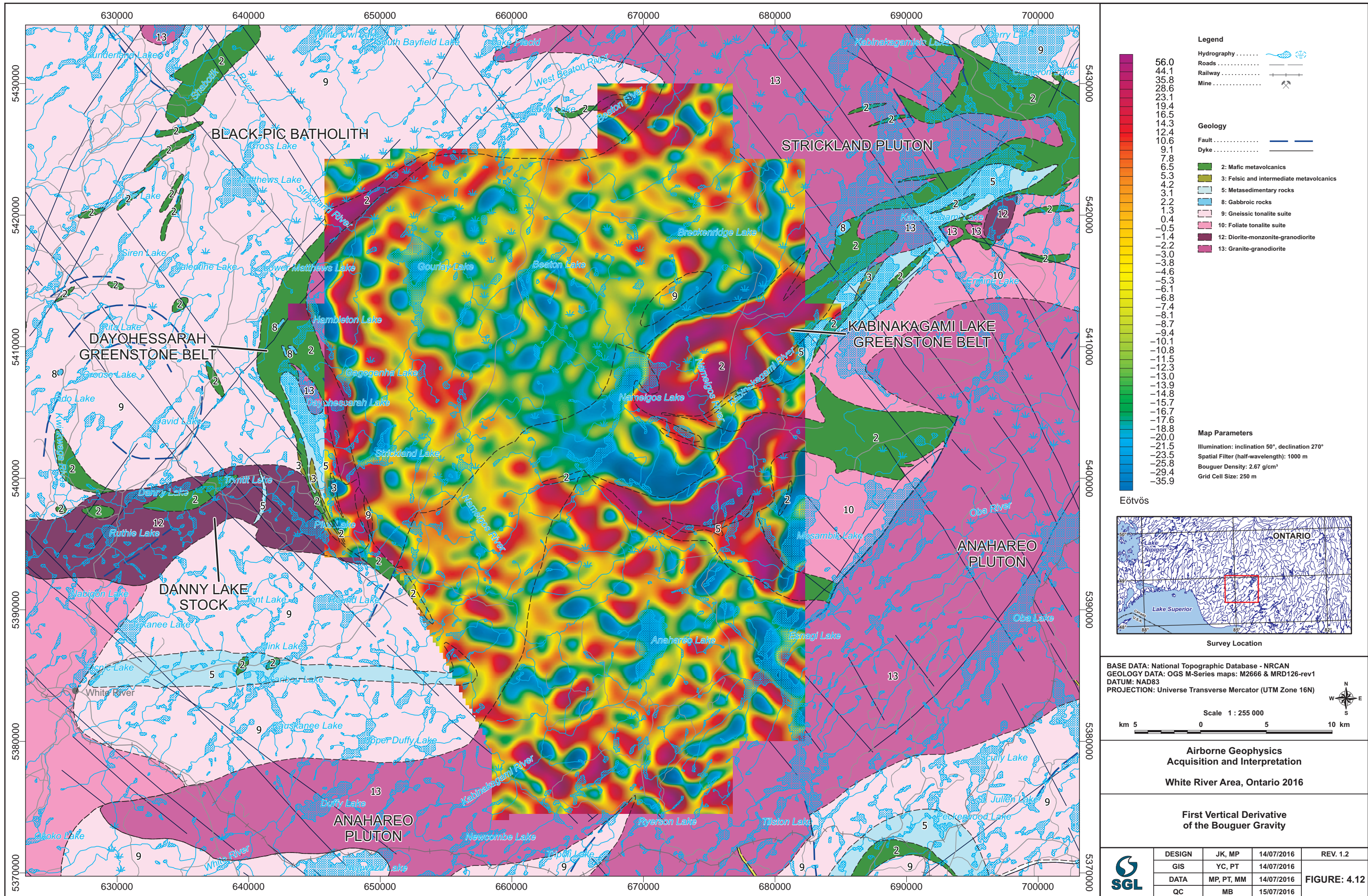








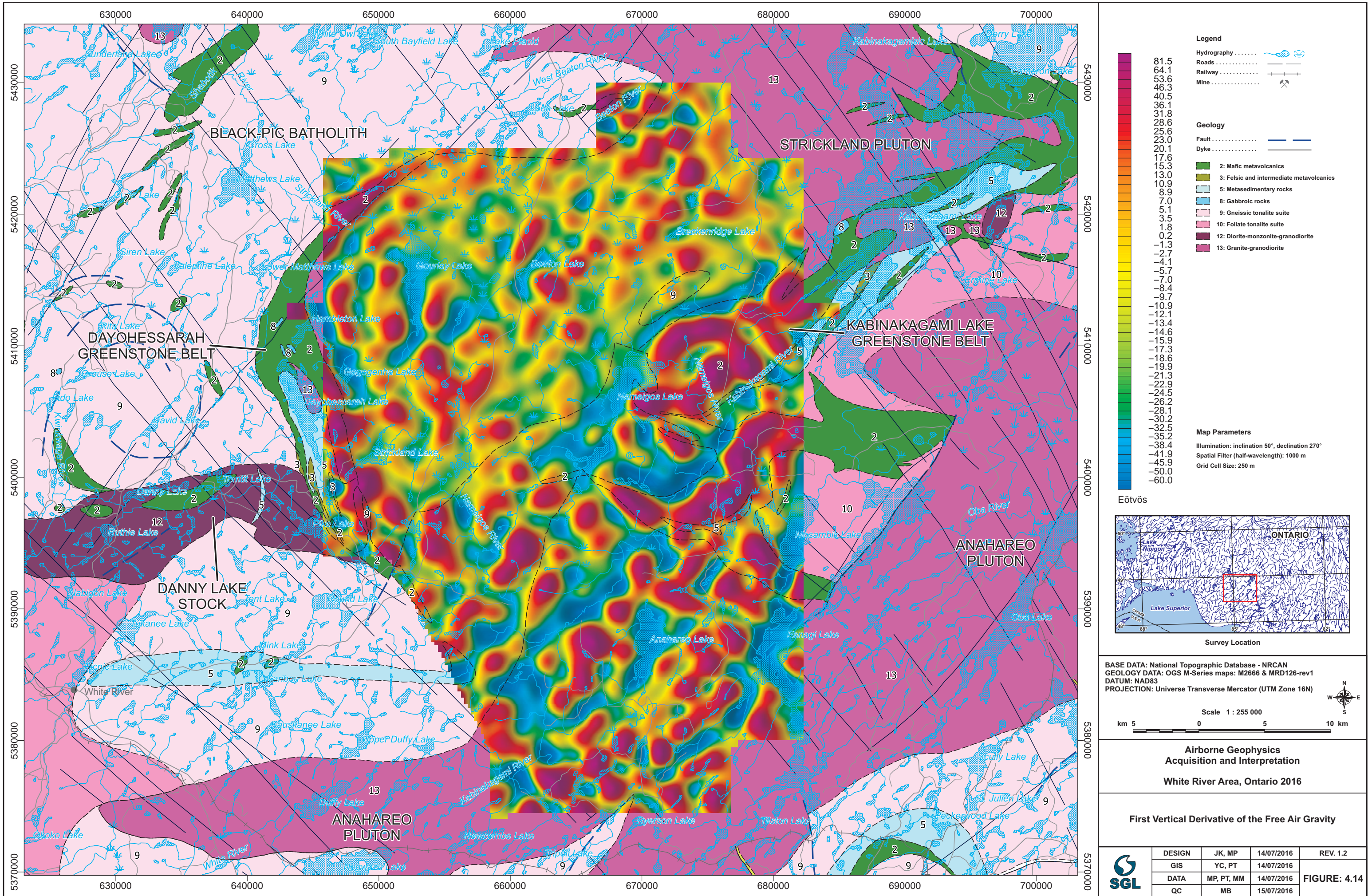








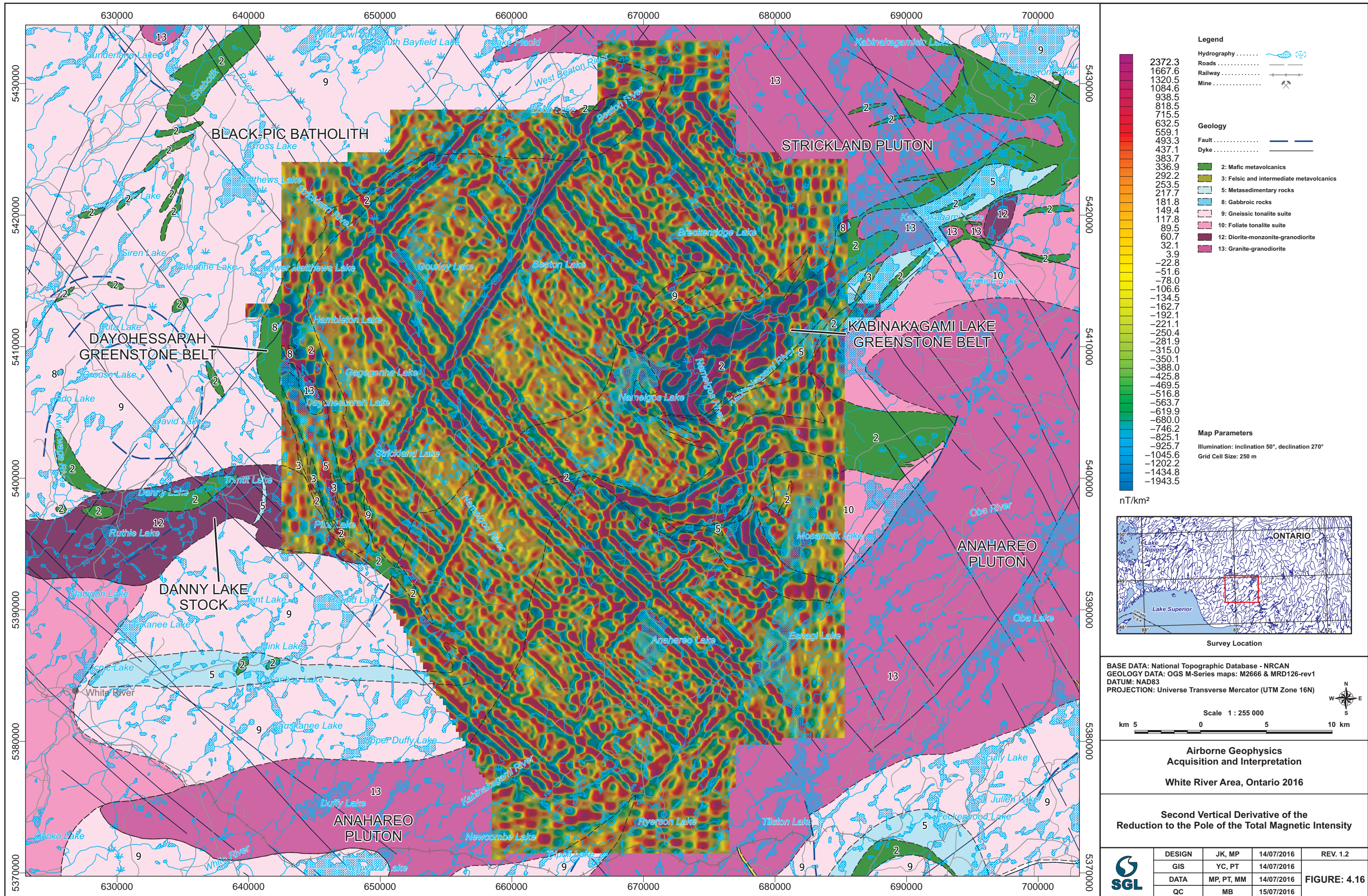








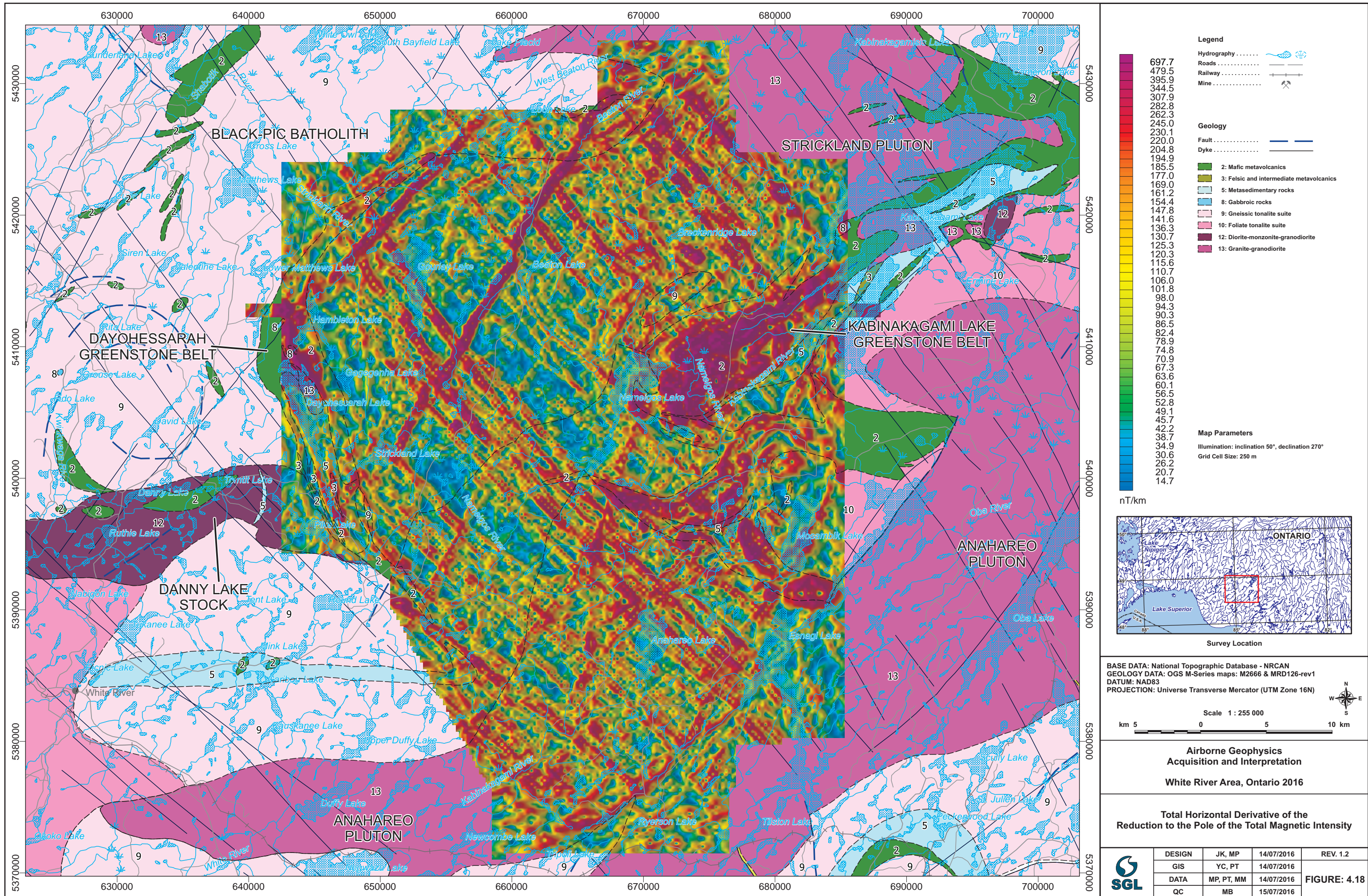




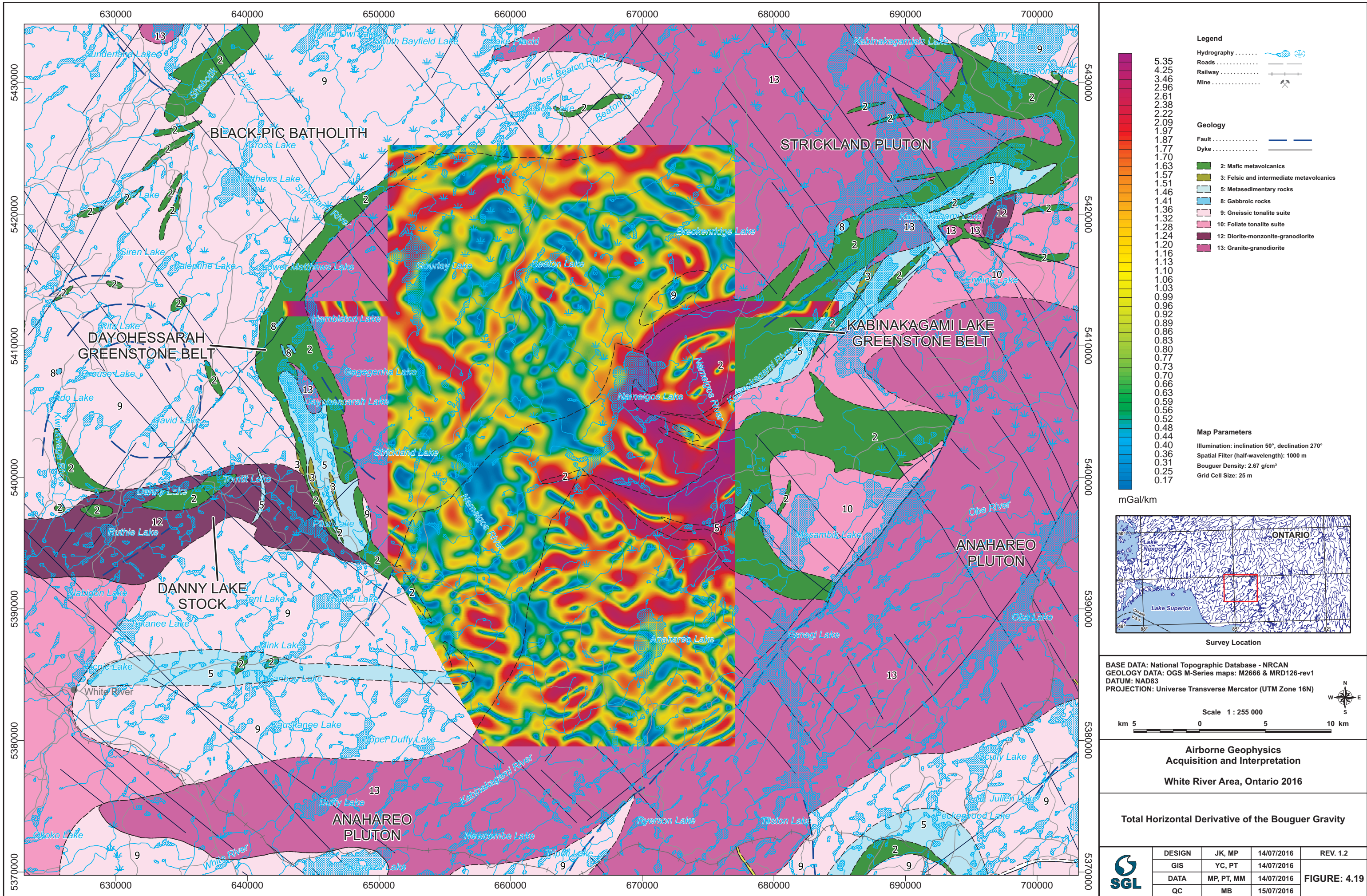




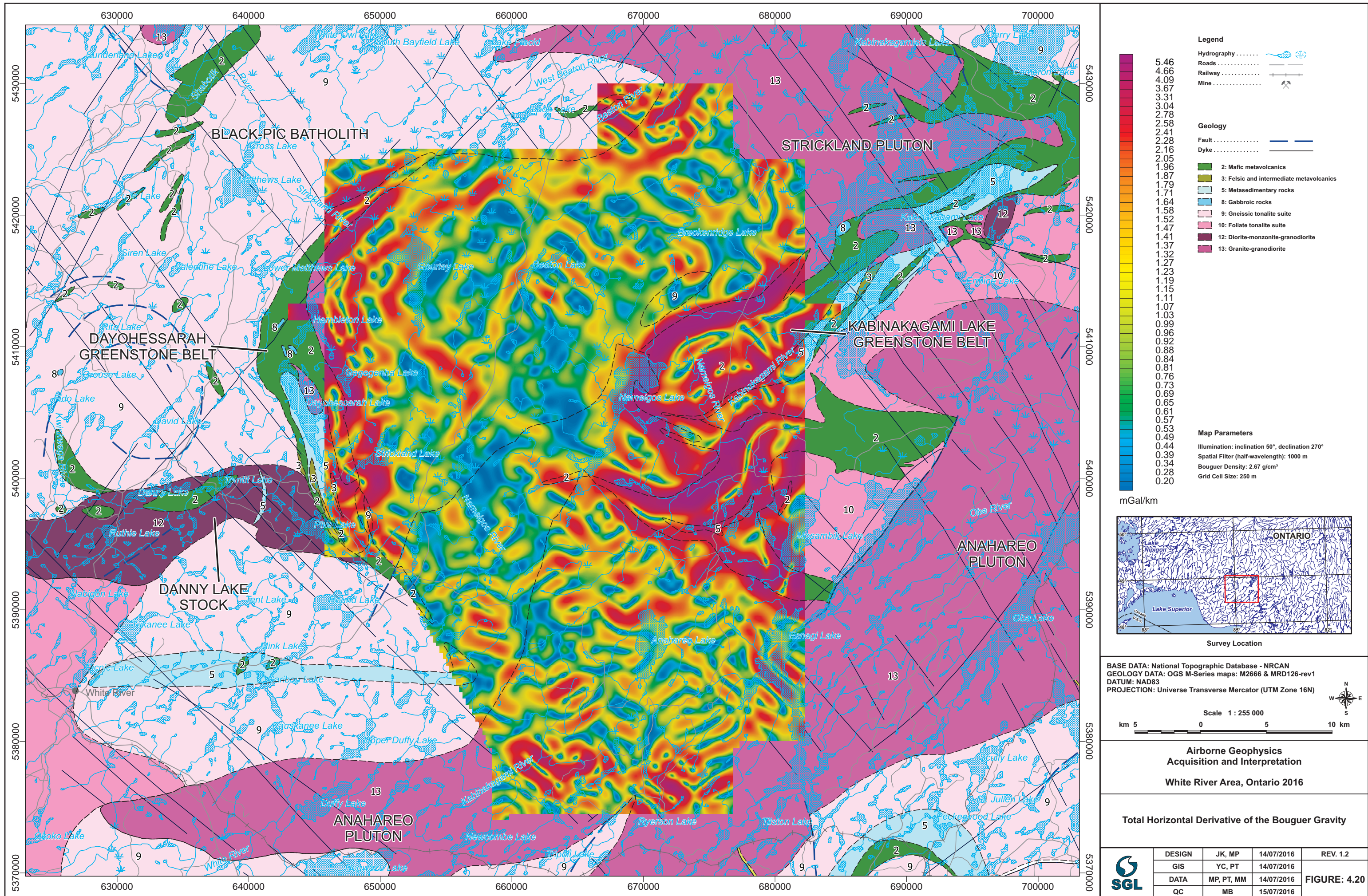








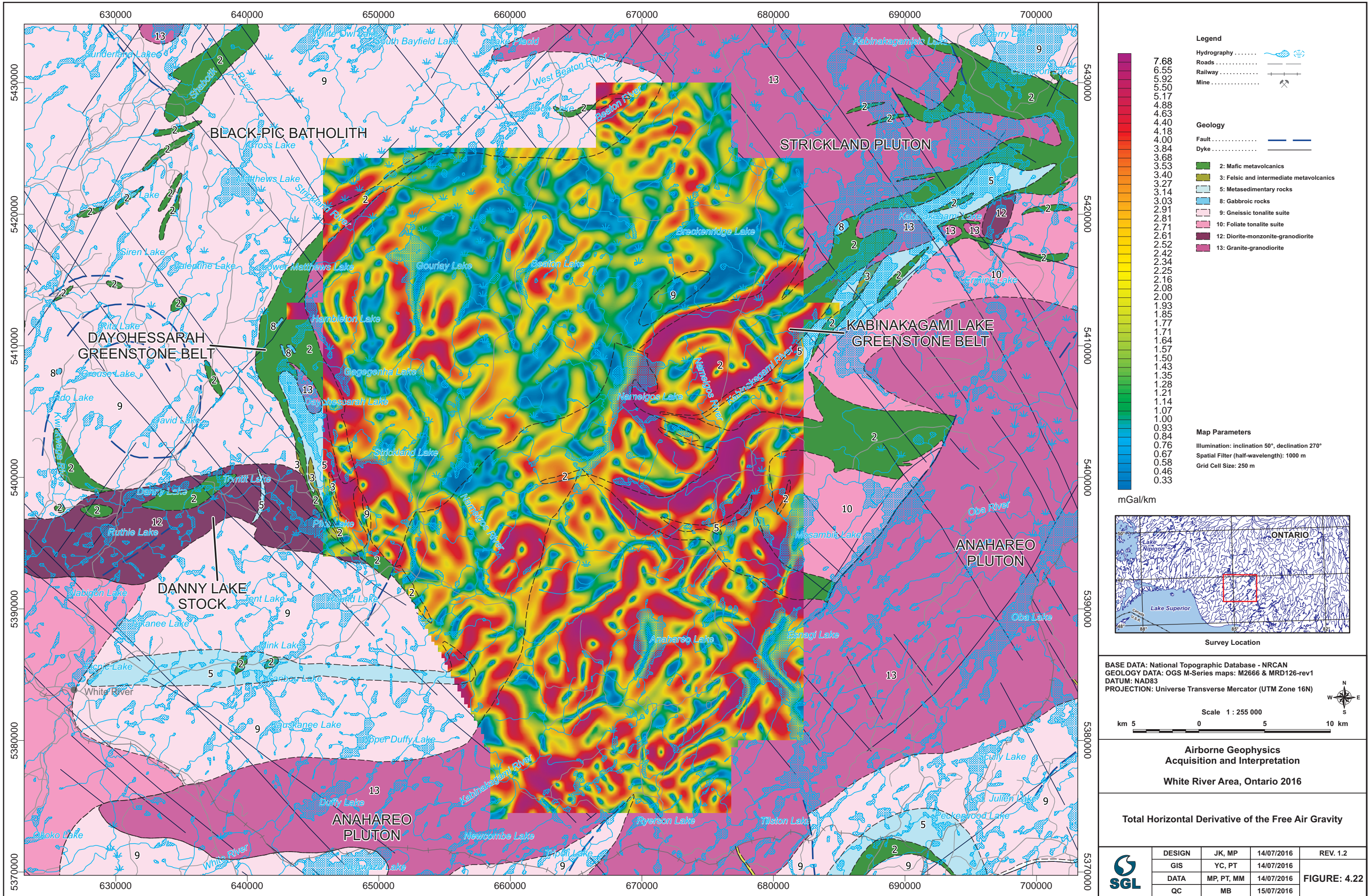




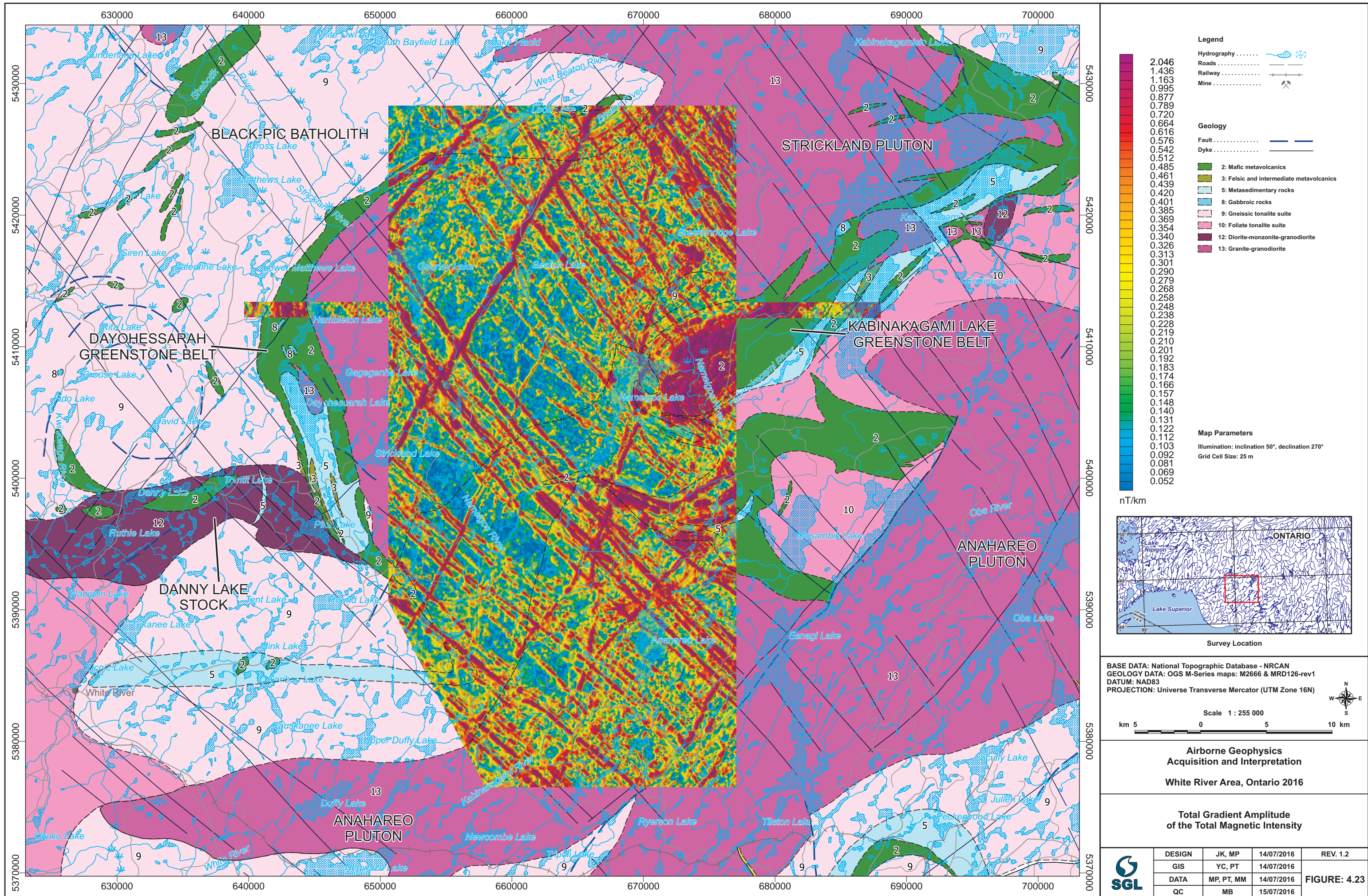




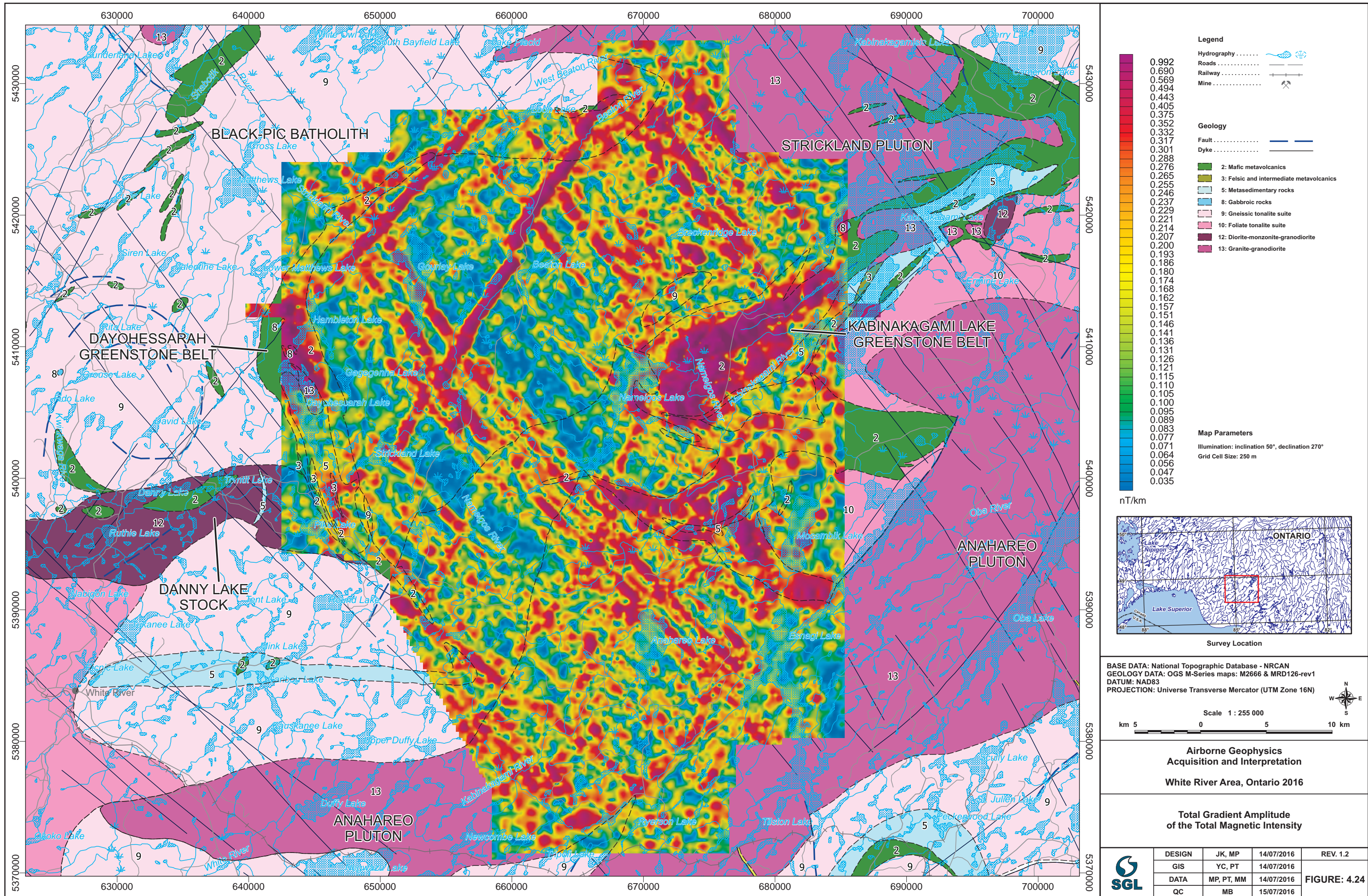




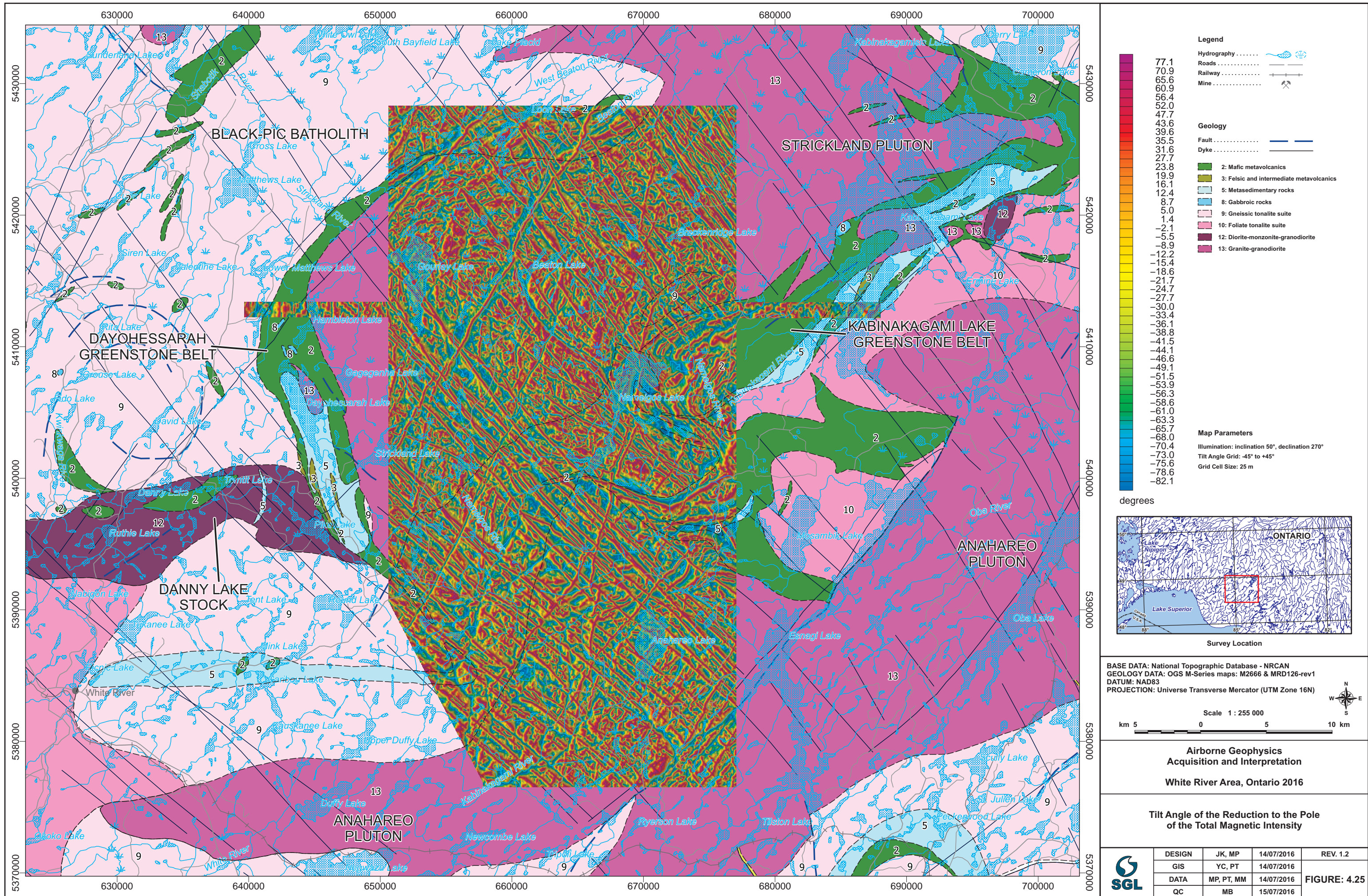




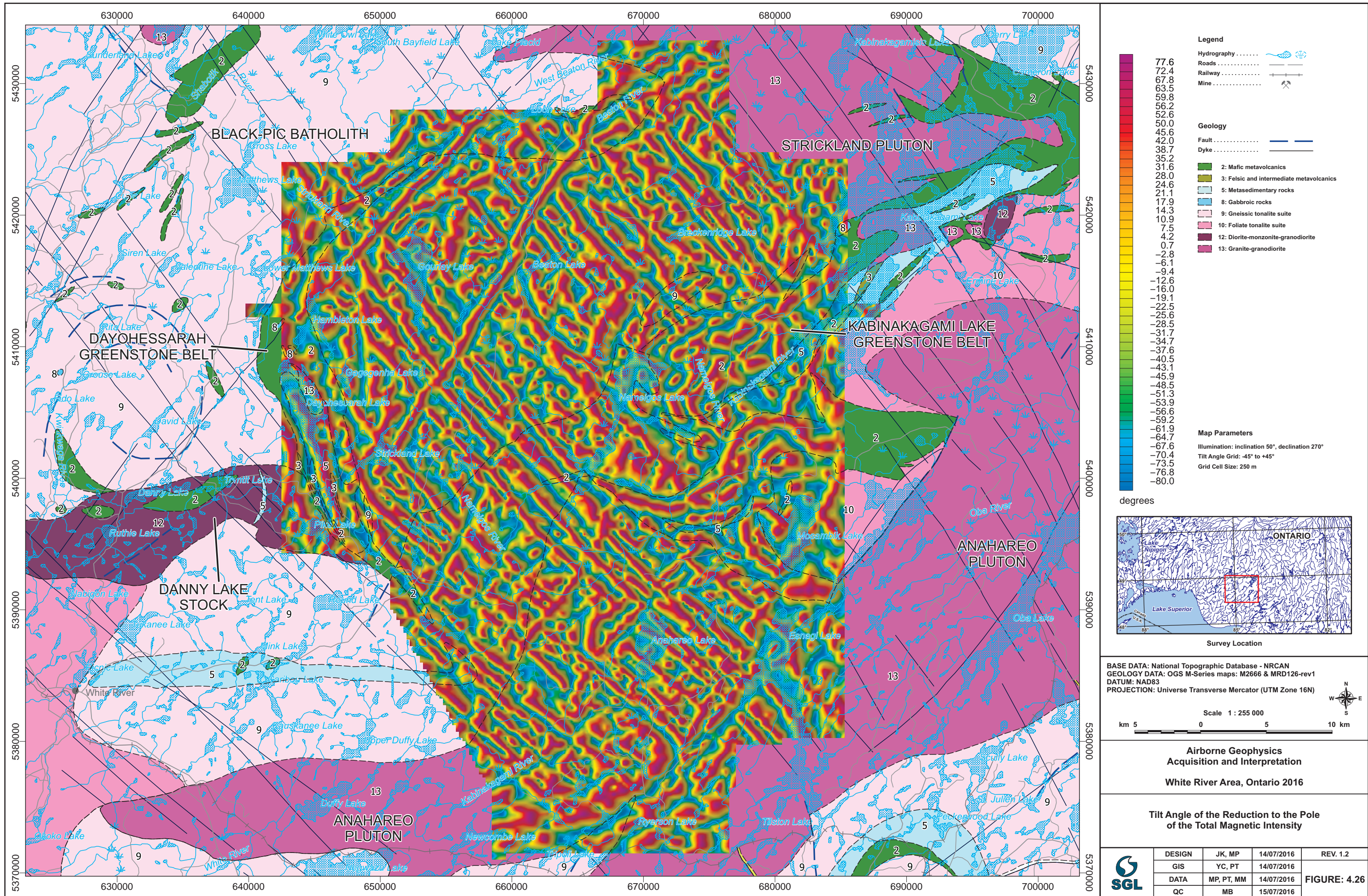




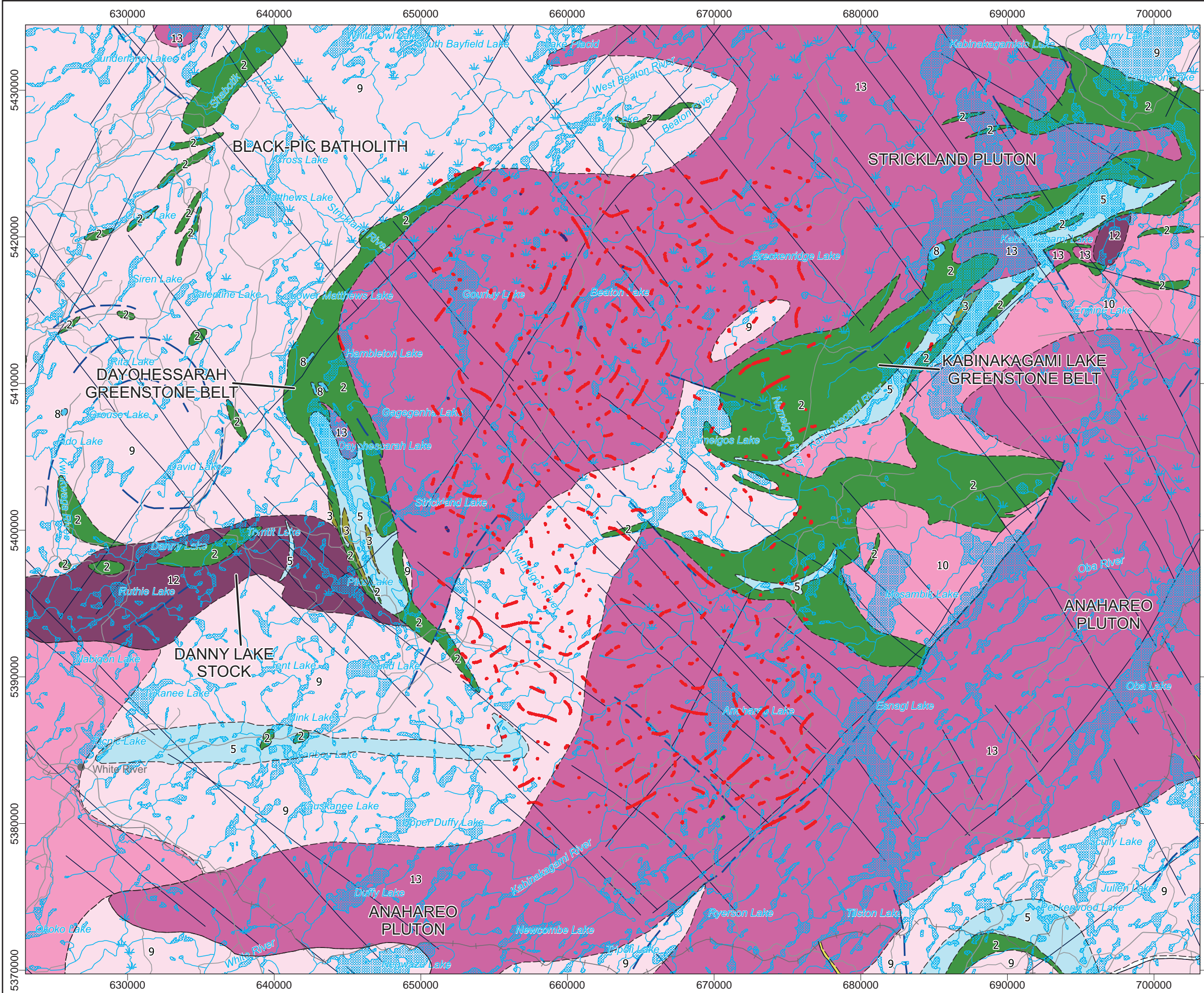












**Legend**

Hydrography .....

Roads .....

Railway .....

Mine .....

**Geology**

Fault .....

Dyke .....

2: Mafic metavolcanics

3: Felsic and intermediate metavolcanics

5: Metasedimentary rocks

8: Gabbroic rocks

9: Gneissic tonalite suite

10: Foliate tonalite suite

12: Diorite-monzonite-granodiorite

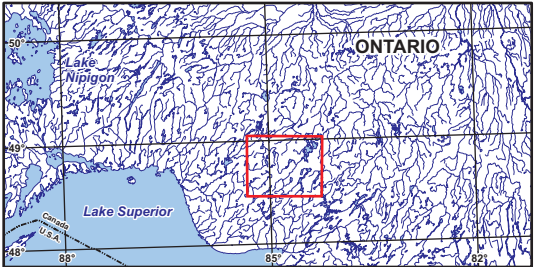
13: Granite-granodiorite

**Trend Analysis Solutions**

0 - 100 m

101 - 200 m

> 200 m



Survey Location

BASE DATA: National Topographic Database - NRCAN  
GEOLOGY DATA: OGS M-Series maps: M2666 & MRD126-rev1  
DATUM: NAD83  
PROJECTION: Universe Transverse Mercator (UTM Zone 16N)



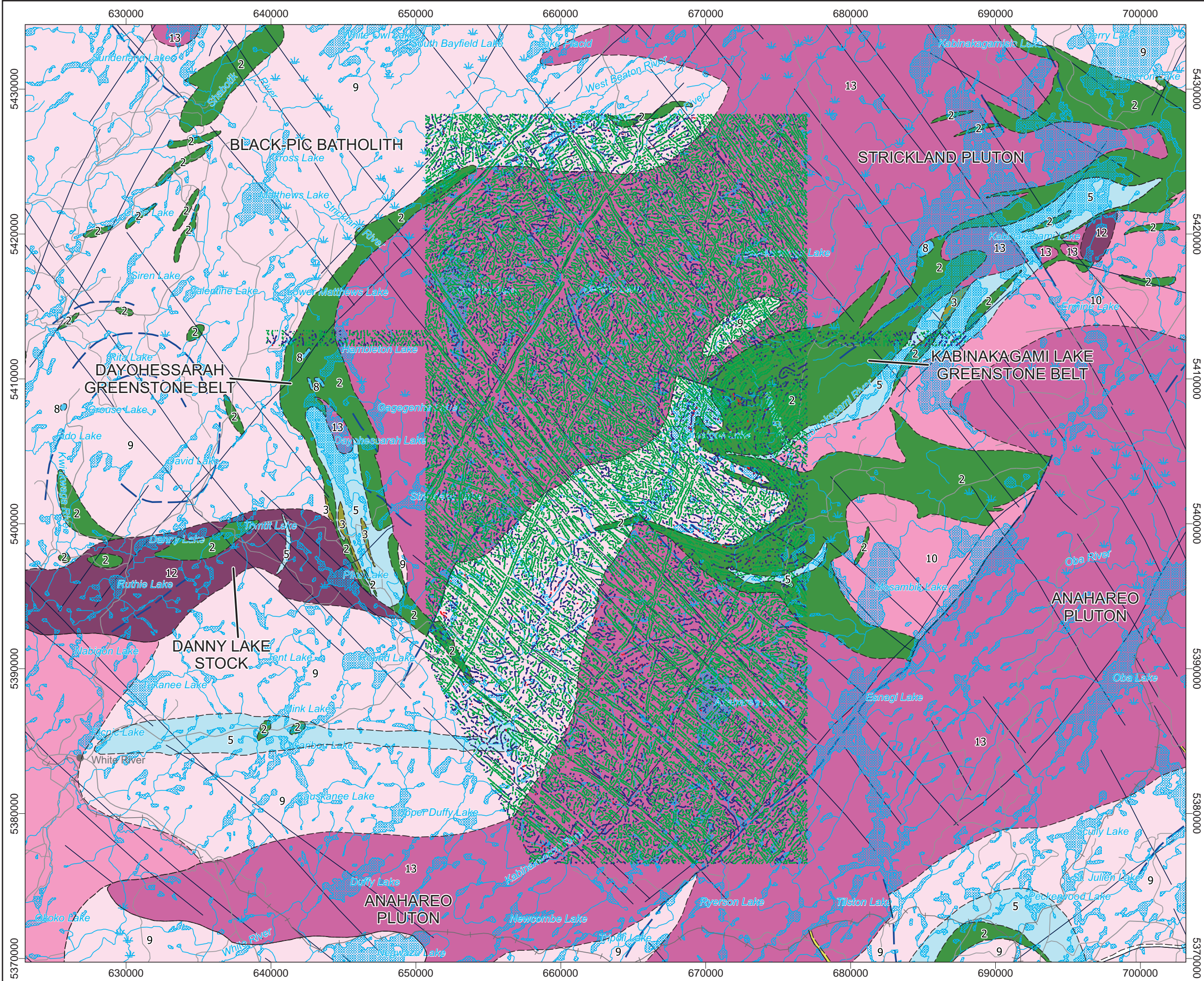
**Airborne Geophysics  
Acquisition and Interpretation**

**White River Area, Ontario 2016**

**Trend Analysis Solutions of Bouguer Gravity**

	DESIGN	JK, MP	14/07/2016	REV. 1.2
	GIS	YC, PT	14/07/2016	
	DATA	MP, PT, MM	14/07/2016	FIGURE: 4.27
	QC	MB	15/07/2016	





**Legend**

Hydrography .....  
Roads .....  
Railway .....  
Mine .....

**Geology**

Fault .....  
Dyke .....

**Trend Analysis Solutions**

Depth from sensor

- 0 - 100 m
- 101 - 200 m
- > 200 m

**Geology**

- 2: Mafic metavolcanics
- 3: Felsic and intermediate metavolcanics
- 5: Metasedimentary rocks
- 8: Gabbroic rocks
- 9: Gneissic tonalite suite
- 10: Foliate tonalite suite
- 12: Diorite-monzonite-granodiorite
- 13: Granite-granodiorite

**Survey Location**

BASE DATA: National Topographic Database - NRCAN  
GEOLOGY DATA: OGS M-Series maps: M2666 & MRD126-rev1  
DATUM: NAD83  
PROJECTION: Universe Transverse Mercator (UTM Zone 16N)

Scale 1 : 255 000

km 5 0 5 10 km

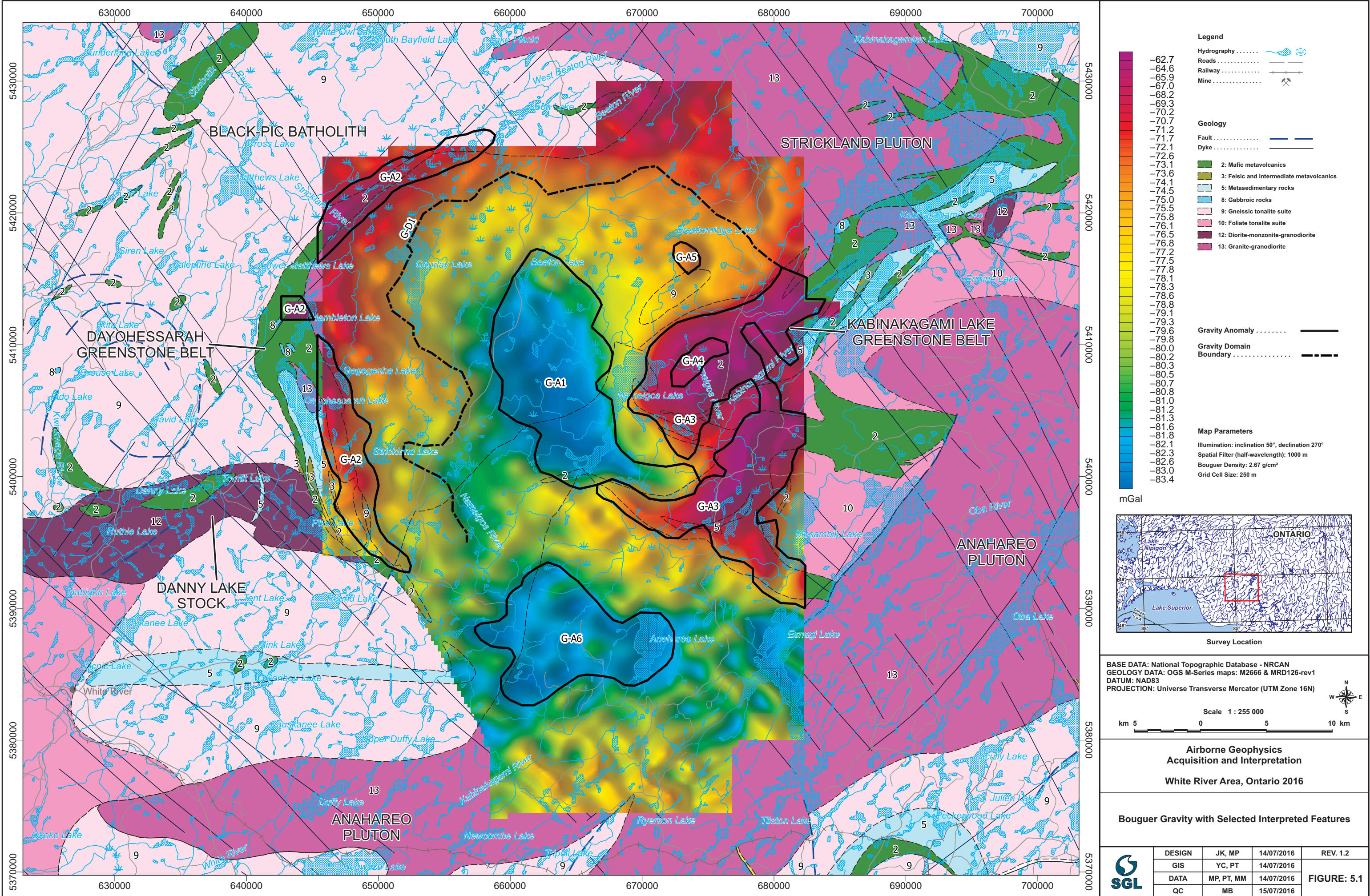
**Airborne Geophysics  
Acquisition and Interpretation**

**White River Area, Ontario 2016**

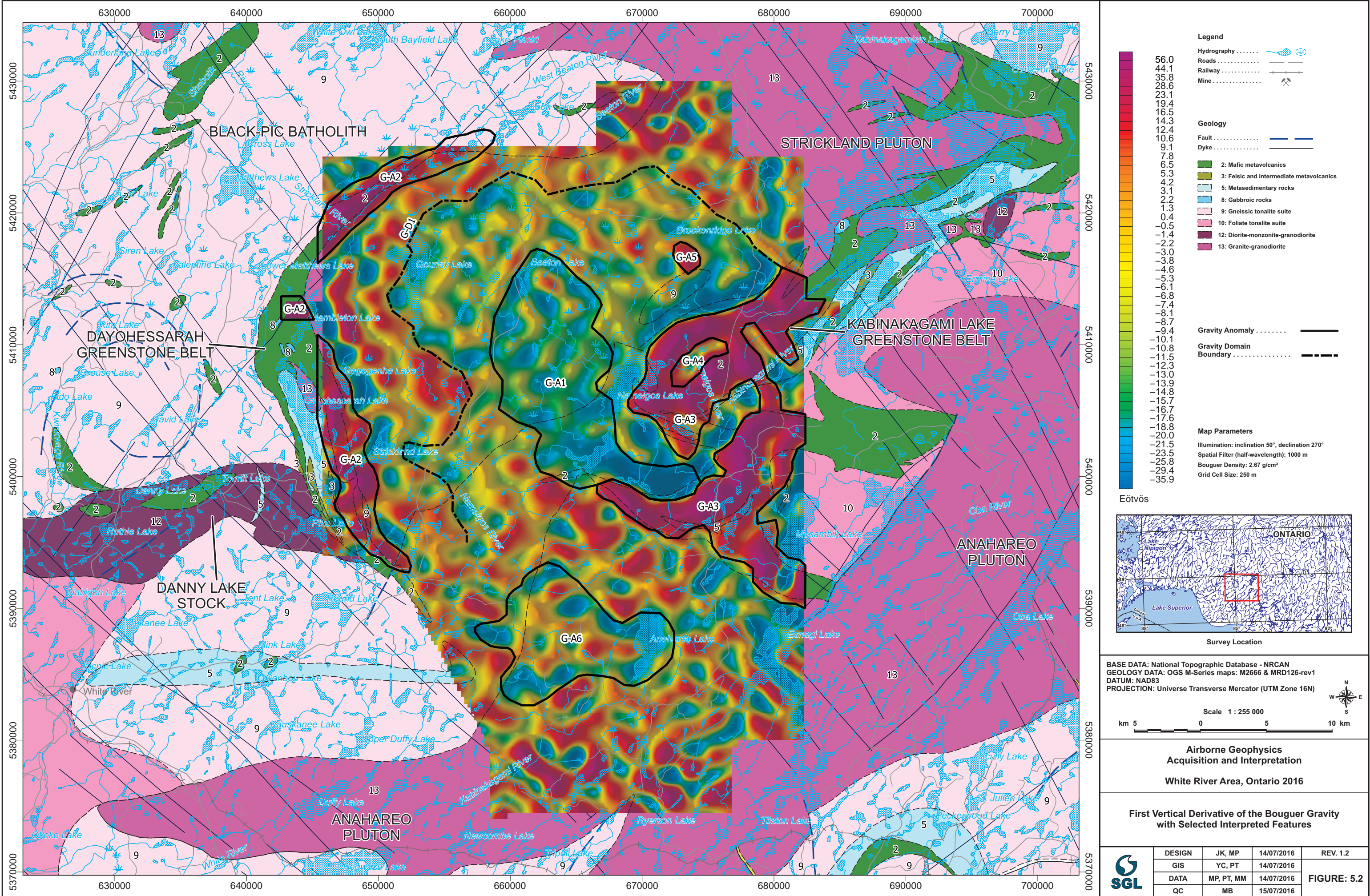
**Trend Analysis Solutions of Reduction to the Pole  
of the Total Magnetic Intensity**

	DESIGN	JK, MP	14/07/2016	REV. 1.2
	GIS	YC, PT	14/07/2016	
	DATA	MP, PT, MM	14/07/2016	FIGURE: 4.28
	QC	MB	15/07/2016	

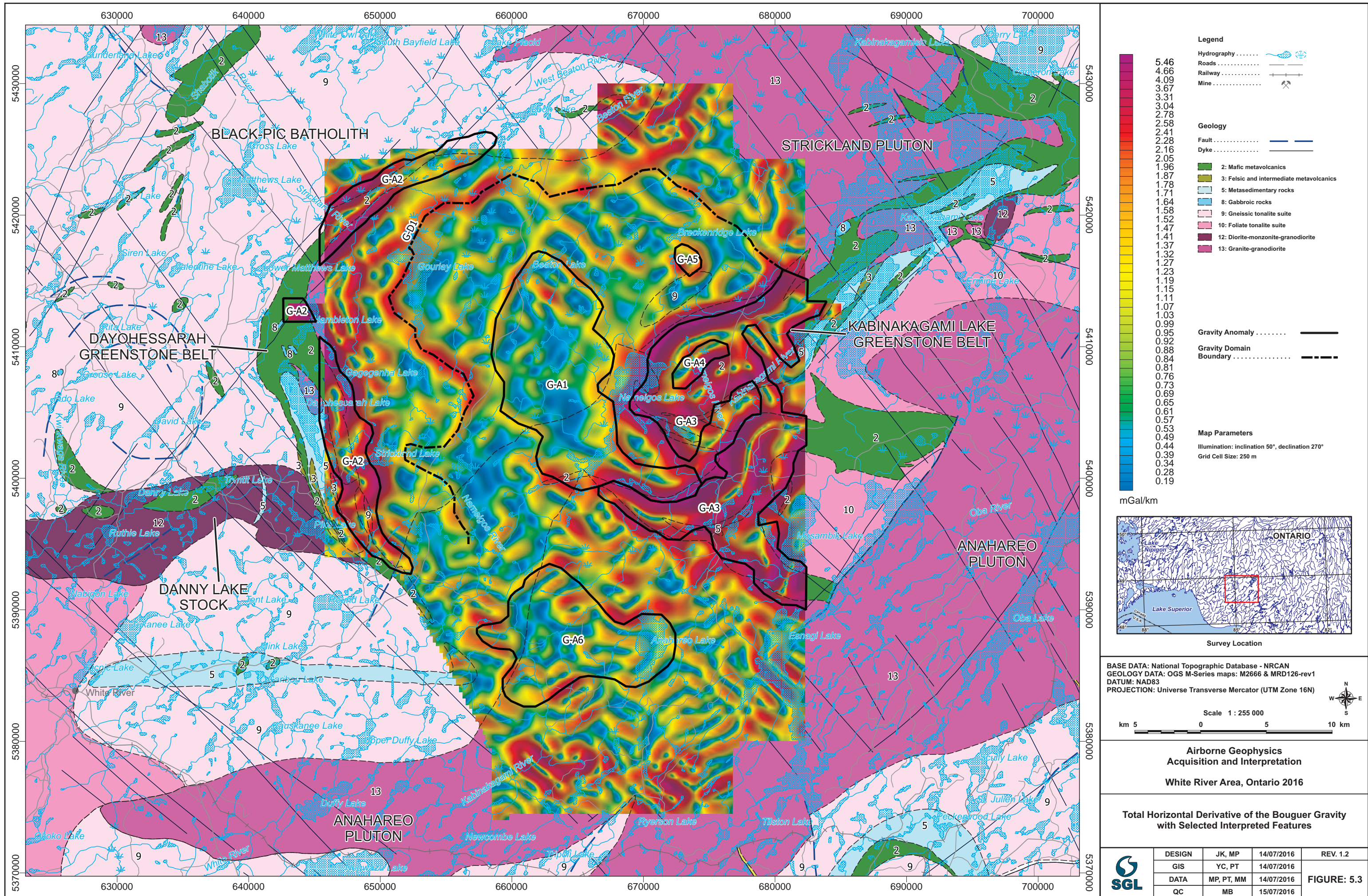




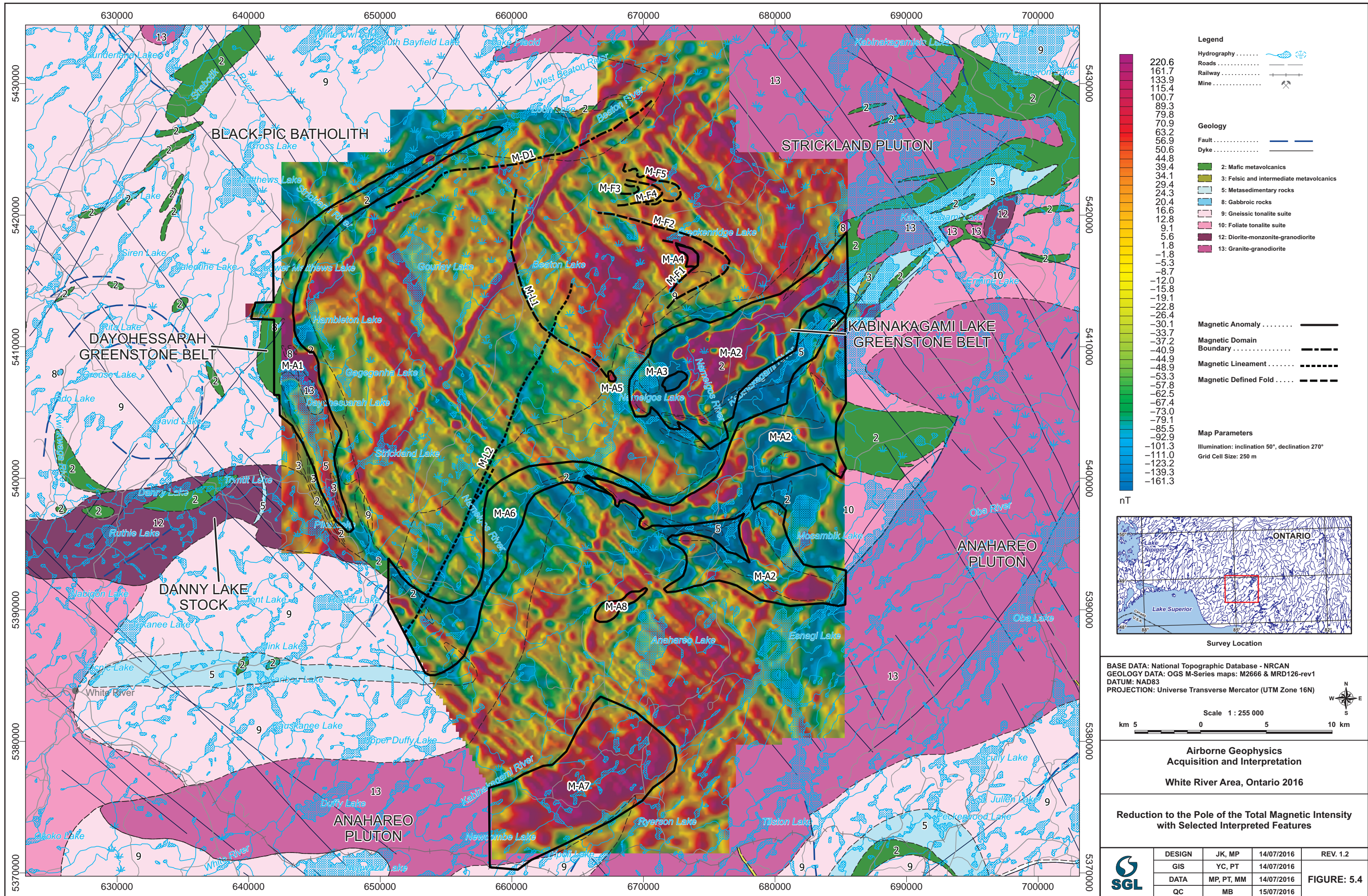




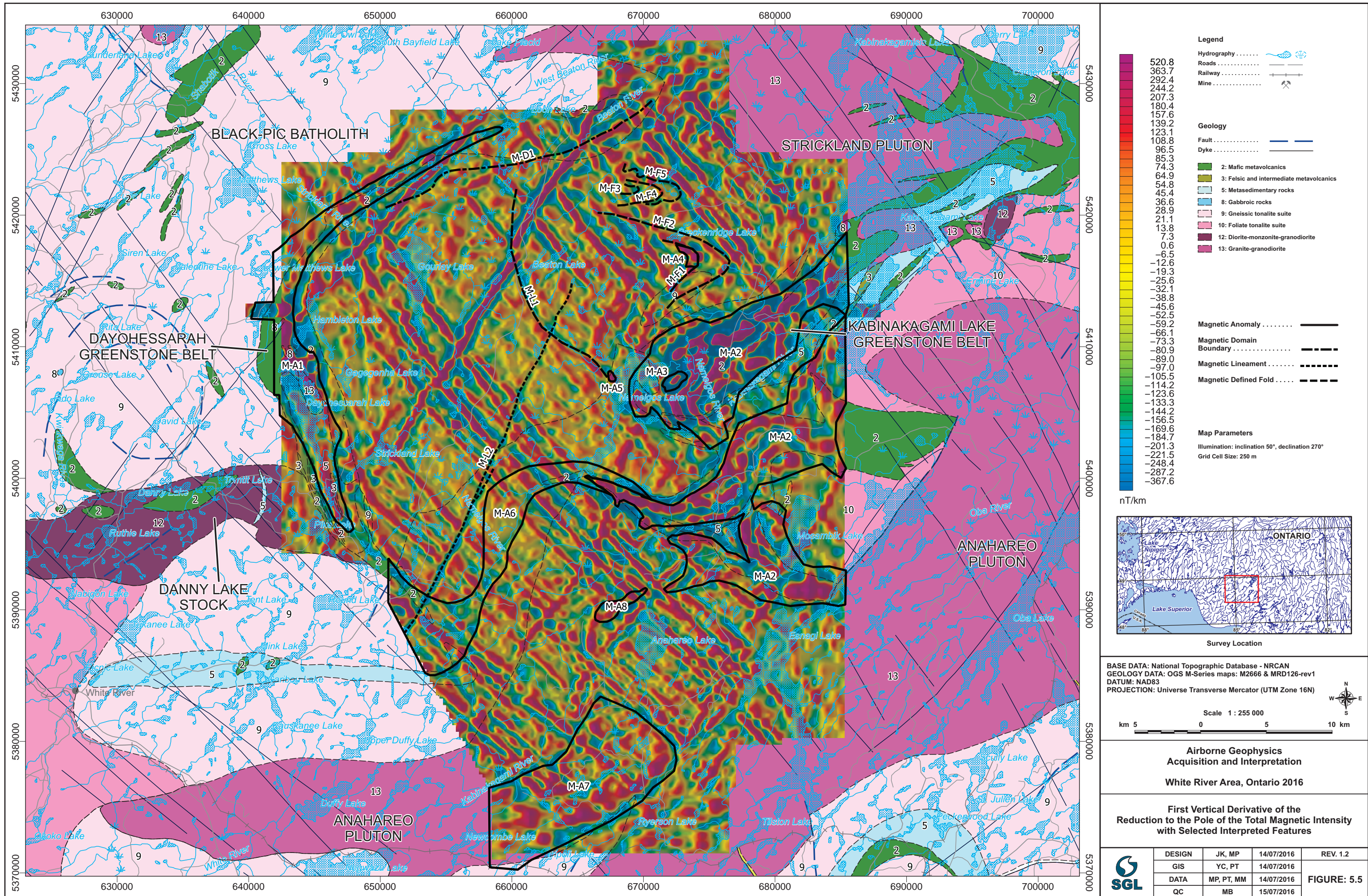




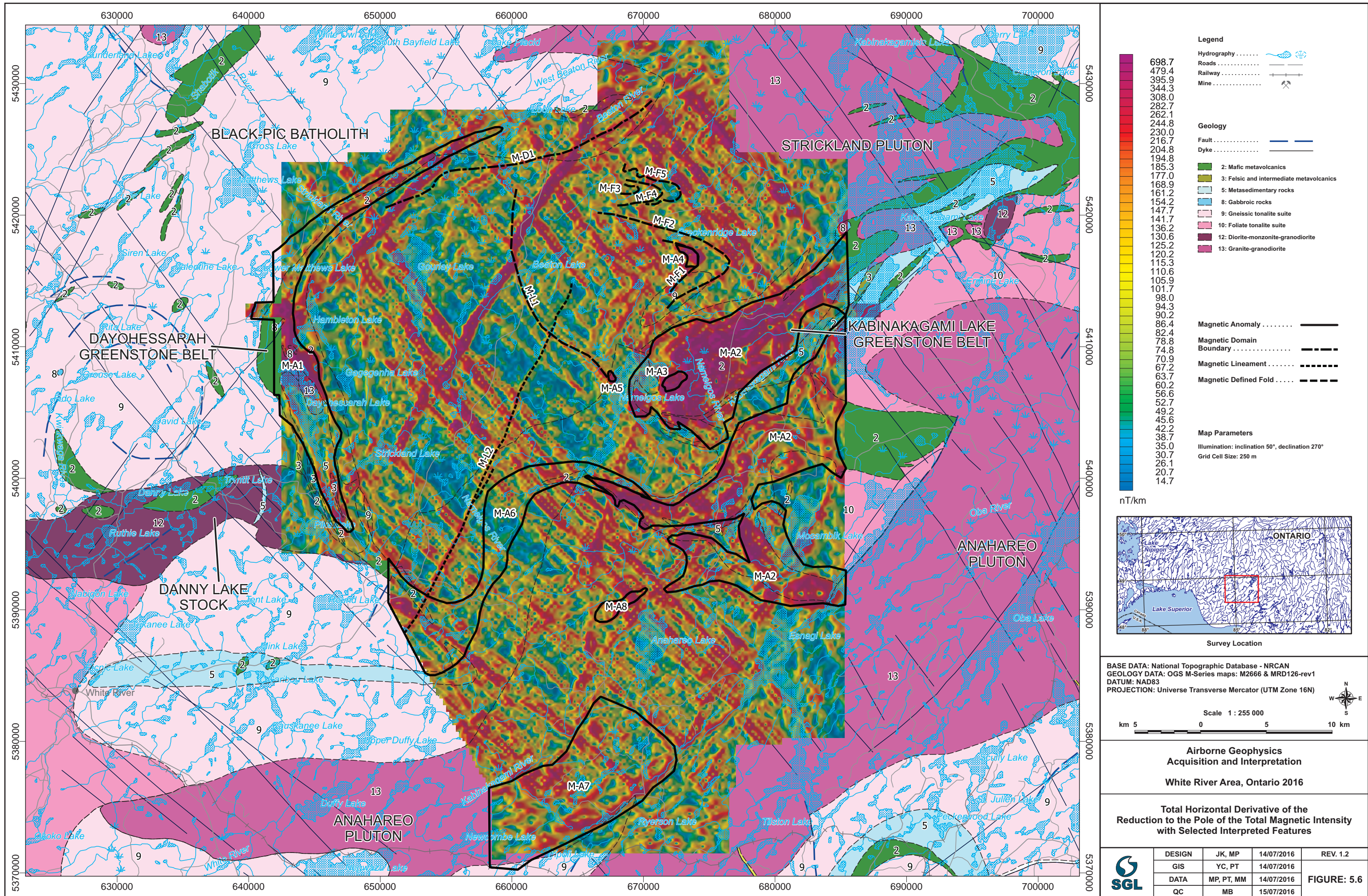




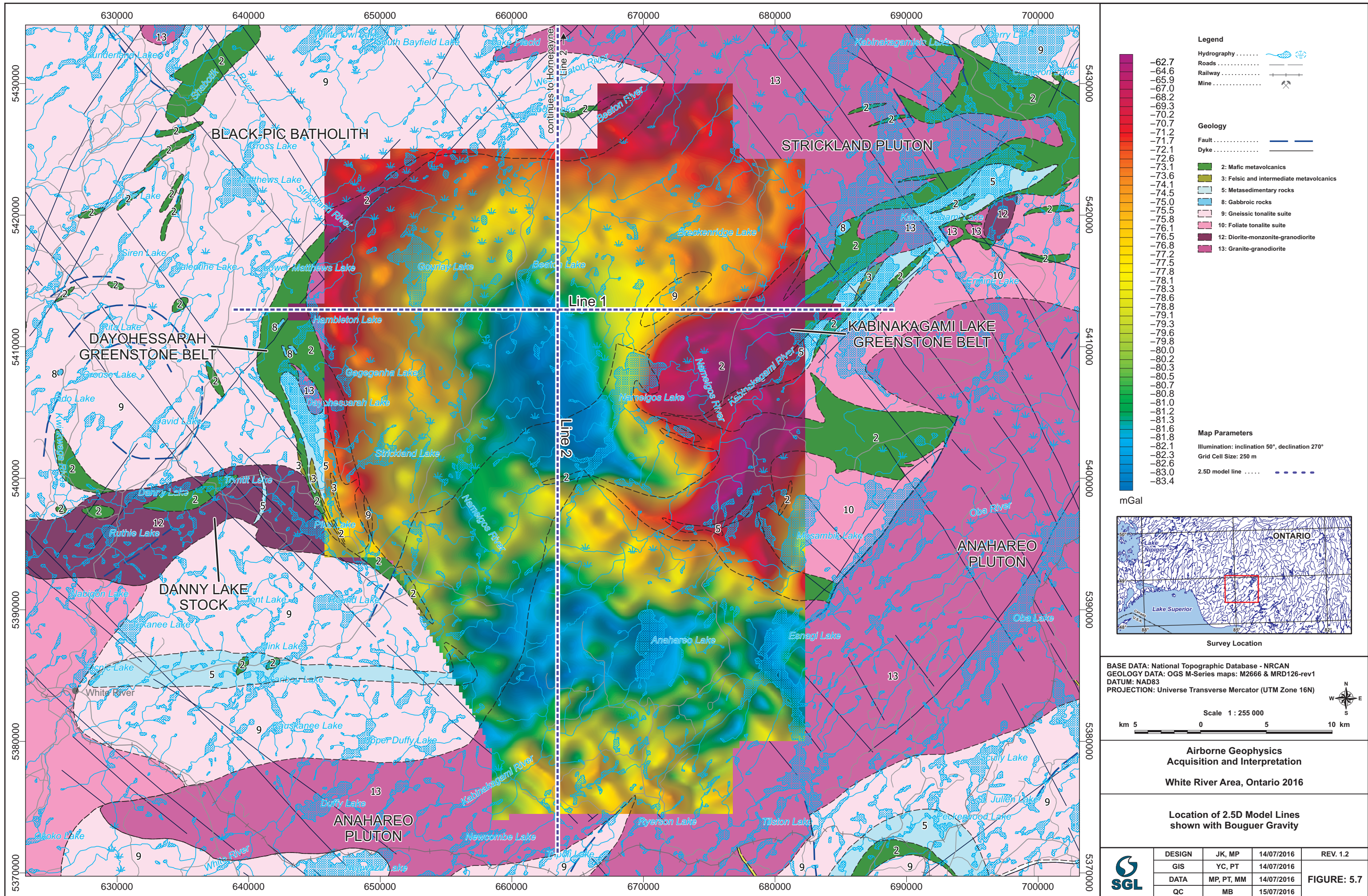














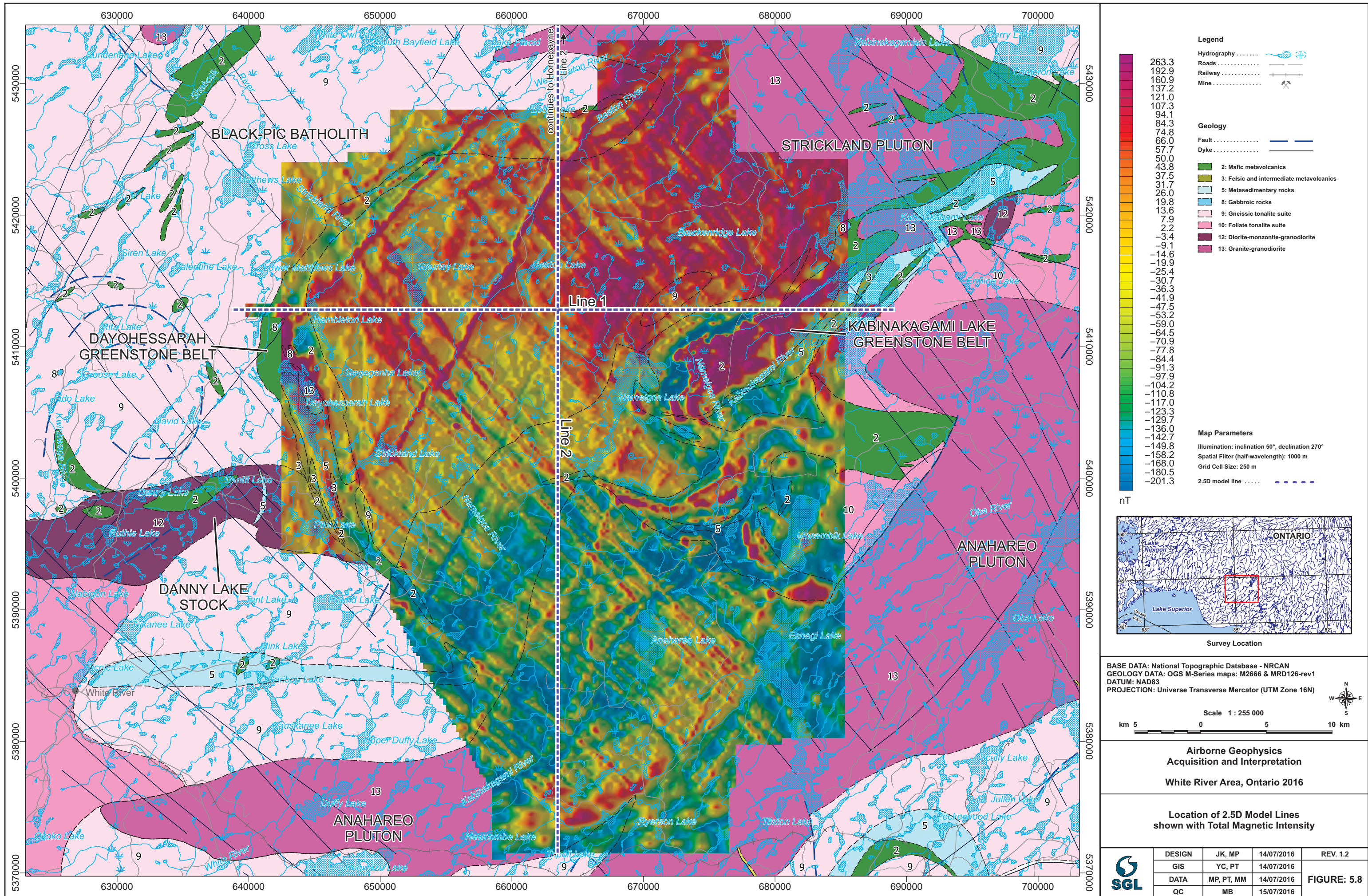




Figure 5.9 - Forward Modeling Results: Line 1, White River, Ontario

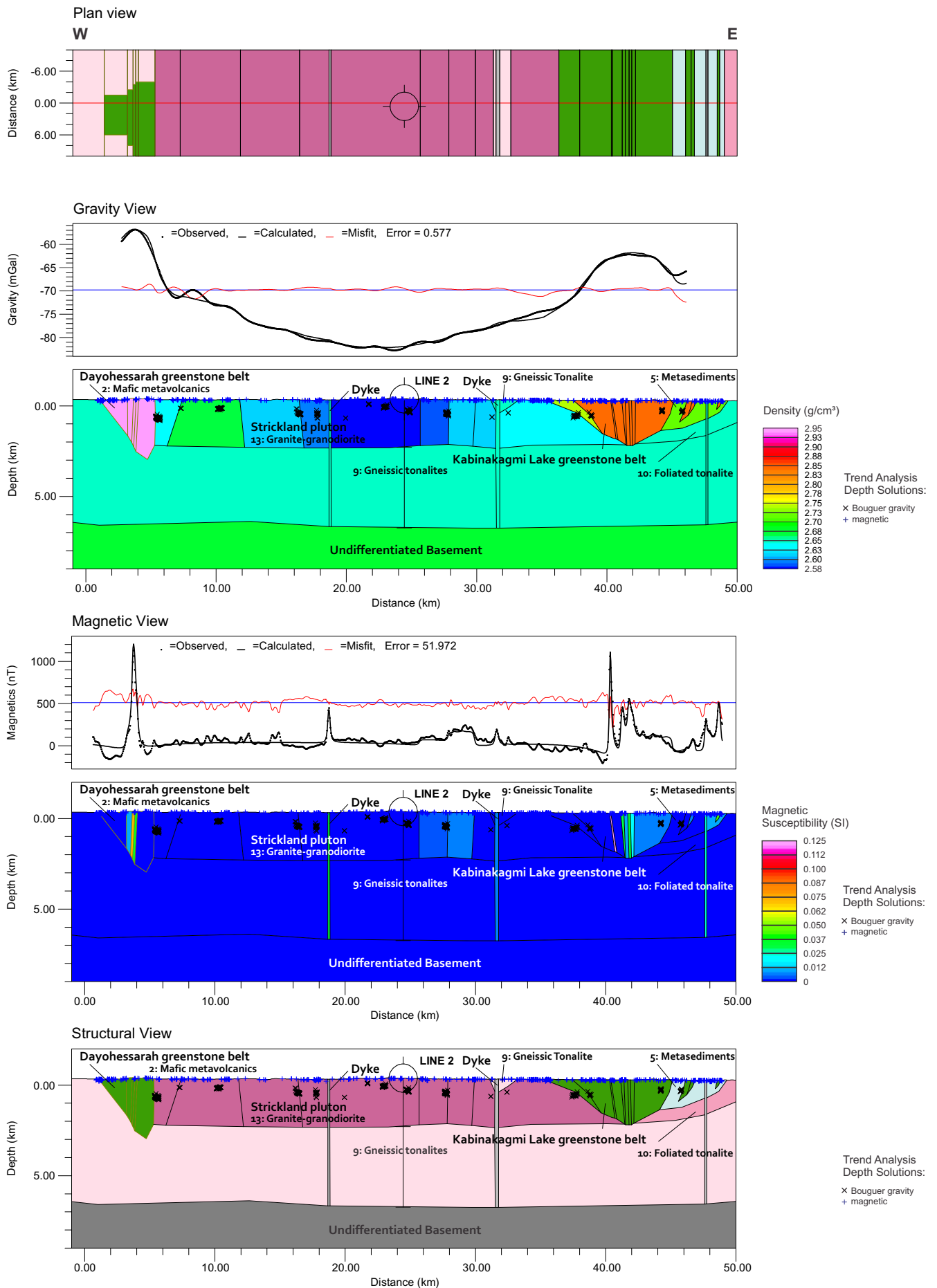




Figure 5.10 - Forward Modeling Results: Line 1-Alternative, White River, Ontario

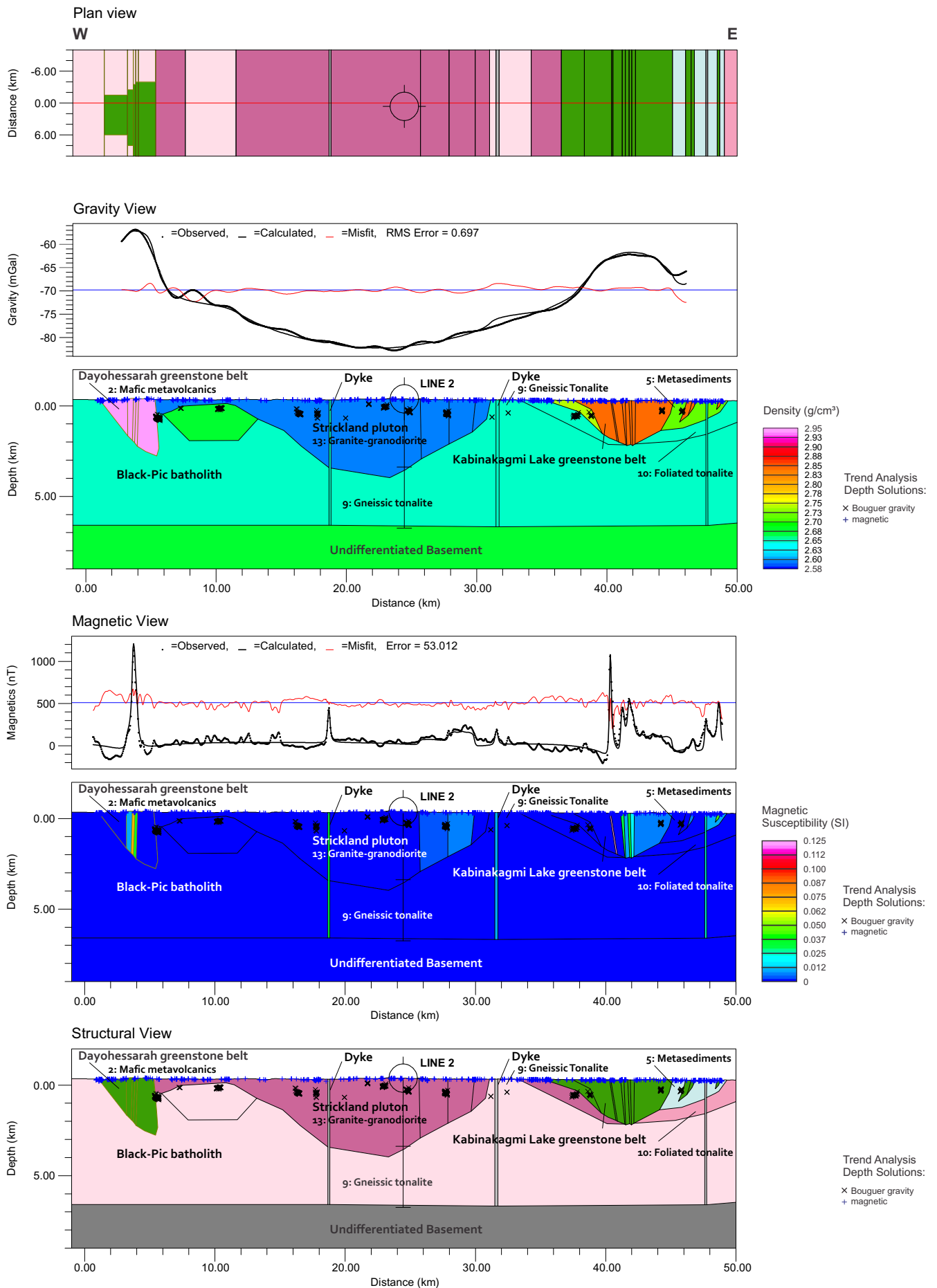




Figure 5.11 - Forward Modeling Results: Line 2, White River, Ontario

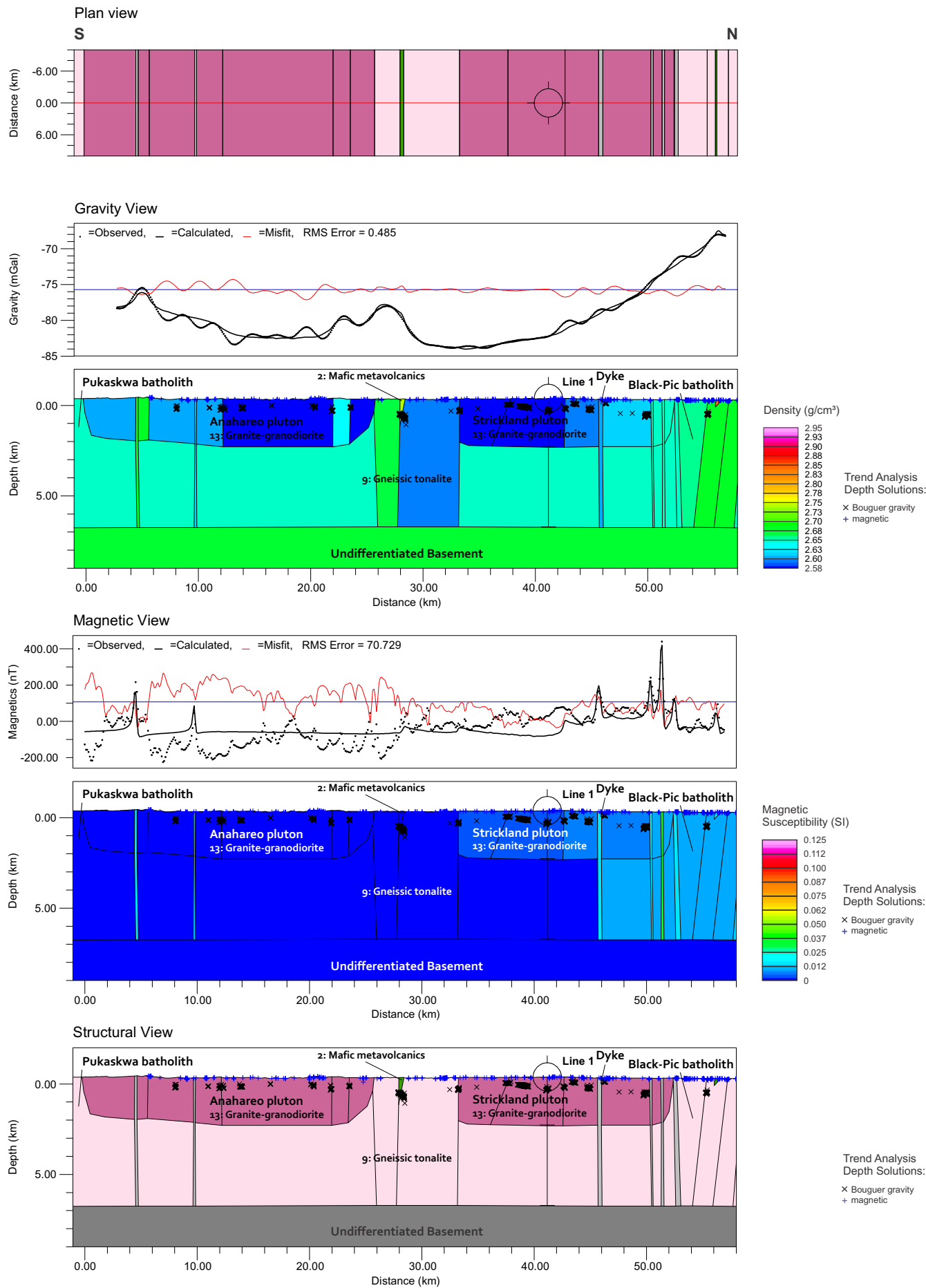




Figure 5.12 - Forward Modeling Results: Line 2-Alternative, White River, Ontario

